Check for updates

The Meteoritical Society

Meteoritics & Planetary Science 1–45 (2026)
doi: 10.1111/maps.70233

Xenoliths in meteorites: Insights into the dynamics of material exchange between asteroids

J. GATTACCECA[1]*, B. DEVOUARD[1], L. BONAL[2], Y. MARROCCHI[3], A. GRESHAKE[4], R. TARTÈSE[5], M. GOUNELLE[6], D. AUYANG[1], C. SONZOGNI[1], M. HUTSON[7], A. IRVING[8], C. AGEE[9], T. SHISSEH[9], A. LOVE[10], V. VIDAL[1], D. BORSCHNECK[1], S. A. ECKLEY[11], and A. MORBIDELLI[12,13]

[1]CEREGE, CNRS, Aix-Marseille Univ, IRD, INRAE, Aix-en-Provence, France
[2]Univ. Grenoble Alpes, CNRS, CNES, IPAG, Grenoble, France
[3]Université de Lorraine, CNRS, CRPG, Nancy, France
[4]Museum für Naturkunde, Leibniz-Institut für Biodiversitätsforschung, Invalidenstraße 43, Berlin, Germany
[5]Department of Earth and Environmental Sciences, The University of Manchester, Manchester, UK
[6]Muséum National d'Histoire Naturelle, Sorbonne Université, UMR CNRS 7590, Institut de Minéralogie, de Physique des Matériaux et de Cosmochimie, Paris, France
[7]Cascadia Meteorite Laboratory, Portland State University, School of Earth, Environment and Society, Portland, Oregon, USA
[8]Department of Earth & Space Sciences, University of Washington, Seattle, WA, USA
[9]Institute of Meteoritics, University of New Mexico, Albuquerque, New Mexico, USA
[10]Department of Geology, Appalachian State University, Boone, North Carolina, USA
[11]Amentum, JETS 2, NASA Johnson Space Center, Houston, Texas, USA
[12]Observatoire Lagrange, Univ. Côte d'Azur, Observatoire de la Côte d'Azur, France
[13]Collège de France, Paris, France

***Correspondence**
J. Gattacceca, CEREGE, CNRS, Aix-Marseille Univ, IRD, INRAE, Aix-en-Provence, France.
Email: gattacceca@cerege.fr

(Received 18 May 2026; revision accepted 01 September 2026)

Abstract–A minor fraction of meteorites contains xenoliths, that is, clasts that were formed on a different parent body than that of the host lithology. The occurrence of xenoliths is direct evidence for the exchange of material between asteroids, including exchanges between asteroids from the carbonaceous (CC) and non-carbonaceous (NC) reservoirs. Overall xenolith population statistics may therefore inform us about the dynamical mixing of these two asteroid reservoirs. Xenoliths are also intrinsically interesting because they may sample parent bodies that are not represented in the meteorite collection. In this work, we conducted a critical and exhaustive review of xenoliths described in the literature and performed a new large-scale search for macroscopic lithic xenoliths. We identify 89 xenolith-bearing meteorites in the literature, and report 18 new ones. We expand the diversity of known host/xenolith pairs with occurrence that had not been reported before: a CM clast in a L chondrite, a CO3 clast in a eucrite, a pallasite and H clasts in howardites, and two CO-CM breccias. Based on our observations, we reinterpret a number of previously described xenoliths. In particular, many "CI-like" xenoliths should rather be classified as ungrouped C1 or C2 chondrite xenoliths. At least a third of xenoliths do not belong to the known meteorite groups, suggesting that they represent a flux of meteoroids different from the present-day one that is dominated by the products of recent (~<50 Ma) collisions. Although xenoliths are present in only 0.14% of meteorites, the statistics of the total data set of 107 xenolith-bearing meteorites can be discussed in relation with the asteroid population. Xenoliths are more abundant in the regolith breccias of large asteroids, in agreement with

© 2026 The Author(s). *Meteoritics & Planetary Science* published by Wiley Periodicals LLC on behalf of The Meteoritical Society.
This is an open access article under the terms of the Creative Commons Attribution License, which permits use, distribution and reproduction in any medium, provided the original work is properly cited.

their ability to maintain an old and mature regolith. Chondritic xenoliths represent 95% of xenolith occurrence, in line with a higher number of chondritic asteroids with respect to achondritic ones. Xenoliths from the CC and NC reservoirs are found in host meteorites from both reservoirs, and a majority was implanted at low collisional speed (below about 2 km s^{-1}). The low proportion of CC meteorites with NC xenoliths can be related to the fact that the present-day outer asteroid belt that hosts the majority of CC asteroids is depleted in NC asteroids. The broad agreement between the xenolith population and the present-day architecture of the asteroid belt, as well as the low collisional speed between CC and NC materials suggest that the implantation of most xenoliths occurred after the main scattering event of the asteroids triggered by the formation of Jupiter a few Myr after the formation of the solar system. Conversely, CV, CK, and CO chondrites contain only xenoliths from a meteorite group of their own meteorite clan suggesting that these intra-clan xenoliths were implanted while their parent bodies were still orbiting in a narrow range of heliocentric distance, that is, before the main scattering event of the asteroids triggered by the formation of Jupiter. Eventually, a few xenoliths were incorporated in asteroids that were still accreting. Therefore, xenolith implantation seems to have been a universal and protracted phenomenon, active for most of solar system history.

INTRODUCTION

The formation of planetesimals (solid bodies ~50–100 km in diameter), within a few Myr after the formation of calcium–aluminum rich inclusions (CAIs), was a crucial step of planetary formation. In the scenario of a non-empty primordial asteroid belt, it is estimated that about 99.9% of these planetesimals that originally formed were subsequently ejected from the solar system. This strong mass depletion occurred in two steps, with a main depletion event associated to the formation of the giant planets in the first Myr after the formation of the solar system (e.g., Morbidelli et al., 2015), and a later undated depletion by a factor of ~10 triggered by the giant planets instability (e.g., Deienno et al., 2018). It is noteworthy that, in addition to mass removal, the initial mass depletion is accompanied by the implantation of planetesimals formed beyond the orbit of the giant planets between Mars and Jupiter (Raymond & Izidoro, 2017). The remnants of the original planetesimal population are now in the main asteroid belt that hosts about 1 million asteroids over 1 km in diameter (Burbine et al., 2002). This high number is the result of 4.5 billion years of collisional history, and asteroids today are much more numerous than their parent planetesimal population (e.g., Bottke et al., 2015; Weidenschilling, 1988). About 100 intact planetesimals are estimated to be present in the asteroid belt (Delbo et al., 2017), and a few dozens of asteroid dynamical families that were formed by successive shattering of other planetesimals have been identified. The total number of planetesimals that survived ejection from the solar system, either intact or shattered as asteroids, can thus be estimated at around 200. Meteorites are fragments of the present-day asteroid population, and originate mostly from young (<50 Myr-old) asteroid families (Brož et al., 2024a). It has been estimated that they originate from between 100 and 150 distinct parent bodies (Gattacceca et al., 2020; Greenwood et al., 2020). Therefore, meteorites are a fair yet incomplete representation of the diversity of the original population of ~200 surviving planetesimals.

Most meteorites are brecciated (Bischoff et al., 2006), which reflects, at a smaller scale, the asteroid collisional activity integrated over the age of the solar system (e.g., Marrocchi et al., 2021). Most brecciated meteorites are formed by comminuted material from a single asteroid. However, some meteorites contain clasts (lithic or mineral fragments), called xenoliths, that are made of material genetically unrelated to the host rock. These xenoliths, that are material exchanged from an asteroid to another asteroid deriving from a different parent planetesimal, are nothing else than meteorites or micrometeorites that fell on asteroids.

Xenoliths are particularly relevant to the study of the formation and evolution of the solar system. First, it is possible that some xenoliths originate from parent bodies that are not yet represented in the recognized meteorite groups (Weisberg et al., 2006). For macroscopic xenoliths, this may be because their initial parent body is not in a favorable position to deliver meteoroids to Earth-crossing orbits (i.e., close to a dynamical resonance, see Brož et al., 2024b), and/or because they are made of material that is too friable to survive atmospheric entry. It is also possible that some xenoliths originate from the 99.9% of planetesimals that have been ejected from the solar system during its early history or

19455100, 0, Downloaded from https://onlinelibrary.wiley.com/doi/10.1111/maps.70233 by Portland State University, Wiley Online Library on [06/11/2026]. See the Terms and Conditions (https://onlinelibrary.wiley.com/terms-and-conditions) on Wiley Online Library for rules of use; OA articles are governed by the applicable Creative Commons License

were not implanted in the main asteroid belt. Second, the presence of xenoliths can be direct evidence for the mixing of the different asteroid reservoirs. In particular, non-carbonaceous (NC) and carbonaceous (CC) meteorite reservoirs, distinguished by their distinct nucleosynthetic isotopic anomalies, are suggested to represent inner and outer solar system materials. As such, any mixing of CC and NC material at the meteorite scale is of particular interest to constrain the dynamical mixing of these two reservoirs (e.g., Kruijer et al., 2017; Warren, 2011). This is all the more interesting if a third reservoir is to be considered. Indeed, the existence of a distinct reservoir, the "CI" reservoir represented by CI1 chondrites and asteroid Ryugu material, has been suggested based on iron, chromium, and oxygen isotopic compositions (Dauphas et al., 2024; Gattacceca et al., 2025; Hopp et al., 2022). The existence of this third reservoir is however debated, other studies having suggested that CI1 like dust was ubiquitously distributed throughout the CC reservoir (Marrocchi et al., 2023; Yap & Tissot, 2023).

Xenoliths have been identified in many meteorites (see reviews by Wilkening, 1977; Keil, 1982; Bischoff et al., 2006, 2018; Briani et al., 2012). Most of the previous works, however, were focused on clasts within a single meteorite (e.g., Keil & Fodor, 1980; Zolensky et al., 1992), or in one meteorite group (e.g., Goodrich et al., 2021; Gounelle et al., 2003). Patzek et al. (2018, 2020) studied submillimeter-sized xenoliths in a larger suite of meteorites, including 15 howardite–eucrite–diogenite (HED) meteorites, 11 polymict ureilites, 7 CR2 chondrites, 3 paired CH3 chondrites, and one H chondrite. Lee et al. (2025) provided a review of the typology of hydrated chondritic xenoliths.

The present work is focused on a statistical evaluation of the population of xenoliths in meteorites, as a step to better exploit their potential to constrain the dynamics of the solar system evolution. We present a critical review of the existing literature on xenoliths in meteorites, and a new large-scale survey of meteorites aimed at the discovery and description of new unusual and possibly xenolithic clasts. Xenoliths in meteorite are usually small (<cm), and many of them are much smaller than a millimeter, which is in the range of dust or micrometeorite size (e.g., Briani et al., 2012; Gounelle et al., 2003). Our survey is focused on lithic clasts, typically larger than a millimeter, which fall in the meteorite rather than in the micrometeorite size range (Rubin & Grosmann, 2010), and allow for a comparison with the established meteorite groups. Based on our survey and the literature review, we then discuss the implications of the overall xenolith population statistics for constraining the dynamical evolution of the asteroid belt.

MATERIALS AND METHODS

Meteorite Samples

This work is based in part on a search for unusual clasts in meteorites from the CEREGE (Centre de Recherche et d'Enseignement en Géosciences de l'Environnement, Aix-en-Provence) meteorite collection, that contains 4025 meteorites as of September 2026, and the Museum National d'Histoire Naturelle (MNHN, Paris) meteorite collection, that contains 1800 meteorites as of September 2026. By unusual, we mean clasts that are not obviously cognate. We investigated chondrites, HED, and ureilites. For ordinary chondrites, we surveyed type 3 chondrites exhaustively (including cognate breccias containing type 3 material), while only a small fraction of the equilibrated ordinary chondrites was investigated. This choice was dictated by the elevated number of equilibrated ordinary chondrites that makes it difficult to be exhaustive. Also, unequilibrated ordinary chondrites contain a higher proportion of brecciated meteorites compared to equilibrated ordinary chondrites. This is particularly true for H and L chondrites: 67% of H3 chondrites and 70% of L3 chondrites are brecciated, whereas only 18% of equilibrated H chondrites and L chondrites are brecciated (based on statistics in Bischoff et al., 2018).

In the MNHN collection, we visually inspected the cut surfaces of all meteorite slices with surfaces above about 2 cm^2. We investigated a total of 117 meteorite cut surfaces (from 104 distinct meteorites), amounting to observing 4900 cm^2 of meteorite surface. For this visual inspection, potential xenoliths were identified based on the difference in color, grain size, texture, and opaque content between the clasts and the host rock. The clasts identified by visual inspection of cut surfaces were further examined with an optical microscope. If they were deemed interesting, the samples were cut and polished sections encompassing the clast were prepared. A list of the investigated slices is given in Table S1. The CEREGE collection does not host many large meteorite slices and the search for interesting clasts was therefore focused on the polished sections of the 377 meteorites of interest that had been prepared for routine classification work over the last two decades. These 377 polished sections, with an average observed surface for each meteorite of about 1.5 cm^2, represent about 560 cm^2 of investigated surface. The MNHN survey is biased toward large slices of a limited number of already well-studied meteorites. The CEREGE survey is statistically more robust in terms of meteorite variety but with a limited surface investigated for each meteorite (1.5 cm^2). We also looked for xenoliths in a non-exhaustive selection of meteorites from other collections in the USA (University of Washington,

19455100, 0, Downloaded from https://onlinelibrary.wiley.com/doi/10.1111/maps.70233 by Portland State University, Wiley Online Library on [06/11/2026]. See the Terms and Conditions (https://onlinelibrary.wiley.com/terms-and-conditions) on Wiley Online Library for rules of use; OA articles are governed by the applicable Creative Commons License

University of New Mexico, Appalachian State University, Portland State University, and ANSMET).

Petrography and Mineral Composition

Optical microscopic petrographic examinations were performed with a Leica DM polarizing microscope and a Keyence VHX-7000 digital microscope. Scanning electron microscopy was performed at CEREGE with a Hitachi S3000N microscope fitted with a Bruker X-Flash/Esprit Electron Dispersive Spectrometer (EDS) at CEREGE, and a Hitachi TM4000Plus tabletop microscope equipped with an Oxford instrument detector at the University of Manchester. Both instruments were used to acquire backscattered electron (BSE) images and EDS X-ray chemical maps of the studied samples. We estimated the bulk composition of some clasts by acquiring EDS spectra over areas of a few mm^2. Although such analyses should be considered only semiquantitative, because inter-element matrix corrections cannot be properly applied when scanning heterogeneous assemblages, they appear to be sufficient to distinguish between chondritic versus achondritic bulk compositions.

Quantitative mineral elemental compositions were obtained by electron probe microanalyses (EPMA) using a SX-Five microprobe at the Camparis facility (CNRS, Sorbonne Université, Paris). The operating conditions were 15 kV accelerating voltage, a beam current of 10 nA, and a focused beam ~1 μm in diameter. Both natural and synthetic standards were used for calibration: albite for Na; anorthite for Al; apatite for P; diopside for Mg, Si, Ca; orthoclase for K; pyrite for S; $MnTiO_3$ for Mn and Ti; Cr_2O_3 for Cr; Fe_2O_3 for Fe; and NiO for Ni. For meteorites containing fine-grained matrix, the matrix analyses were obtained with the same operating conditions but a beam defocused to a diameter of ~10 μm. The fine-grained matrix of the host lithology, when available, was analyzed the same way for comparison. The matrix FeO content and the analytical totals are given in Table 1, and detailed analyses are given in Table S2. Defocused EPMA totals in the matrix are reduced by the presence of elements such as H and C, from hydrated minerals such as phyllosilicates (interlayered H_2O and −OH groups), or hydration in the amorphous materials, as well as organic matter (C, H) and carbonates (C) not measured during matrix EMPA. Porosity does not lower the analytical total unless it is completely filled with epoxy resin (C-, H-, and O-rich) (Prêt et al., 2010). The samples used in this study were mostly thick sections prepared without impregnation under vacuum. Therefore, only a negligible part of the porosity may be filled with epoxy, making our EPMA totals data set internally consistent. However, the comparison with similar literature data may be less accurate since there is usually no information about how the polished sections were prepared. Based on Prêt et al. (2010), it can be estimated that in the worst-case, CI-like or CM-like scenario of material with low grain density (~2.7) and highly porosity (~20%) that has been perfectly (100%) filled by epoxy down to the nanometer scale, the EPMA totals would be lowered by 10 wt% compared to a non-impregnated sample. This is the maximum bias that may be observed when comparing our EPMA totals data set with the literature data set.

For a few samples (NWA 14981, NWA 15819, and in part for NWA 17470 and Bholghati), EPMA were performed at the Museum für Naturkunde Berlin using a JEOL JXA 8500F field-emission electron microprobe. The analyses of the silicates, sulfides, and metals were done at 15 kV acceleration voltage, 15 nA beam current, and a fully focused electron beam with a spot size <1 μ. For matrix analyses, a defocused 5-μm beam size was applied. The EPMA of NWA 10472 was performed at the Institute of Meteoritics of the University of New Mexico.

To determine mineral trace element abundances, we used laser ablation inductively coupled mass spectrometry (LA-ICP-MS) at the University of Manchester, using a Teledyne Photon Machines Analyte Excite+193 nm ArF excimer laser ablation system with a HelEx II active 2-volume ablation cell, coupled to an Agilent 8900 ICP-MS via a SQUID-type signal-smoothing device. The material ablated from target phases was carried to the ICP-MS by high-purity He, which was mixed with Ar before injection into the plasma source. Initial tuning of the ICP-MS and mass calibration were performed at the start of the analytical session by optimizing the ion signals during ablation of NIST 612 while maintaining low levels of oxide formation (ThO/Th < 0.3%) and a $^{238}U/^{232}Th$ ratio close to unity. We analyzed masses ^{7}Li, ^{9}Be, ^{23}Na, ^{26}Mg, ^{27}Al, ^{29}Si, ^{31}P, ^{39}K, ^{45}Sc, ^{47}Ti, ^{51}V, ^{52}Cr, ^{55}Mn, ^{57}Fe, ^{59}Co, ^{60}Ni, ^{63}Cu, ^{66}Zn, ^{71}Ga, ^{85}Rb, ^{88}Sr, ^{89}Y, ^{90}Zr, ^{93}Nb, ^{95}Mo, ^{137}Ba, ^{139}La, ^{140}Ce, ^{141}Pr, ^{146}Nd, ^{147}Sm, ^{153}Eu, ^{157}Gd, ^{159}Tb, ^{163}Dy, ^{165}Ho, ^{166}Er, ^{169}Tm, ^{172}Yb, ^{175}Lu, ^{178}Hf, ^{181}Ta, ^{208}Pb, ^{232}Th, and ^{238}U (0.5660 s for a complete mass sweep; see Table S5 for details on analytical protocol). In NWA 14826, olivine and pyroxene from the xenolith and from chondrules from the host lithology were analyzed using a spot size of 65 μm, a fluence of 5 J cm^{-2}, and a repetition rate of 5 Hz. Each analysis lasted 40 s and was preceded by a 15 s counting time of the gas blank (background). Because of the smaller grain sizes in the xenolith in NWA 15116, we used mapping to extract trace element abundances from different phases. We mapped a 300 × 150 μm area by stacking individual LA-ICP-MS line analyses, using a 5-μm rectangular laser spot, a 20 Hz repetition rate, 5 J cm^{-2} fluence, 5 μm vertical

19455100, 0, Downloaded from https://onlinelibrary.wiley.com/doi/10.1111/maps.70233 by Portland State University, Wiley Online Library on [06/11/2026]. See the Terms and Conditions (https://onlinelibrary.wiley.com/terms-and-conditions) on Wiley Online Library for rules of use; OA articles are governed by the applicable Creative Commons License

TABLE 1. Xenolith-bearing meteorites reported in this work.

	Classification					Olivine		Low-Ca pyroxene		Matrix			Chondrule diameter
	Host	Clast	*n*	Largest clast (mm)	Total clast surface (mm^2)	Fa	Cr_2O_3 in ferroan olivine wt%	Fs	Wo	vol %	EPMA total wt%	FeO wt%	μm
Xenolith-bearing meteorites													
Bholghati	Howardite	CM2	6	2.6 × 1.4	3.4	1.09 ± 0.26 (*n* = 7)		3.87 ± 1.34 (*n* = 3)	0.35 ± 2.41	74	89.5 ± 2.7 (*n* = 5)	33.3 ± 2.6	268 (*n* = 2)
Bholghati	Howardite	C2-ung	4	0.58 × 0.47	0.34	1.48 (*n* = 1)				92	84.4 ± 2.5 (*n* = 30)	20.1 ± 2.1	
NWA 3197	Howardite	H (H4?)	1	16 × 8	96	17.8 ± 1.3 (*n* = 6)		16.5 ± 0.7 (*n* = 7)	1.3 ± 0.4				483 ± 144 (*n* = 12)
NWA 10472	Howardite	CM2	2	1.4 × 0.8	0.86	1.1 (*n* = 2)				82			
NWA 10472	Howardite	pallasite	1	0.54 × 0.35	0.15	9.1 ± 0.2 (*n* = 17)							
NWA 10674	Eucrite-pmict	H (H6?)	1	2.0 × 1.3	2.3	19.0 ± 0.4 (*n* = 3)		16.8 ± 0.5 (*n* = 3)	1.8 ± 0.2				
NWA 11490	Howardite	CM2	2	6.4 × 3.2	18.6	17.6 ± 18.9 (*n* = 17)	0.33 ± 0.16 (*n* = 9)	17.8 ± 9.7 (*n* = 4)	1.0 ± 0.1	78	77.4 ± 1.0 (*n* = 2)	28.6 ± 0.0	289 ± 120 (*n* = 12)
NWA 13143	Howardite	CM2	1	4.6 × 5.1	13.6	10.6 ± 14.7 (*n* = 12)	0.43 ± 0.16 (*n* = 11)	1.1 ± 0.3 (*n* = 4)	1.0 ± 0.2	81	80.1 ± 1.7 (*n* = 3)	28.6 ± 2.5	187 ± 70 (*n* = 11)
NWA 14804	Howardite	CM2	4	2.7 × 1.4	4.7	13.0 ± 17.2 (*n* = 9)	0.42 ± 0.24 (*n* = 9)	8.4 ± 15.7 (*n* = 7)	2.5 ± 1.3		89.5 ± 1.4 (*n* = 6)	32.95 ± 4.49	157 ± 83 (*n* = 17)
NWA 14981	Eucrite-pmict	CM2	14	4.6 × 2.5	22.1								
NWA 17470	Eucrite-pmict	CM2	2	1.5 × 1.2	2.3	1.82 ± 0.79 (*n* = 11)	0.52 ± 0.19 (*n* = 10)	1.2 (*n* = 2)	2.5	79	83.7 ± 1.1 (*n* = 12)	28.8 ± 4.5	No intact chondrule
NWA 17470	Eucrite-pmict	CO3.05	1	3.6 × 1.6	5.5	18.8 ± 19.8 (*n* = 18)	0.32 ± 0.11 (*n* = 34)	1.6 ± 0.4 (*n* = 11)	1.0 ± 0.2	58	89.9 ± 1.5 (*n* = 4)	26.9 ± 1.1	154 ± 45 (*n* = 5)
NWA 17597	Howardite	OC3	1	0.9 × 0.6	0.37	33.8 ± 7.3 (*n* = 8)		22.1 ± 0.4 (*n* = 4)	2.3 ± 0.4				738 (*n* = 1)
NWA 14086	Ureilite-pmict	CI1-like	Several								84.75 ± 2.08 (*n* = 4)	30.28 ± 4.87	
NWA 16454	Ureilite-pmict	CI1-like	Several								83.8 (*n* = 2)	24.5	
GRO 06054	LL3.1	Graphite-bearing	1	5 × 4	>9.9	25.3 ± 0.8 (*n* = 7)		19.9 ± 0.6 (*n* = 4)	2.2 ± 0.1				
NWA 13177	L3-6	CM2	1	1.1 × 0.7	0.59	3.6 ± 2.1 (*n* = 4)	0.50 ± 0.15 (*n* = 4)	2.2 ± 0.5 (*n* = 7)	1.7 ± 0.9	68	86.1 ± 0.8 (*n* = 9)	30.9 ± 8	229 μm (*n* = 1)
NWA 15116	LL3	Achondrite	1	10.3 × 9.1	58.4			23.7 ± 5.7 (*n* = 6)	4.3 ± 1.3				

19455100, 0, Downloaded from https://onlinelibrary.wiley.com/doi/10.1111/maps.70233 by Portland State University, Wiley Online Library on [06/11/2026]. See the Terms and Conditions (https://onlinelibrary.wiley.com/terms-and-conditions) on Wiley Online Library for rules of use; OA articles are governed by the applicable Creative Commons License

TABLE 1. *Continued.* Xenolith-bearing meteorites reported in this work.

	Classification					Olivine		Low-Ca pyroxene		Matrix			Chondrule diameter
	Host	Clast	*n*	Largest clast (mm)	Total clast surface (mm^2)	Fa	Cr_2O_3 in ferroan olivine wt%	Fs	Wo	vol %	EPMA total wt%	FeO wt%	μm
NWA 16109	LL3	H3	Several	45 × 45	>2000	18.5 ± 10.7 (*n* = 19)	0.09 ± 0.07 (*n* = 16)	17.1 ± 12.3 (*n* = 11)	1.6 ± 1.3	55	36.5 ± 1.6 (*n* = 3)	91.4 ± 2.4	445 ± 229 (*n* = 40)
Los Vientos 200	CH3	CI1-like	>10	3.1 × 2.8	7						76.5 ± 14.7 (*n* = 5)	17.5 ± 5.1	
NWA 15819	CO3	CM2	1	>1		18.6 ± 15.1 (*n* = 30)	0.39 ± 0.11 (*n* = 19)	3.8 ± 2.3 (*n* = 20)	0.7 ± 0.4 (*n* = 20)	60	77.2 ± 0.9 (*n* = 5)	33.0 ± 0.9	
NWA 17518	CO3[a]	CM2	1	>5		27.6 ± 26.3 (*n* = 6)	0.38 ± 0.14 (*n* = 6)	4.8 (*n* = 1)	1.4	51	87.5 (*n* = 2)	32.8	190 ± 90 (*n* = 13)
Other unusual clast-bearing meteorites													
NWA 10472	Howardite	Mesosiderite		0.64 × 0.34	0.21			55.7 ± 1.6 (*n* = 5)	11.7 ± 1.6				
NWA 14981	Eucrite-pmict	Mesosiderite	2	10.7 × 7.6	72.7			40.8 ± 0.1 (*n* = 10)	3.9 ± 0.1				
NWA 13271	LL3.15	Matrix-rich inclusion (possibly R)	1	2.7 × 1.6	4.3	38.1 ± 1.2 (*n* = 9)					90.7 (*n* = 2)	26.5	
NWA 14826	LL3	Achondrite (possibly xenolithic)	1	6.5 × 5.3	28.4	6.3 ± 1.4 (*n* = 8)	0.51 ± 0.12 (*n* = 8)	1.54 ± 1.9 (*n* = 8)	1.7 ± 1.6				
NWA 13385	CV3	Cognate matrix-rich inclusion	1	2 × 3	7.8	3.2 ± 2.1 (*n* = 4)	0.14 ± 0.04 (*n* = 3)	1.6 ± 1.1 (*n* = 5)	1.4 ± 0.9	71	93.1 ± 0.9 (*n* = 3)	35.1 ± 0.3	176 ± 50 (*n* = 5)
NWA 7502	CR2	Cognate matrix-rich inclusion	5	2	4.9	1.67 ± 0.38 (*n* = 5)		4.5 ± 5.0 (*n* = 6)	1.6 ± 1.4	92	85.3 ± 1.5 (*n* = 8)	21.1 ± 4.0	64 ± 40 (*n* = 5)
NWA 13724	CR2	Cognate matrix-rich inclusion	1	1.9 × 0.8	1.3						84.4 ± 6.2 (*n* = 3)	30.2 ± 6.1	
NWA 14250	CR2	Cognate matrix-rich inclusion	2	4.7 × 2.8	23.2	7.8 ± 14.8 (*n* = 12)		1.9 ± 0.8 (*n* = 8)	1.0 ± 0.2		77.3 ± 3.7 (*n* = 3)	27.7 ± 0.5	525 (*n* = 2)
NWA 15175	CR2	Cognate matrix-rich inclusion	1	2.8 × 2.1	5.1								

Abbreviation: *n*, number of clasts.

[a]Classified as CM2 in the Meteoritical Bulletin Database, but proposed to be classified as CO3 in this study, based on the geometry of the contact between the CO3 and CM2 material.

19455100, 0, Downloaded from https://onlinelibrary.wiley.com/doi/10.1111/maps.70233 by Portland State University, Wiley Online Library on [06/11/2026]. See the Terms and Conditions (https://onlinelibrary.wiley.com/terms-and-conditions) on Wiley Online Library for rules of use; OA articles are governed by the applicable Creative Commons License

distance between lines, and a laser scan speed of 5 μm s^{-1}. This resulted in a spatial resolution of 2.83 × 5 μm per pixel. After each laser line, there was a pause of 5 s during which background counts for the masses of interest were integrated. We used known Si abundances for standards and those measured by EDS on the samples for internal standardization. For the spots analyses (NWA 14826), we used the BHVO-2G glass standard as our primary reference material, and repeated analyses of ML3B-G and BCR-2G glass standards treated as unknown for quality control (most trace element abundances were within 10% of the recommended abundances; Table S6). For the maps (NWA 15116), we used the BHVO-2G glass standard as our primary reference material, and repeated analyses of BCR-2G treated as unknown for quality control (most trace element abundances were within 15% of the recommended abundances; Table S6). All LA-ICP-MS results are provided in Table S6.

X-ray diffraction data were acquired at CEREGE using a MalvernPanalytical X'Pert Pro diffractometer equipped with a cobalt tube (λ = 1.79 A) running at 40 kV and 40 mA. Sample was deposited on a low background silicon plate and analyzed from 5° (2θ) to 70° (2θ) with a step size of 0.026° and a total counting time of 3.5 h. Sample was spun at 5 rpm to improve statistics. Phase identification was performed using the X'pert Highscore plus software (MalvernPanalytical) together with the PDF-2 ICDD database (International Center for Diffraction data, Powder Diffraction Files 2).

X-ray microcomputed tomography (micro-XCT) of a 1.36 g stone of NWA 17158 was performed using the micro-XCT-400 X-ray microscope (Zeiss) of the MATRIX platform at CEREGE. Data were acquired with a tungsten X-ray source at an accelerating voltage of 80 kV and a power of 10 W. The scan consists of 1201 projections at an exposure time of 2 s per projection collected over a 360° rotation of the sample. The volume reconstruction using back-projection filtering (by XMReconstructor, Xradia software) achieved an isotropic voxel size of 28.8 μm and a field of view of 28.8 × 28.8 × 28.8 mm^3. Avizo 2020 software was used for the visualization, processing, and analysis of the 3-D images.

Micro-XCT was also performed on GRO 06054,38 (6.039 g) and GRO 06054,39 (2.818 g) using the Nikon XTH 320 large cabinet XCT scanner in the Astromaterials X-ray Fluorescence and Computed Tomography (X-FaCT) Laboratory at NASA Johnson Space Center. Data for both samples were acquired using a 225 kV reflection tungsten X-ray source at an accelerating voltage of 150 kV and a power of 12 W with 1.5 mm of aluminum beam filtration. The scans consisted of 2831 projections at an exposure of 1.42 s per frame and 4 frames averaged per projection collected over a 360° rotation of the sample. The volume reconstruction using back-projection filtering (by CTPro3D [v. 5.4], Nikon software) achieved an isotropic voxel size of 16.0 μm (GRO 06054,38) and 13.1 μm (GRO 06054,39) and fields of view of 32.0 × 32.0 × 32.0 mm^3 and 26.2 × 26.2 × 26.2 mm^3, respectively. Dragonfly™ 2022 (Comet Technologies Inc., Canada) software was used for the visualization, processing, and analysis of the 3-D images.

Oxygen Isotopes

The oxygen isotopic composition of nine clasts was measured in this work (Table 2). Three bulk clast samples were analyzed using laser fluorination and isotope ratio mass spectrometry (IRMS), and six clasts were analyzed in situ on polished sections using secondary ion mass spectrometry (SIMS). Results are reported in δ notation: $\delta^{17,18}O = ([^{17,18}O/^{16}O]_{sample}/[^{17,18}O/^{16}O]_{reference} - 1) \times 1000$ (‰), and normalized to VSMOW (Vienna Standard Mean Ocean Water). Mass-independent variations are expressed by $\Delta^{17}O = \delta^{17}O - 0.525 \times \delta^{18}O$.

IRMS measurements were performed at CEREGE. Bulk fragments of the clasts were broken or cut with a wire saw, and gently powdered. For NWA 15116, the clast was microdrilled using a Micromill (Elemental Scientific). Aliquots of 1.6 to 3 mg were analyzed. Molecular O_2 extracted using the infrared laser-heating fluorination technique was passed through a −114 °C slush to trap any molecule interfering with the mass 33. The gas was directly sent to the dual-inlet mass spectrometer (ThermoQuest Finnigan Delta V Plus). The method is detailed in Outrequin et al. (2021). The maximal uncertainty (1σ) on the quartz laboratory standard measurement during the analytical sessions was 0.2‰ for $\delta^{18}O$, 0.1‰ for $\delta^{17}O$, and 0.03‰ for $\Delta^{17}O$ (n = 6).

SIMS measurements were performed using a CAMECA IMS 1270 E7 at CRPG-CNRS (Bouden et al., 2021; Morin et al., 2022). $^{16}O^-$, $^{17}O^-$, and $^{18}O^-$ ions generated by a Cs^+ primary beam (~4 μm, 500 pA) were collected in multi-collection mode, with $^{16}O^-$ and $^{18}O^-$ measured on off-axis Faraday cups and $^{17}O^-$ on the axial electron multiplier. To eliminate $^{16}OH^-$ interference on $^{17}O^-$ and optimize peak flatness, the EM slits were adjusted to achieve a mass resolving power of ~6000, resulting in negligible OH contribution (<0.1%). The Faraday cups operated at MRP ~2500. Each analysis lasted 260 s, including 60 s of pre-sputtering and 200 s of data acquisition. Instrumental mass fractionation (IMF) was defined using three terrestrial standards (San Carlos olivine, Ipanko spinel, and Rockport fayalite) and corrected for matrix effects in olivine. San Carlos olivine was reanalyzed every 10 measurements to monitor

19455100, 0, Downloaded from https://onlinelibrary.wiley.com/doi/10.1111/maps.70233 by Portland State University, Wiley Online Library on [06/11/2026]. See the Terms and Conditions (https://onlinelibrary.wiley.com/terms-and-conditions) on Wiley Online Library for rules of use; OA articles are governed by the applicable Creative Commons License

TABLE 2. Oxygen isotopic composition of xenoliths measured in this study.

	Host	Clast		$\delta^{18}O$ ‰	*SD.*	$\delta^{17}O$ ‰	*SD.*	$\Delta^{17}O$ ‰*	*SD.*
Laser fluorination			*mass (mg)*						
Los Vientos 200	CH3	"CI-like"	1.62	12.742	0.20	6.694	0.10	0.004	0.03
NWA 15116	LL3	Achondritic	1.97	4.822	0.20	2.881	0.10	0.349	0.03
NWA 16109	LL3	H3	2.01	5.232	0.20	3.037	0.10	0.290	0.03
SIMS			*Analyzed mineral*						
Bholghati	Howardite	C2-ung	Fine-grained matrix	19.94	0.10	13.67	0.524	3.20	0.72
Bholghati	Howardite	C2-ung	Fine-grained matrix	23.36	0.90	13.08	0.550	0.82	0.72
Bholghati	Howardite	C2-ung	Fine-grained matrix	17.42	0.90	12.13	0.531	2.98	0.71
Bholghati	Howardite	C2-ung	Fine-grained matrix	17.91	0.85	11.56	0.554	2.15	0.71
GRO 06054	LL3.1	Graphite-rich	Olivine	8.79	0.66	4.96	0.394	0.35	0.52
GRO 06054	LL3.1	Graphite-rich	Olivine	8.31	0.63	4.57	0.238	0.21	0.41
GRO 06054	LL3.1	Graphite-rich	Olivine	8.88	0.62	4.62	0.344	−0.04	0.47
NWA 11490	Howardite	CM2	Olivine	−4.37	1.05	−8.92	0.395	−6.63	0.67
NWA 11490	Howardite	CM2	Olivine	−3.91	0.86	−8.34	0.331	−6.28	0.56
NWA 11490	Howardite	CM2	Olivine	−5.08	0.83	−8.58	0.332	−5.91	0.54
NWA 11490	Howardite	CM2	Olivine	−4.22	0.85	−8.76	0.352	−6.54	0.57
NWA 13143	Howardite	CM2	Olivine	−4.49	1.09	−8.25	0.439	−5.89	0.72
NWA 13143	Howardite	CM2	Olivine	−1.71	1.06	−5.85	0.471	−4.96	0.73
NWA 13143	Howardite	CM2	Olivine	−4.28	1.02	−8.06	0.372	−5.82	0.65
NWA 13143	Howardite	CM2	Olivine	−2.74	1.10	−6.96	0.388	−5.52	0.69
NWA 13143	Howardite	CM2	Olivine	−2.34	0.81	−4.65	0.453	−3.42	0.62
NWA 13143	Howardite	CM2	Olivine	−1.75	0.92	−4.16	0.322	−3.24	0.58
NWA 13143	Howardite	CM2	Olivine	−4.14	0.88	−7.91	0.398	−5.74	0.61
NWA 13271	LL3.15	R or LL	Olivine	9.30	0.90	5.90	0.350	1.02	0.59
NWA 14826	LL3	Achondritic	Olivine	6.53	0.94	4.33	0.542	0.91	0.73
NWA 14826	LL3	Achondritic	Olivine	6.61	1.04	4.98	0.586	1.51	0.80
NWA 14826	LL3	Achondritic	Olivine	10.85	1.04	5.89	0.532	0.19	0.76
NWA 14826	LL3	Achondritic	Olivine	8.37	1.03	5.95	0.541	1.56	0.76
NWA 14826	LL3	Achondritic	Olivine	7.45	0.89	5.66	0.529	1.75	0.70
NWA 14826	LL3	Achondritic	Olivine	10.07	0.94	6.51	0.556	1.23	0.74

*$\Delta^{17}O = \delta^{17}O - 0.525 \times \delta^{18}O$.

instrumental drift. Typical 2σ uncertainties are ~0.9‰ for $\delta^{18}O$, ~0.4‰ for $\delta^{17}O$, and ~0.7‰ for $\Delta^{17}O$, with $\Delta^{17}O$ uncertainties calculated by quadratic error propagation of $\delta^{17}O$ and $\delta^{18}O$. The oxygen isotopic compositions determined by SIMS were calibrated against a San Carlos olivine standard as no standards for serpentine-group minerals were available. Matrix effects between olivine and serpentine-group phyllosilicates produce isotopic shifts of up to about +3‰ and −1‰ (Scicchitano et al., 2018). Although these offsets exceed the analytical precision, they remain small compared to the isotopic variations observed in chondrites and are mass-dependent, thus not affecting the $\Delta^{17}O$ values reported in this study.

REVIEW OF XENOLITHIC CLASTS DESCRIBED IN THE LITERATURE

There is ample literature on meteorite breccias, with several comprehensive reviews (e.g., Bischoff et al., 2006, 2018; Bridges & Hutchison, 1997; Keil, 1982), including some specifically on xenoliths (e.g., Goodrich et al., 2021; Wilkening, 1977). Our own critical review of macroscopic xenoliths described in the literature is given in Table S3. It is based on the existing reviews (Bischoff et al., 2006; Briani et al., 2012; Goodrich et al., 2021), with an update based on papers describing new xenoliths or reanalyzing previously described xenoliths (e.g., Alevy et al., 2025; Kerraouch et al., 2021; Patzek et al., 2018, 2020).

We did not include most chondritic xenoliths much smaller than a millimeter, that are more analogous to micrometeorites (see, e.g., Briani et al., 2012). This small size prevents obtaining a representative petrographic characterization and bulk chemical composition or oxygen isotopic composition of the clast, information that would allow a reliable comparison with the established meteorite groups. For instance, microxenoliths in H chondrites were found to have affinities with CR2 or CM2 chondrites based on their matrix properties (Briani et al., 2012), but a strict attribution to these two meteorite groups is tentative

19455100, 0, Downloaded from https://onlinelibrary.wiley.com/doi/10.1111/maps.70233 by Portland State University, Wiley Online Library on [06/11/2026]. See the Terms and Conditions (https://onlinelibrary.wiley.com/terms-and-conditions) on Wiley Online Library for rules of use; OA articles are governed by the applicable Creative Commons License

based on the absence of other petrographic evidence (matrix abundance, chondrule size, etc). A hydrated carbonaceous chondrite microclast in Rumuruti chondrite NWA 6828 could not be matched with known meteorite groups (Greshake, 2014). These small xenoliths have been interpreted, at least in H chondrites, as samples from the zodiacal cloud (Briani et al., 2012; Gounelle et al., 2003), and they likely represent a different population of objects compared to meteorites. We did not include in our review the possible cometary microxenolith described in LAP 02342 CR2 chondrite (Nittler et al., 2019). We also did not include possibly xenolithic material observed only in the form individual components such as chondrule or CAIs (unless these are found in achondrites) or mineral fragments, as opposed to lithic clasts. For instance, the components possibly originating from enstatite, ordinary and carbonaceous chondrite described in ALH 85085 CH3 (Kimura & El Goresy, 1989) are not included in our review. Similarly, we did not include the exotic mineral clasts likely originating from ordinary and enstatite chondrites described in Nilpena and North Haig polymict ureilites (Prinz et al., 1986). We did not include xenoliths that are only briefly mentioned in abstracts with any details, like a supposedly LL chondrite xenolith in Tanezrouft 039 L3 chondrite (Funk et al., 2011).

We include in our review only clasts that can be convincingly interpreted as xenoliths. For chondritic xenoliths, this is usually based on petrographic observations like the nature of the interchondrule matrix, the opaque mineralogy, the overall texture, and in some cases on oxygen isotopic composition. For igneous clasts in chondrites, the xenolithic nature is usually difficult to prove based on mineralogy and texture only, because such clasts may have been be formed on the same chondritic parent body by partial or total melting by large-scale internal heating or by smaller scale impact heating (see discussion in, e.g., Goodrich et al., 2021). In particular, we do not include the many igneous clasts that have been shown to be macrochondrules or to derive from melting of material from the same parent body as the host lithology with a variable degree of fractionation (e.g., Ruzicka et al., 2019). We also excluded igneous clasts whose xenolithic nature was not convincingly proven. For instance, a melt rock clast in Bovedy whose H parentage was proposed but not firmly established (Rubin et al., 1981) is not considered as a xenolith. However, based on mineral chemistry, bulk chemistry, and/or oxygen isotopic composition (e.g., Bischoff et al., 2018), a few igneous clasts have been demonstrated to be xenolithic, and are therefore listed in Table S3. Small and well-studied achondritic xenoliths, like the 70 μm-sized achondritic pyroxene clast described in NWA 12651 CM2 chondrite (Ebert et al., 2019), have been included in the present review. Indeed, despite their small size and almost monomineralic nature, their geochemical and oxygen isotopic signatures allows establishing their xenolithic nature. The majority of igneous xenoliths in chondrites are found in ordinary chondrites and derive from another ordinary chondrite group.

A few clasts described as xenoliths in the literature have been reinterpreted and are not listed in Table S3. For instance, in the absence of oxygen isotopic composition data, the xenolithic nature of the matrix-rich clasts found in Krymka (Grossman et al., 1980; Semenenko et al., 2001) is not considered here as demonstrated. A dark clast in Bencubbin CBa, originally interpreted as a carbonaceous xenolith (Lovering, 1962; McCall, 1968), was later interpreted as a matrix lump (Weisberg et al., 1990). Cognate clasts, even if they have suffered intense thermal processing like the granoblastic clast described in Murchison, originally attributed to the R group (Isa et al., 2014), but later described as the result of metasomatism within the CM parent body (Kerraouch et al., 2019), are not considered xenoliths either. A 3×4 cm^2 clast originally interpreted as a H melt rock xenolith in MET 01004 LL5 chondrite (Corrigan et al., 2015) is not considered in our review as the classification of the host meteorite has been questioned, and it may need to be reclassified as a H chondrite (Corrigan & Lunning, 2016).

We also did not consider as xenoliths the matrix-rich dark inclusions that are found in almost all chondrite groups: CO3 chondrites (Itoh & Tomeoka, 2003), $CV_{Ox}3$ and $CV_{Red}3$ chondrites (e.g., Buchanan et al., 1997; Johnson et al., 1990; Krot et al., 1999), CK chondrites (e.g., Chaumard et al., 2014), and ordinary chondrites (Ikeda et al., 1981). They are most likely formed from similar material as their host meteorite (Ikeda et al., 1981; Itoh & Tomeoka, 2003). These inclusions have experienced aqueous alteration and/or thermal processing, and some authors have suggested that they may have been affected by nebular processes before being accreted (e.g., Johnson et al., 1990), although this view is debated (e.g., Itoh & Tomeoka, 2003; Krot et al., 1999). These inclusions are better referred to as fine-grained matrix-rich cognate inclusions (e.g., Bischoff et al., 2006). Like chondrules, CAIs, metal grains, and other chondrite constituents, these inclusions are part of the initial microconglomeratic assemblage that we call chondrite. As such, they lie beyond the scope of our study and are not discussed in further details. For instance, in the absence of oxygen isotopic composition measurements, we do not consider that the dark clasts reported as carbonaceous xenoliths in Supuhee (Leitch & Grossman, 1977), or Dimmitt (Rubin et al., 1983) are xenoliths since their petrographic description is compatible they being matrix-rich cognate inclusions.

19455100, 0, Downloaded from https://onlinelibrary.wiley.com/doi/10.1111/maps.70233 by Portland State University, Wiley Online Library on [06/11/2026]. See the Terms and Conditions (https://onlinelibrary.wiley.com/terms-and-conditions) on Wiley Online Library for rules of use; OA articles are governed by the applicable Creative Commons License

Dark inclusions have been described in many CR2 chondrites (Endress et al., 1994; Lee et al., 2025; van Kooten et al., 2024; Weisberg et al., 1991). Their nature is discussed in more detail in section §4.6. Indeed, the oxygen isotopic composition of dark inclusions in CR2 chondrites indicates that they may have originated from a different precursor material than their host (Endress et al., 1994; van Kooten et al., 2024) and, therefore, be true xenoliths, although they seem to have been incorporated during the initial accretion (Endress et al., 1994; Patzek et al., 2018).

CH and CB chondrites are a particular case because of their peculiar accretion style compared to other chondrites, from recondensation of an impact plume and admixture of an impactor component (e.g., Krot et al., 2005; Wölfer et al., 2023). Therefore, the CI-like clasts in CH chondrites are true xenoliths, although they accreted together with the other components forming the host rock (see discussion in Patzek et al., 2018). Therefore, they were considered in the present review.

In some cases, we reconsidered the classification of the xenoliths. For instance, the H3 xenolith described in Weatherford CBa chondrite is better described as an ungrouped type 3 ordinary chondrite in view of its oxygen isotopic composition (Prinz et al., 1993) that is identical, for example, to the oxygen isotopic composition of the lithology B described in the ungrouped type 3 ordinary chondrite NWA 5717 (Bunch et al., 2010).

Because the reduced and oxidized CV groups have been proposed to originate from two distinct parent bodies (Gattacceca et al., 2020), we included Vigarano CV_{Red} as a xenolith-bearing meteorite since it contains clasts of CV_{Ox} material (Krot et al., 2000). Brecciated CV chondrites containing CV_{OxA} and CV_{OxB} material are not included, as these two subgroups are interpreted as variably metamorphosed material from the same parent body (e.g., Gattacceca et al., 2020). We included Camel Donga 003, a CK3 chondrite that contains $CV_{Ox}3$ lithologies (Alevy et al., 2025).

Xenoliths with igneous textures have been described in ordinary chondrites, and in the CM2 carbonaceous chondrite NWA 12651 (Ebert et al., 2019). Although many ordinary chondrites contain igneous inclusions (e.g., Ruzicka et al., 1998, 2019), there are only very few xenoliths in ordinary chondrites that are igneous rock with non-chondritic bulk composition formed by crystallization from a differentiated melt on another parent body (see Goodrich et al., 2021). Only five have been described so far, all originating from the NC reservoir. Three of them originate from a non-ordinary chondrite parent body: two in Parnallee and one in Villalbeto de la Peña. A well-characterized differentiated xenolith of LL parentage has been described in Study Butte H3-6 chondrite (Fredriksson et al., 1989; Sokol et al., 2007). A ≥ 20 cm^3 differentiated xenolith has been recently described in Hassi el Madani 002 (Agee et al., 2024). Although this meteorite is classified as an ungrouped achondrite, the host lithology has all the characteristics of a L-melt rock. Although originally proposed to originate from Mars (Agee et al., 2024), the clast has been later interpreted as coming from another large differentiated body (Kruijer et al., 2025). Its oxygen isotopic composition (Agee et al., 2024) point to an origin from an ungrouped ordinary parent body. The other xenoliths with igneous textures found in ordinary chondrites have retained a chondritic composition, and have been shown to originate from another ordinary chondrite parent body. Such occurrences have been described in NWA 092, NWA 8645, Farmington, Barwell, MET 01004, Ngawi, Parnallee, and Paragould. There are additional occurrences, not included in this review, of igneous non-fractionated clasts in ordinary chondrites for which the parent body and therefore the xenolithic nature cannot be established with certainty, usually by lack of oxygen isotopic composition data.

We do not include in our review and discussion the exceptional case of Kaidun that has been extensively documented elsewhere. Kaidun consists of millimeter-sized fragments of EH, EL, CV, CM, and R chondrites, as well as other exotic components, so that it is difficult to define a host lithology (e.g., Zolensky & Ivanov, 2003).

Our literature review comprises 89 xenolith-bearing meteorites (Table S3). Xenoliths have been reported in howardites and polymict eucrites, aubrites, ureilites, all ordinary chondrite groups, and in some carbonaceous chondrite groups (CV, CM, CH, CB). The vast majority of these xenoliths are clasts of carbonaceous chondrites, and are categorized as "CI-like," "CR-like," or "CM-like." It is noteworthy that the affinities comparison with CI or CM is based mostly on the clast texture (quasi-absence vs presence of significant amounts of anhydrous silicates in "CI-like" and "CM-like" clasts, respectively). Eight occurrences of graphite-bearing clasts are described (e.g., Storz et al., 2021). In some cases, the oxygen isotopic composition of the chondritic xenoliths has been measured to ground their attribution to a specific chondrite group (Table S4). This includes "CI-like" clasts in Sahara 98645 H3 chondrite (Bischoff et al., 2018), PAT 91546 CH3 (Weisberg et al., 1995), and polymict ureilites (Clayton & Mayeda, 1988; Patzek et al., 2025), CM2-like clasts in HED achondrites (Patzek et al., 2025; Van Drongelen et al., 2016), carbonaceous clast in Zag H3-5 (Kebukawa et al., 2019) and Plainview H5 (Clayton & Mayeda, 1978), and ordinary chondrite-related clasts in Bencubbin CBa (Clayton & Mayeda, 1978), Cumberland Falls aubrite (Clayton & Mayeda, 1978), Weatherford (Prinz et al., 1993) and NWA 7531 C-ung (Bunch et al., 2013). In view of their abundance and variety, xenoliths

19455100, 0, Downloaded from https://onlinelibrary.wiley.com/doi/10.1111/maps.70233 by Portland State University, Wiley Online Library on [06/11/2026]. See the Terms and Conditions (https://onlinelibrary.wiley.com/terms-and-conditions) on Wiley Online Library for rules of use; OA articles are governed by the applicable Creative Commons License

in polymict ureilites have been the focus of detailed oxygen isotopic studies (Downes et al., 2008; Ikeda et al., 2003; Kita et al., 2003; Patzek et al., 2025).

NEW SURVEY OF XENOLITHS IN METEORITES

Introduction

In this survey, we did not actively look for xenoliths much smaller than ~1 mm that are more analogous to micrometeorites (see, e.g., Briani et al., 2012). We restricted our study to larger lithic xenoliths that can be more readily compared to the established meteorite groups. However, we included a few xenolithic clasts smaller than this 1 mm threshold when they consisted of lithic clasts whose petrography could be compared to meteorites.

One of the difficulties of such survey is the choice of a priori criteria for studying a clast that may be a xenolith. Our survey is likely biased toward dark clasts that are easy to distinguish by optical observations of slices, polished sections, and thin sections. However, most of these dark clasts are not xenoliths (e.g., Lee et al., 2025). In chondrites, a large proportion of dark clasts are shock-darkened or melt rock material belonging to the same group. Melt rock clasts can be identified by their microporphyritic texture, mineral composition close to that of equilibrated members of the same group, and chondritic bulk composition. We observed such melt rock clasts in, for example, Catalina 456, Chug Chug 092, Great Sand Sea 008, NWA 7965, NWA 12290, NWA 13145, NWA 13152, NWA 14102, and NWA 16035. Shock-darkened clasts can be identified by the presence of opaque veinlets, and μm-sized opaque inclusions in silicates. We observed shock-darkened clasts in, for example, Adzhi-Bogdo, NWA 6135, Sahara 97210, and Wells. Microbrecciated inclusions that contain a fine-grained clastic matrix can also be misleading at macroscopic scale and reminiscent of fine-grained matrix-rich xenoliths. But their mineral chemistry, texture, and matrix composition allows distinguishing them from xenoliths containing pristine fine-grained matrix. We observed dark matrix-rich inclusions in many L3 and LL3 chondrites, and in several $CV_{Red}3$ chondrites, but as discussed above, these are not xenoliths and are better called fine-grained matrix-rich cognate inclusions (Bischoff et al., 2006). The nature of the dark inclusions in CR2 chondrites is discussed below in more detail.

Among light-colored clasts, a number of clasts with igneous textures were observed in ordinary chondrites. In most cases, their mineralogy, mineral chemistry, and/or bulk composition indicate that they are large chondrule fragments, or the result of crystallization of an impact melt from the same parent body as their host (Goodrich et al., 2021; Ruzicka et al., 2019). We observed this type of igneous clast in, for example, GRO 06054, NWA 17170. Cognate clasts, that are simply clasts of a different petrologic type as the host lithology can also be misleading. They are particularly abundant in Rumuruti and CK3 chondrites. For example, we investigated the large (up to 3 cm) dark gray inclusions described in the initial declaration of Tanezrouft 057 CK4, and concluded that they are metamorphosed matrix-rich cognate clasts. Even in a relatively simple case like howardites and polymict eucrites, where numerous dark carbonaceous chondrite xenoliths have already been described, the occurrence of dark clasts of shocked eucrite and diogenite lithologies is also common and can be misleading during a macroscopic survey (e.g., in Bununu howardite).

Eventually, this study reports new xenoliths from 18 meteorites, some of them containing different types of xenoliths (Table 1). Except for the xenoliths in Bholghati, all reported xenoliths are from meteorites that were never studied before for that purpose. The macroscopic observation of the 118 slices (4900 cm^2) from the MNHN collection revealed only one meteorite containing xenoliths: Bholghati howardite in which xenoliths had already been described in details (Buchanan et al., 1993; Zolensky et al., 1996). Unusual clasts observed during this survey are the centimeter-sized metal-deprived clast in Sahara 97158 (EH3), and the centimeter-sized matrix-dominated clast in DaG 417 (R3-4), described below. The survey of the 377 polished sections (560 cm^2) from the CEREGE collection revealed eight meteorites containing xenoliths. Nine xenolith-bearing meteorites selected from other meteorite collections were also studied. We report below only a relatively short petrographic description of these clasts, the aim of this study not being to provide a detailed description of each xenolith and discuss their petrogenesis, but rather to reach a statistical significance in terms of numbers of xenoliths. Note that although in some cases, the xenolithic nature of the clasts is trivial (e.g., chondritic clasts in howardites), in other cases, the interpretation as xenolith requires a longer demonstration.

Xenoliths in Howardite and Polymict Eucrites

We report 36 carbonaceous chondrite xenoliths in six howardites and polymict eucrites in which they had not been described previously (NWA 10472, NWA 11490, NWA 13143, NWA 14804, NWA 14981, NWA 17470), and in Bholghati howardite whose clasts have already been extensively studied (Buchanan et al., 1993; Zolensky et al., 1996). These xenoliths are up to several millimeter in size (Figure 1a). The contact between the clasts and the host is sharp, with no dust rim around the clast

19455100, 0, Downloaded from https://onlinelibrary.wiley.com/doi/10.1111/maps.70233 by Portland State University, Wiley Online Library on [06/11/2026]. See the Terms and Conditions (https://onlinelibrary.wiley.com/terms-and-conditions) on Wiley Online Library for rules of use; OA articles are governed by the applicable Creative Commons License

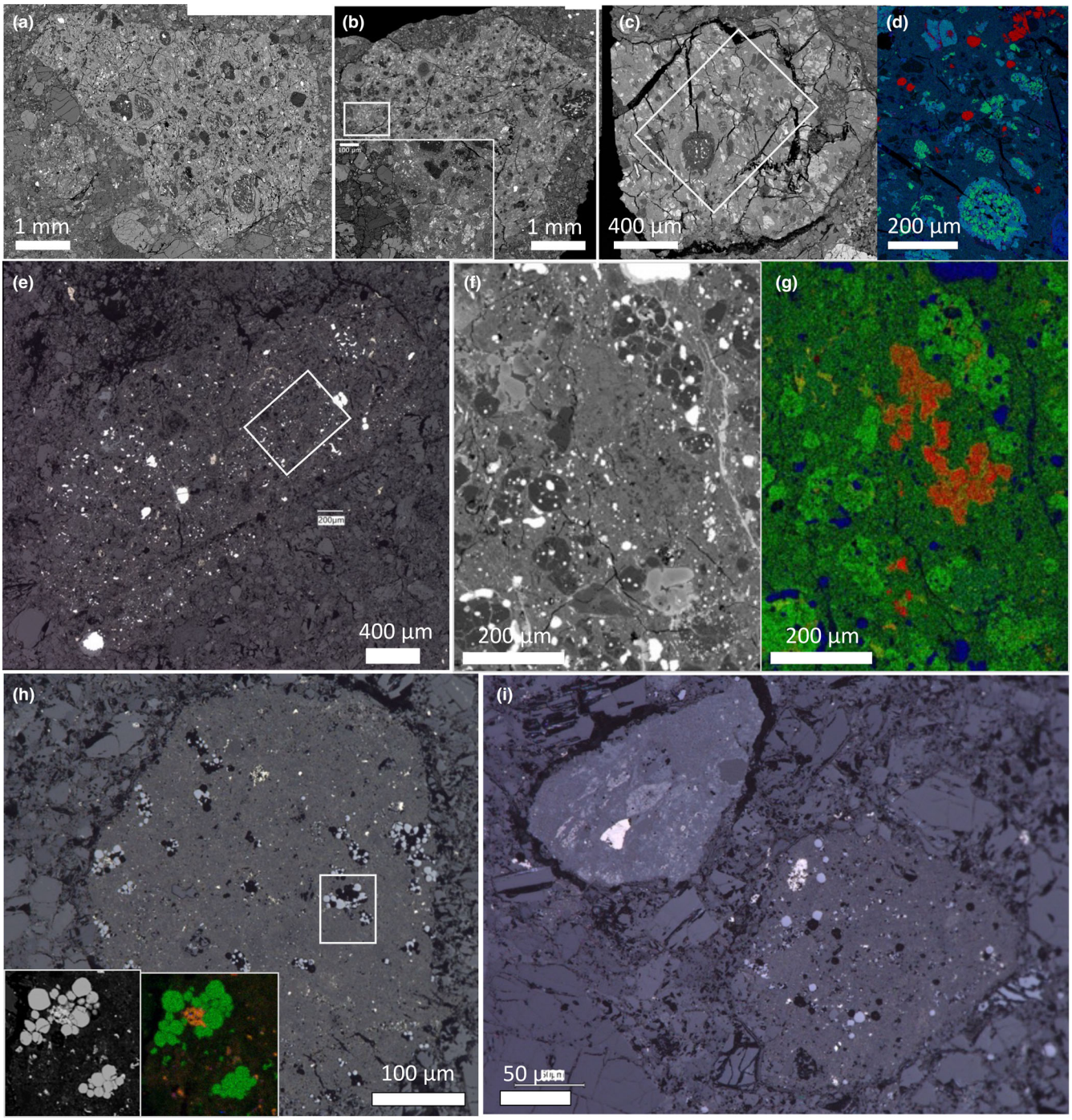


FIGURE 1. Xenoliths in howardites and polymict eucrites. (a) CM2 xenolith in NWA 11490 (BSE image). (b) CM2 xenolith in NWA 13143 (BSE image). The inset shows the sharp contact between the xenolith and the host lithology. (c) CM2 clast in Bholghati (clast Bholghati#1, BSE image). The inset is shown in panel (d). (d) RGB composite image (R=Ca, G=Mg, B=Si) evidencing carbonates in red. (e) CO3 xenolith in NWA 17470 (reflected light image). The inset is shown in panels (f) (BSE image) and (g) (RGB composite image (R=Al, G=Si, B=Fe) evidencing a CAI in red). (h) Magnetite-rich clast in Bholghati (clast Bholghati#5, reflected light). The inset shows a BSE image and a RGB composite image (R=S, G=Fe, B=Ni) highlighting the magnetite crystals in green and troilite in orange. (i) Two different types of xenoliths coexisting in Bholghati (clasts Bholghati#6 and #7, reflected light image).

19455100, 0, Downloaded from https://onlinelibrary.wiley.com/doi/10.1111/maps.70233 by Portland State University, Wiley Online Library on [06/11/2026]. See the Terms and Conditions (https://onlinelibrary.wiley.com/terms-and-conditions) on Wiley Online Library for rules of use; OA articles are governed by the applicable Creative Commons License

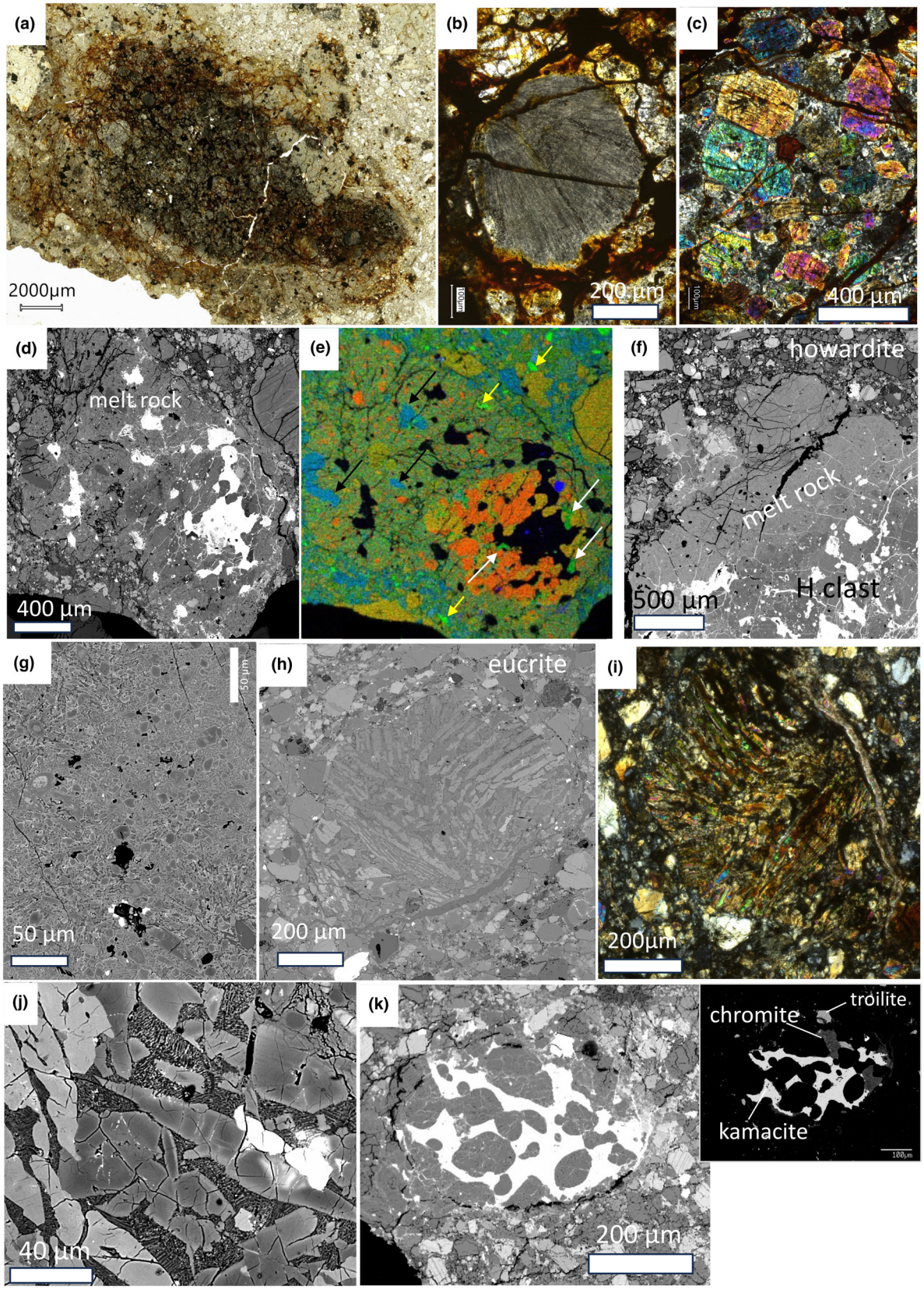
(Figure 1b). Their shape varies from subangular (Figure 1a) to subrounded (Figure S1a,b). In some meteorites, several clasts can be found in the same meteorite over centimeter scale. Most of these carbonaceous chondrite clasts (31 out of 36 studied carbonaceous clasts) are similar to the CM2-like clasts of Zolensky et al. (1996). In fact, they share many similarities with CM2 chondrites: overall texture with abundant and often foliated fine-grained matrix (Figure 1a–c), mineralogy including the presence of calcium carbonates (Figure 1d), tochilinite–cronstedtite intergrowths (TCI), magnetite, and only rare metal found as kamacite encased within the anhydrous silicates (Figure S1a,b). These 31 CM2-like clasts represent 5.5 vol% of the observed polished sections. The average fine-grained matrix abundance of the clasts is 80 vol%, with a narrow range of 78–81 vol%. The relatively few intact chondrules have an average apparent diameter of 208 ± 104 μm (n = 43). For estimating chondrule diameter, we selected only circular objects. In fact, as noted by Zolensky et al. (1996), the CM2-like clasts contain small (<200 μm) porphyritic objects that are not circular and do not qualify as microchondrules. Chondrules, as well as chondrule fragments and mineral clasts, show fine-grained dust rims with thickness in the 10 to 40 μm range. The olivine composition shows a pronounced peak around Fa_1. The defocused EPMA analyses of matrix yield FeO content in the total 20–32 wt% range, and totals in the 77–89 wt% range. In situ oxygen isotopic analyses by SIMS of anhydrous silicates in two of these clasts in NWA 11490 and NWA 13143 give a composition that is in the range of similar analyses in chondrules of CV, CO, and CM, and different from chondrules of OC, EC, and CR chondrites (Marrocchi et al., 2024), but these data are not very diagnostic to link the clasts to a specific chondrite group. However, these clasts have all the petrographic and mineralogical characteristics of CM2 chondrites and can be safely classified as such.

A small number of carbonaceous chondrite clasts in the studied HED meteorites are not CM2 clasts. In addition to two CM2 clasts, NWA 17470 contains a 3.6 mm^2 chondritic xenolith with 7 vol% metal (Figure 1e), an average apparent chondrule diameter of 154 ± 45 μm (n = 5), relatively abundant calcium–aluminum-rich inclusions (CAIs, Figure 1f,g), and 58 vol% of fine-grained matrix. We assign this clast to the CO3 group based on its mineralogy and texture. The Cr_2O_3 content of ferroan olivine is 0.316 ± 0.108 wt% (n = 34), similar to Colony and Yamato 81020 and indicative of a petrologic type of 3.05 (Grossman & Brearley, 2005).

In Bholghati, in addition to six CM2-like clasts (Figure 1c), we observed four clasts (our Bholghati clasts #5-7-10-11) that have a markedly different texture and mineralogy. These clasts, that make up 0.25 mm^2 of the observed section, consist mostly of fine-grained matrix (92 vol%), and do not contain chondrules (Figure 1h). The defocused EPMA of the matrix yielded totals of 84.4 ± 2.5 wt% (n = 30), indicating the presence of hydrous phases. These clasts contain anhydrous olivine crystals with $Fa_{1\text{-}2}$, aggregates of magnetite dodecahedron 5–12 μm in size. Ni-rich (pentlandite) and Ni-poor (troilite) sulfides are found as grains up to 5 μm in size forming composite aggregates up to 20 μm (Figure 1h). Carbonates are present with grain size up to 15 μm. Their chemical composition is in the calcite/aragonite range (Table S10). The composition is Fe-, Mg-, and Mn-poor, significantly different from that of carbonates in CI1 chondrites that contain mostly dolomite and magnesite (see, e.g., Gattacceca et al., 2025, and fig. 5 in Patzek et al., 2018). Metal is absent. The presence of both aqueous alteration phases and anhydrous silicates indicates that these clasts are of petrologic type 2. Their matrix is particularly iron-poor with only 20.1 ± 2.0 wt% FeO (n = 30), compared to 33.3 ± 2.6 wt% FeO (n = 5) in the CM2-like clasts and 30–40 wt% in CR2 chondrites. The complete absence of metal also advocates against a CR2 classification. The EPMA totals of the matrix (84.4 ± 2.5 wt%, n = 30) are much higher than the 76.4 ± 5.9 wt% average of totals in the matrix of CI1 chondrites computed using average data from McSween and Richardson (1977), Zolensky et al. (1993) and Gattacceca et al. (2025) for Alais, Ivuna, Orgueil, and Oued Chebeika 002. The EPMA totals of the clast matrix are more in the range observed in CM2 and CR2 chondrites, although some aqueously altered type 3 chondrites, such as CO3 and CV3, can have totals in this range (see review of carbonaceous chondrite matrix analyses by Krämer Ruggiu et al., 2022, their fig. 11, or by Ebert et al., 2018, their figure 19). We assign a petrologic type 2 to these clasts, based on the low EPMA totals of the matrix and the composition of low-Ni sulfides. The oxygen isotopic composition of the matrix of clast #5, determined by in situ SIMS analyses, is close to the CI1 meteorite cluster, but significantly different (Figure 11). We classify these two clasts as ungrouped C2 chondrites, with possible affinities with CI chondrites. It is noteworthy that these ungrouped C2 clasts can be found in close proximity with CM2 clasts, down to 50-μm distance (Figure 1i).

We observed equilibrated chondrite lithic clasts in NWA 3197 howardite, and NWA 10674 polymict eucrite (Figure 2). The clast in NWA 3197 contains chondrules of various types: barred olivine, radial pyroxene, and porphyritic olivine (Figure 2a–c). The clast in NWA 10674 contains a single highly recrystallized chondrule with an apparent diameter of 830 μm (Figure 2d,e). The

19455100, 0, Downloaded from https://onlinelibrary.wiley.com/doi/10.1111/maps.70233 by Portland State University, Wiley Online Library on [06/11/2026]. See the Terms and Conditions (https://onlinelibrary.wiley.com/terms-and-conditions) on Wiley Online Library for rules of use; OA articles are governed by the applicable Creative Commons License



19455100, 0, Downloaded from https://onlinelibrary.wiley.com/doi/10.1111/maps.70233 by Portland State University, Wiley Online Library on [06/11/2026]. See the Terms and Conditions (https://onlinelibrary.wiley.com/terms-and-conditions) on Wiley Online Library for rules of use; OA articles are governed by the applicable Creative Commons License

FIGURE 2. Xenoliths in howardites and polymict eucrites. (a) H xenolith in NWA 3197 howardite (plane polarized transmitted light image). The clast is made of a chondrite core mantled by melt rock. (b) Radial pyroxene chondrule in the clast of NWA 3197 (plane polarized transmitted light image). (c) Shock features in a porphyritic olivine chondrule in the clast of NWA 3197 (crossed polarized transmitted light image). (d, e) H xenolith in NWA 10674 polymict eucrite (BSE image and RGB composite image with R=Mg, G=Si, B=Ca highlighting olivine in orange, anorthositic plagioclase in blue (in the host eucrite and the melt rock, black arrows), albitic plagioclase in dark green (in the chondrule, white arrows), silica in bright green (in the host eucrite and melt rock, yellow arrow), and pyroxene in light brown). (f) Contact between the H clast and the howardite host in NWA 3197 (BSE image). (g) Melt rock clast in NWA 10674 (BSE image). This clast is not xenolithic (see text). (h–j) Chondrule in NWA 17597 eucrite: BSE image, cross-polarized transmitted light image, and BSE image of the devitrified mesostasis. (k) Pallasite clast in NWA 10472 (BSE image). The inset has contrast adjusted to reveal the opaque mineralogy.

clasts in both meteorites have silicate composition in the H range (Table 1). The opaque mineralogy consists of metal (mostly kamacite, but taenite is present) and troilite. In NWA 3197, the metal abundance in the clast is 8.0 vol%. The clast in NWA 10674 is too small and weathered to allow a robust estimate of the metal abundance, but it is at least several vol%. The average apparent chondrule size in NWA 3197 (483 ± 144 μm, n = 12) is in the range observed in H chondrites. We classify these clasts as H chondrites. Although their petrologic type is difficult to ascertain because of the intense shock effects (see below), the absence of interchondrule plagioclase in the clast of NWA 3197 suggests a petrologic type 4. In NWA 10674, the chondrule is equilibrated and the presence of albitic plagioclase with a grain size of ~70 μm in the chondrule (Figure 2e) suggests a petrologic type 6. In both meteorites, the clasts show evidence of strong shock: undulatory extinction, planar fractures, planar deformation features and mosaicism in olivine (Figure 2c), and the presence of melt pockets with eutectic mixtures of metal and troilite. Evidence for strong shock in the clast of NWA 3197 is also indicated by the mantling of the clast by a millimeter-thick rim of chondritic melt rock penetrated by opaque veinlets (Figure 2f). However, the contact between the clast and the host howardite is sharp and does not show evidence for high-speed collision. NWA 10674 also contains numerous microporphyritic clasts, up to 3 cm across, making up about 10 vol% of the studied thin section. These clasts have a grain size of about 10 μm and slightly zoned silicates, a texture typical of melt rocks (Figure 2g). They contain 7 vol% metal on average (both kamacite and taenite) and have olivine composition $Fa_{14.4–16.7}$ (FeO/MnO = 31–38, n = 2), in the range of equilibrated H chondrites. However, these melt rock clasts contain relict exsolved pyroxene, silica polymorph grains, and Ca-rich plagioclase with composition An_{80-87}. We interpret these clasts as eucrite melt rock clasts that have incorporated exogenous metal. The H chondrite clast in NWA 10674 is itself mantled by a 1-mm thick layer of similar eucrite melt rock (Figure 2d).

We observed a single composite barred olivine chondrule in NWA 17597 howardite (Figure 2h). The chondrule is highly shocked, with olivine showing mosaicism (Figure 2i). It is unequilibrated and has devitrified mesostasis (Figure 2j). It contains chromite, troilite, and Fe,Ni metal. Although it is a single chondrule, its apparent diameter (738 μm), olivine and low-Ca pyroxene composition (average $Fa_{33.8}$ and $Fs_{22.1}Wo_{2.3}$) and mineralogy suggest it may originate from an unequilibrated ordinary chondrite, possibly L chondrite.

In NWA 10472 howardite, in addition to CM2 clasts, we observed a clast with 100 μm-sized rounded olivine set in a Fe,Ni metal network making 22 vol% of the clast (Figure 2k). Chromite and troilite are also present. Olivine has composition $Fa_{9.1\pm0.2}$, Fe/Mn = 43.7 ± 2.5 (n = 17). Kamacite has 4.81 ± 0.11 wt% Ni and 0.63 ± 0.02 wt% Co (n = 4). A single chromite analysis yielded Cr/(Cr + Al) = 0.83 and Fe/(Fe + Mg) = 0.76. Although the grain size is small compared to usual main group pallasites, we interpret this clast as a pallasite xenolith based on its texture, mineralogy, and mineral chemistry.

Xenoliths in Polymict Ureilites

We report carbonaceous chondrite xenoliths in two polymict ureilites: NWA 14086 and NWA 16454. These two meteorites contain dozens of chondritic clasts each (Figure S2). The clasts are usually small, with longest dimensions about 250 μm, but the largest ones have a surface of 0.35 mm^2 and 0.55 mm^2 in NWA 14086 and NWA 16454, respectively. In both studied meteorite sections, the xenoliths amount to over 1 mm^2 of material. The clast shapes range from subangular (Figure S2a) to subrounded (Figure S2b). They consist mostly of fine-grained matrix that yields low EPMA total in the 82–86 wt% range and contain abundant opaque minerals: magnetite (including framboids) and pyrrhotite. These clasts are referred to as "CI1-like" based on their texture, mineralogy, and similarity with CI1-like clasts found in other polymict ureilites.

19455100, 0, Downloaded from https://onlinelibrary.wiley.com/doi/10.1111/maps.70233 by Portland State University, Wiley Online Library on [06/11/2026]. See the Terms and Conditions (https://onlinelibrary.wiley.com/terms-and-conditions) on Wiley Online Library for rules of use; OA articles are governed by the applicable Creative Commons License

Xenoliths in CH3 Chondrites

Los Vientos 200 (CH3) contain numerous (>10 per cm^2) rounded carbonaceous chondritic xenoliths mostly in the 100–200 μm range (Figure S3a). They represent about 0.5 mm^2 in the studied section. The clasts are made mostly of fine-grained phyllosilicate-rich matrix containing abundant iron sulfides in the form of elongated laths, and abundant magnetite in the form of platelets, spheroids, and framboid (Figure S3b,c). One clast shows indentation by a euhedral enstatite crystal from the host lithology (Figure S3d). A larger clast, 1.3 × 0.8 mm in size, visible on the cut surface of the meteorite was sampled for measurements of oxygen isotopic composition and X-ray diffraction analyses. Due to the small amount of material, the sample was not finely grinded but in the form of grains several tens of μm in size, making the interpretation of X-ray diffraction patterns qualitative. However, the X-ray data clearly indicate the dominance of serpentine, magnetite, pyrrhotite, and possibly smectite (broad peak at ~13 Å). The oxygen isotopic composition measured for a 1.62 mg bulk sample of the same large clast is ($\delta^{18}O$ = 12.742‰, $\delta^{17}O$ = 6.694‰, $\Delta^{17}O$ = 0.004‰). Although it is closer to CI1 material than from other chondrite groups, it lies significantly outside of the CI1/Bennu/Ryugu cluster, and plots in a relatively empty area of the $\Delta^{17}O$ versus $\delta^{18}O$ plot (Figure 11). It is noteworthy that Los Vientos 200 is virtually unweathered, with almost no traces of metal weathering, so that the oxygen composition of the clast is likely unaffected by terrestrial alteration.

Xenoliths in CM and CO Chondrites

NWA 17518, classified as a CM2 chondrite, contains two contrasted lithologies, separated by a relatively sharp and curvilinear contact (Figure 3a,b). The dominant lithology, at the scale of the studied polished section has 69 vol% matrix (determined by point counting, n = 467) and an apparent chondrule diameter of 310 ± 150 μm (n = 27). Its matrix contains abundant phyllosilicates and iron sulfides. Metal is rare. The second lithology has 51 vol% matrix and average apparent chondrule size 190 ± 90 μm (n = 13). It contains 4.4 vol% metal, as determined by point counting, and CAIs up to 200 μm in size (Figure 3c). No phyllosilicates are visible in the matrix. The texture of the matrix in the two lithologies is contrasted: foliated in the metal-poor lithology, homogeneous in the metal-rich lithology (Figure 3a). The two contrasted lithologies (metal-poor and metal-rich) have all the characteristics of CM2 and CO3 chondrites, respectively: chondrule size (although chondrule size has been recently questioned as a criterion to distinguish CO and CM, see Floyd et al., 2024), mineralogy, matrix abundance and mineralogy, and texture. The contact between the two lithologies is not reminiscent of the alteration fronts observed in some CM chondrites (e.g., Musolino et al., 2024). In any case, in situ alteration processes would not account for the difference in chondrule size and matrix abundance. Therefore, our interpretation is that NWA 17518 is a meteorite containing both CM2 and CO3 lithologies. The Cr_2O_3 content of 0.38 ± 0.14 (n = 6) in the ferroan olivine in the CO3 lithology suggests a petrographic subtype ~3.1 (Grossman & Brearley, 2005). The geometry of the contact alone, visible on the available polished section does not allow determining which lithology is the host and which one is the clast. X-ray tomography of a 1.36 g sample, showed metal-rich (CO3) and metal-poor (CM2) areas and evidenced an overall convex contact between the CM2 and the CO3 lithologies (Figure 3d). This suggests that the former may be the xenolith and the latter may be the host.

Because NWA 17518 has a low terrestrial weathering degree, magnetic susceptibility is a relevant petrographic proxy to estimate the relative abundance of CO3 and CM2 material. Indeed, although CM and CO chondrites to a lesser extent have a relatively wide range of magnetic susceptibility, they have contrasted average magnetic susceptibility (Rochette et al., 2008). The distribution of magnetic susceptibility measured on 50 samples of NWA 17518 shows a well-defined maximum $\chi = 4.52 \times 10^{-5}$ m^3/kg measured for seven samples totaling 15.5 g of material. This value can be taken as the magnetic susceptibility of the pure CO3 material. Similarly, the susceptibility of the pure CM2 material can be estimated to 9.3×10^{-6} m^3/kg (mass-weighted average for 38 samples totaling 32.7 g). The mass-weighted susceptibility of NWA 17518, $\chi = 2.68 \times 10^{-5}$ m^3/kg measured on 50 samples for a total mass of 48.1 g, is intermediate between the CO and CM poles, a simple mixing model indicating 49 wt% CO3 and 51 wt% CM2 material. Finally, we interpret NWA 17518 as a polymict breccia containing CO3 and CM2 material mixed at the centimeter-scale. Although this remains ambiguous, the CO3 lithology is likely the host lithology, so this meteorite should rather be classified as a CO3 chondrite (containing a CM2 clast) rather than a CM2 chondrite.

NWA 15819, classified as a CO3 chondrite, contains a 3.5 × 2.0 mm clast fragment (Figure 4a). The host lithology (Figure 4b) contains 40 vol% matrix, chondrules with chondrule average apparent diameter of 161 ± 106 μm (n = 137), CAIs, 3.8 vol% metal, about 0.8 vol% iron sulfides (pentlandite, pyrrhotite), no carbonates, and no hydrated phases such as serpentine or TCI. The Cr_2O_3 content of the ferroan olivine in the clast (0.387 ± 0.114 wt%, n = 19) is similar to that in Acfer 094 and MIL 07687, suggesting that NWA 15819 has a

19455100, 0, Downloaded from https://onlinelibrary.wiley.com/doi/10.1111/maps.70233 by Portland State University, Wiley Online Library on [06/11/2026]. See the Terms and Conditions (https://onlinelibrary.wiley.com/terms-and-conditions) on Wiley Online Library for rules of use; OA articles are governed by the applicable Creative Commons License

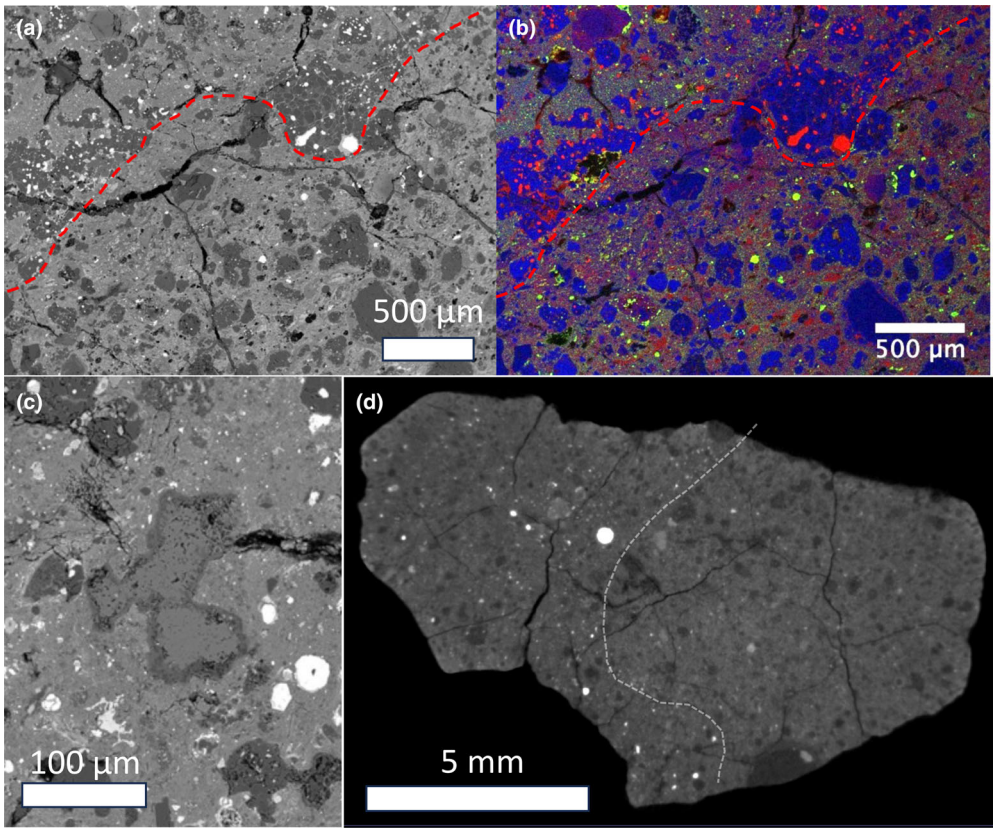


FIGURE 3. NWA 17518 CO-CM chondrite. (a) Reflected light image with the contact between the two lithologies highlighted in red. (b) BSE and RGB composite image (R=Fe, G=S, B=Si) across the contact between the metal-rich lithology (top left) and the metal-poor lithology (bottom right). The RGB image highlights Fe,Ni metal (red) and sulfides (green). (c) CAI in the metal-rich lithology (BSE image). (d) X-ray tomography image showing the contact between the CO3 and CM2 lithology.

low subtype estimated at 3.05 (Grossman & Brearley, 2005). The magnetic susceptibility of the 15 g type specimen (log χ = 4.99 with χ in 10^{-9} m^3/kg) is in the upper range for CO3 chondrites (Rochette et al., 2008). The oxygen isotopic composition is $\delta^{18}O = -2.405‰$, $\delta^{17}O = -6.231‰$, $\Delta^{17}O = -5.17‰$. All this is coherent with a CO3.05 classification for the host lithology. The clast (Figure 4c) contains 60.4 vol% matrix (determined by brightness thresholding of BSE images), about 0.4 vol % iron sulfides (pyrrhotite and pentlandite), calcium carbonates containing 0.80 ± 0.4 wt% FeO, TCI, tochilinite (Figure 4d), and almost no metal present only encased in anhydrous silicates (Figure 4e). Most chondrules are heavily altered and their diameter is difficult to evaluate. The matrix of the clast yields EPMA totals of 77.2 ± 0.9 wt%, confirming the presence of hydrated phases. The hydrated clast has all the characteristics of CM2 chondrites: mineralogy, including abundant alteration phases (phyllosilicates, carbonates, pentlandite, TCI), texture. The contact between the CO3 lithology and the CM2-like lithology is sharp and not reminiscent of an alteration front. The bulk magnetic susceptibility being clearly in the range of CO3 chondrites and outside of the range of CM2 chondrites, we interpret NWA 15819 as a CO3 chondrite containing a mm-sized CM2 xenolith.

Dark Inclusions in CR2 Chondrites

We report chondritic inclusions in four CR2 chondrites: NWA 7502, NWA 13724, NWA 14250, and NWA 15175. Most of these meteorites contain several inclusions. These inclusions are subrounded to subangular, up to several mm in size (Figure 5a,b). They can be abundant, up to several vol%, with, for instance, over five inclusions representing 4.9 mm^2 in a 1.31 cm^2 section of NWA 7502, and two inclusions representing 23.2 mm^2 in a 3.69 cm^2 section of NWA 14250 (Figure 5a). They consist almost entirely of fine-grained matrix (~90 vol%). The abundance of anhydrous silicates in these inclusions is variable between meteorites, ranging from almost absent (in two inclusions of NWA 7502) to

19455100, 0, Downloaded from https://onlinelibrary.wiley.com/doi/10.1111/maps.70233 by Portland State University, Wiley Online Library on [06/11/2026]. See the Terms and Conditions (https://onlinelibrary.wiley.com/terms-and-conditions) on Wiley Online Library for rules of use; OA articles are governed by the applicable Creative Commons License

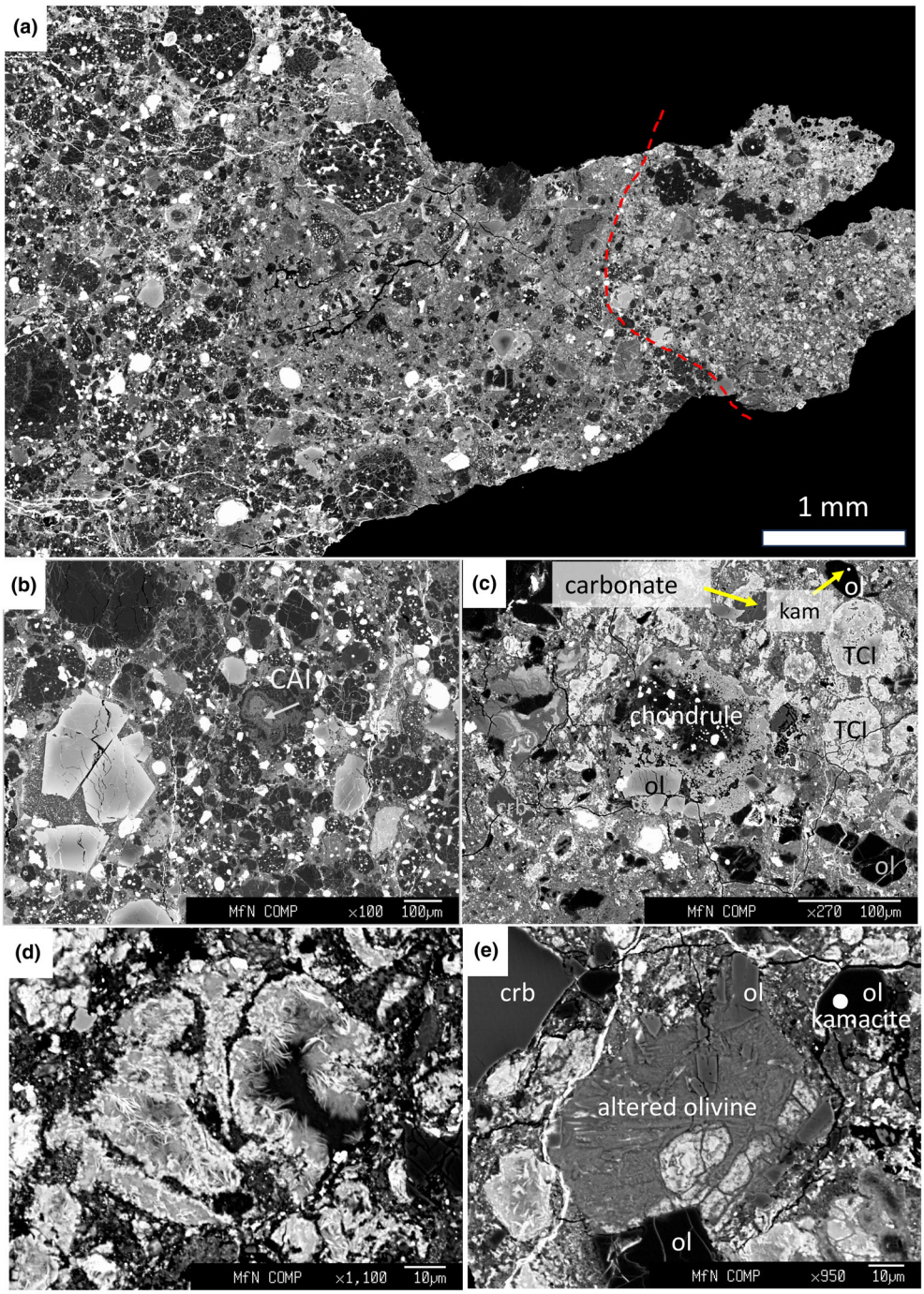


FIGURE 4. BSE images of NWA 15819 CO3 chondrite. (a) BSE image with the contact between the CO3 lithology (left) and the hydrated clast (right) highlighted by the white broken line. (b) CO3 host lithology. (c) Hydrated clast. (d) tochilinite-rich alteration phase in the clast. (e) Altered olivine in the clast. Mineral abbreviations: Ol = olivine, TCI = tochilinite–cronstedtite intergrowths, kam = kamacite, crb = carbonate.

several vol% (NWA 14250, NWA 15175), sometimes present as chondrule or chondrule fragments. The abundance of anhydrous silicates may also vary between inclusions in a given meteorite. For instance, NWA 7502 contains inclusions with no anhydrous silicates and others with up to 6 vol% anhydrous silicates. Defocused EPMA of the matrix yields low totals (75–85 wt% range), indicating that the matrix is hydrated. Matrix analyses are variable, including among different inclusions of a given meteorite, and indicate an overall

19455100, 0, Downloaded from https://onlinelibrary.wiley.com/doi/10.1111/maps.70233 by Portland State University, Wiley Online Library on [06/11/2026]. See the Terms and Conditions (https://onlinelibrary.wiley.com/terms-and-conditions) on Wiley Online Library for rules of use; OA articles are governed by the applicable Creative Commons License

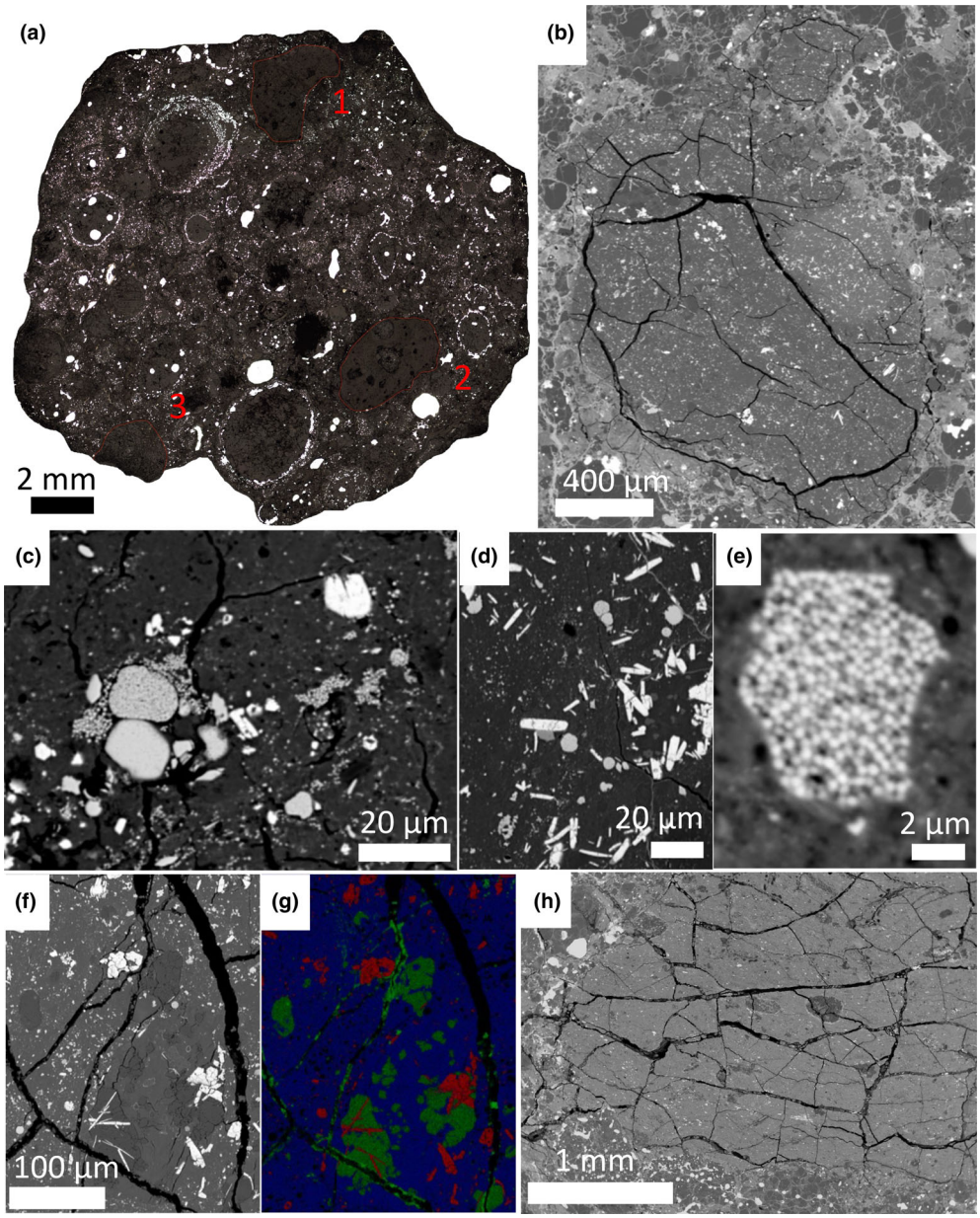


FIGURE 5. Dark inclusions (DIs) in CR2 chondrites. (a) NWA 14250 with three DIs contoured in red (reflected light). (b) DI with desiccation cracks in NWA 7502 (clast NWA7502#1, BSE image. (c, d) Sulfides and magnetite with a variety of morphologies in NWA 7502 (clast NWA7502#2 and #1, BSE image). (e) Magnetite framboids in NWA 14250 (clast NWA14250#1, BSE image). (f) BSE image of clast #1 in NWA 7502. (g) RGB composite image (red = S, green = Ca, blue = Si) of the same field of view as panel f, highlighting carbonates (green) and sulfides (red) in NWA 7502 (clast #1). (h) BSE image of dark inclusion in NWA 15175.

composition of serpentine ± saponite (Table S2). Some anhydrous silicate aggregates may be relicts of altered chondrules. The inclusions show abundant open cracks up to 20 µm wide (Figure 5b). They contain a variety of iron sulfides (troilite, pentlandite, pyrrhotite) with a variety of morphologies (Figure 5c,d) including elongated laths sometimes enclosed in dolomite (Figure 5f,g). Magnetite also displays a variety of morphologies: small framboids, plaquettes, and larger euhedral grains (Figure 5c–e). Rare kamacite is present. The dark inclusion in NWA 15175 (Figure 5h) is different from those in NWA 7502, NWA 13724, and NWA 14250. It contains more abundant anhydrous silicates and chondrule fragments, less abundant iron sulfides, almost no metal, and no carbonates. The main opaque mineral is magnetite, but no magnetite framboids were observed.

19455100, 0, Downloaded from https://onlinelibrary.wiley.com/doi/10.1111/maps.70233 by Portland State University, Wiley Online Library on [06/11/2026]. See the Terms and Conditions (https://onlinelibrary.wiley.com/terms-and-conditions) on Wiley Online Library for rules of use; OA articles are governed by the applicable Creative Commons License

The possible xenolithic nature of these dark inclusions in CR2 chondrites is discussed in section §5.4.

Chondritic Xenolith in NWA 13177 (L3-6)

NWA 13177, classified as L3-6, displays a clastic texture with L4 and L6 clasts set in a host lithology dominated by L3 material (Figure 6a). It also contains a 0.59 mm^2 clast, dark in optical observation that has a texture and mineralogy markedly different from the host rock. This clast contains abundant fine-grained matrix (68 vol% by point counting, 62 vol% by image analyses), a single intact chondrule with a diameter of 230 μm, and mineral fragments (Figure 6b). The matrix analyses by EPMA yield low totals (86.1 ± 0.8 wt%, $n = 9$), indicating the presence of hydrated minerals. Calcite is abundant (Figure 6c), and CAIs are present (Figure 6d). All these objects are mantled by 40-μm-wide fine-grained rims. Troilite, pentlandite, and TCIs are found in the matrix. Metal is rare and found only encased in anhydrous silicates. The anhydrous silicate composition $Fa_{3.6\pm2.1}$ ($n = 4$), $Fs_{2.2\pm0.5}Wo_{1.7\pm0.9}$ ($n = 7$) is at odds with the much higher average FeO content of silicates in unequilibrated ordinary chondrites (e.g., Dodd Jr. et al., 1967). The mineralogy, with presence of calcite, CAI, TCI, pentlandite is similar to that of CM2 chondrites. The matrix electron probe defocused analyses, with FeO 28.9 wt% and analytical total of 86.3 wt% confirming the presence of hydrated minerals, are also in the CM2 range. We interpret this clast as a CM2-like clast. We investigated by optical microscopy 178 cm^2 of sliced polished material of NWA 13177, but could not find additional CM2-like clasts.

Graphite-Rich Clast in GRO 06054 (LL3.1)

GRO 06054, initially classified as L3.6, has been proposed to be a LL3 chondrite based in particular on its magnetic susceptibility (Eschrig et al., 2022). Its petrographic subtype has been revised to 3.1 based on Raman spectroscopy (Bonal et al., 2016). We adopt in the following this LL3.1 classification. We observed a graphite-rich clast in the ANSMET thin section GRO 06054,32 (Figure 7a). The clast size is ≥9.88 mm^2 (lower limit since the clast is cut by the thin section border). The clast has a granoblastic texture with grain size ~40 μm and 120° triple junction indicating intense thermal metamorphism (Figure 7b,c). It is made mostly of olivine (68 vol%), plagioclase (14 vol%), orthopyroxene (9 vol %), Ca-pyroxene (0.6 vol%), graphite (5.1 vol%), and troilite (3.5 vol%). Ca-phosphate (~0.4 vol%) and Fe,Ni are present. Metal has 50.9 wt% Ni and 1.71 wt% Co ($n = 2$). The graphite is found in the form of euhedral laths up to 200 μm in size (Figure 7b). The silicates are equilibrated with the following composition: olivine $Fa_{25.3\pm0.8}$ ($n = 7$), orthopyroxene $Fs_{19.9\pm0.6}Wo_{2.2\pm0.1}$ ($n = 4$), Ca-pyroxene $Fs_{9.2}Wo_{43.9}$ ($n = 1$), plagioclase $An_{19.2\pm0.6}Ab_{78.4\pm1.8}Or_{2.7\pm1.2}$ ($n = 4$). These compositions are close to the range observed for equilibrated L chondrite. The bulk composition of the clast is chondritic (Table S9, Figure 12). The average oxygen isotopic composition determined for three olivine crystals is $\delta^{18}O = 8.66 \pm 0.30$ ‰, $\delta^{17}O = 4.72 \pm 0.21$ ‰, and $\Delta^{17}O = 0.17 \pm 0.20$ ‰ (Figure 11). X-ray tomography was performed at NASA on samples GRO 06054,38 and GRO 06054,39 with voxel sizes of 16 and 13 μm, respectively. Several inclusions were evidenced, but subsequent cutting and microscopic observations of polished sections did not reveal additional graphite-rich clasts in these ~4 cm^3 of material.

Igneous Clasts in NWA 14826 (LL3) and NWA 15116 (LL3)

NWA 14826 contains several inclusions, including a 26.7 mm^2 clast with igneous texture (Figure 8a,b). This clast has a microporphyritic texture with olivine and orthopyroxene subhedral grains with typical size ~250 μm, up to 1 mm for some olivine, set in a plagioclase mesostasis (Figure 8c,d). Olivine is slightly zoned. Troilite is present, and pure metallic Fe is found within some olivine grains (Figure 8e). The olivine $Fa_{6.3\pm1.4}$ (FeO/MnO 17.6 ± 5.7, $n = 8$) and orthopyroxene $Fs_{1.54\pm1.9}Wo_{1.7\pm1.6}$ (FeO/MnO = 3.0 ± 2.6, $n = 9$) compositions (Table S8) are far apart from that of equilibrated LL chondrites. The bulk composition of the clast, estimated by EDS mapping, departs slightly from a chondritic composition, with high Al_2O_3 and low K_2O (Table S9, Figure 12) and is in the basaltic andesite range (SiO_2 = 55.1 wt%, $Na_2O + K_2O$ = 0.85 wt%). The low bulk FeO/MnO ratio of 15.3 suggests a possible origin by crystallization from a melt in a differentiated body with iron depletion in the silicate fraction. Based on the relation between their Mn and Fe content (expressed in atomic formula units), olivine and pyroxene compositions (Table S8) do not follow the trends defined for Mars, Vesta, the Moon, or the angrite parent body based (Papike et al., 2003). The olivine and pyroxene trace element abundances vary slightly across different crystals; overall abundances are globally consistent with those in ungrouped basaltic achondrites and Martian basalts for most elements (Figure S6), in agreement with a differentiated magmatic origin for the clast protolith. The clast is mantled by fine-grained chondritic matrix rim with thickness 50–100 μm. This rim has texture and semiquantitative composition (determined by EDS, Table S2) similar to that of type 3 ordinary chondrite matrix (e.g., Grant et al., 2024). The presence of this rim

19455100, 0, Downloaded from https://onlinelibrary.wiley.com/doi/10.1111/maps.70233 by Portland State University, Wiley Online Library on [06/11/2026]. See the Terms and Conditions (https://onlinelibrary.wiley.com/terms-and-conditions) on Wiley Online Library for rules of use; OA articles are governed by the applicable Creative Commons License

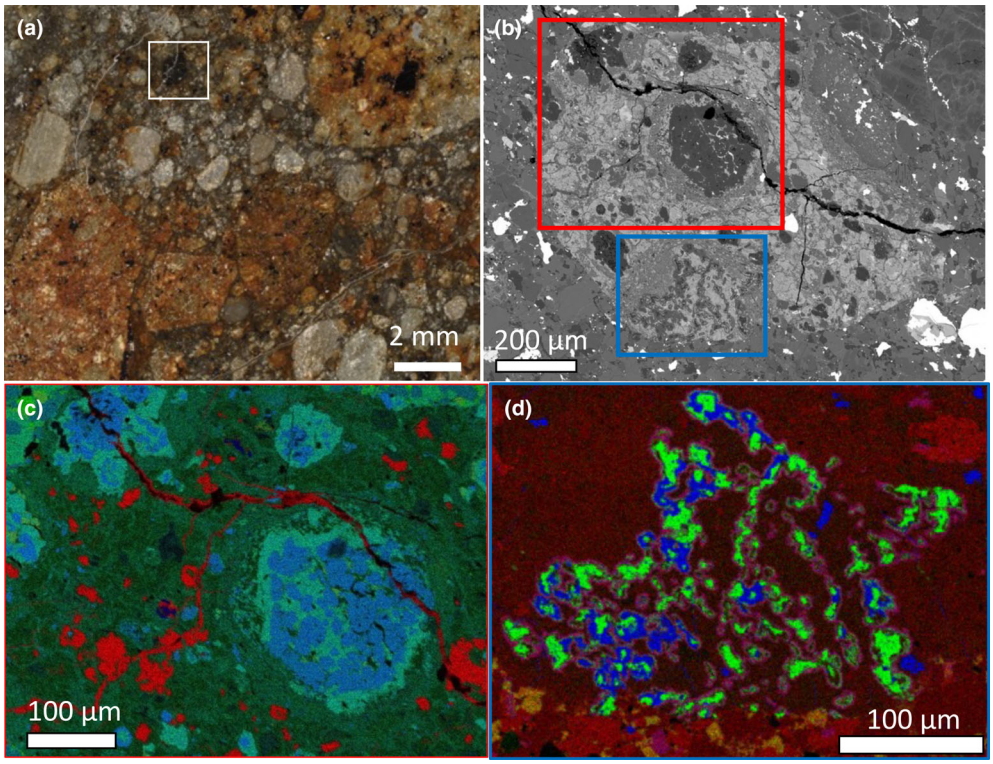


FIGURE 6. Xenolith in the L chondrite NWA 13177. (a) Optical image with the clast highlighted by the white box. (b) BSE image of the clast. The red inset is shown in figure (c), the blue inset in figure (d). (c) RGB composite image (R=Ca, G=Si, B=Mg) of the clast highlighting the calcium carbonates in red. (d) RGB composite image (R=Si, G=Al, B=Ca) of the clast evidencing a CAI.

suggests that the clast was incorporated in the meteorite at the time of accretion. The oxygen isotopic composition of 6 olivine crystals in the basaltic clast was measured by SIMS. It lies in the ordinary chondrite field ($\Delta^{17}O = 1.23 \pm 0.57‰$, $n = 6$ analyses in olivine crystals), and plot close to the equilibrated LL trend ($\Delta^{17}O = 1.21 \pm 0.10‰$ for 35 bulk analyses) but with an average $\delta^{18}O$ of $8.3 \pm 1.8‰$ shifted by about 3‰ from the LL average (Table 2, Figure 11). This suggests a formation by melting and differentiation of a LL precursor, the elevated $\delta^{18}O$ being attributed to mass dependent fractionation during the differentiation process. Therefore, although this clast is a rare occurrence of a truly achondritic clast in an ordinary chondrite, it may not be a xenolith sensu stricto.

NWA 15116 LL3 chondrite contains a 62.4 mm^2 fractured igneous clast (Figure 9a,b). It is composed of elongated zoned clinopyroxene phenocrysts with maximum length ~ 100 µm and composition $Fs_{23.7\pm5.7}$ $Wo_{4.3\pm1.3}$ (range $Fs_{15.8–30.3}$, FeO/MnO = 48.9 ± 13.3, $n = 6$, Table S8), set in a partly crystallized mesostasis containing ~10 µm-sized euhedral olivine crystals with composition $Fa_{66–85}$ (Figure 9c). The clast is mantled by a thin, ~ 20-µm thick, possibly clastic inner rim and an outer fine-grained matrix rim with thickness up to 1 mm (Figure 9d). This fine-grained rim has EPMA FeO content of 32.8 wt% and totals 91.3 wt%. The bulk composition of the clast, estimated by EDS mapping, is basaltic, with SiO_2 = 50.6 wt% and $Na_2O + K_2O$ = 1.79 wt% (Table S9). Although the low-Ca pyroxene is in the range of LL equilibrated chondrite, olivine phenocrysts are absent, the bulk FeO/MnO of 29.3 is much lower than in LL chondrites (50.2 ± 4.5, computed from 16 analyses on LL falls by Jarosewich, 1990), and the bulk composition is clearly non chondritic (Figure 12). This suggests that this clast was also formed by crystallization from a differentiated melt. This is consistent with the trace element abundances in low-Ca pyroxene are at about 5–10 times CI chondrite abundances for most elements, and in general slightly higher than abundances in pyroxene in the NWA 14826 clast (Figure S6). The presence of a well-defined, up to mm-thick fine-grained hydrated dust rim mantling the entire clast suggests that it was incorporated in the meteorite at the time of accretion. The bulk oxygen isotopic composition of the clast ($\delta^{18}O = 4.822‰$, $\delta^{17}O = 2.881‰$, $\Delta^{17}O = 0.350‰$), measured on a 1.97 mg bulk sample (microdrilled from the polished section), is markedly different from that of LL

19455100, 0, Downloaded from https://onlinelibrary.wiley.com/doi/10.1111/maps.70233 by Portland State University, Wiley Online Library on [06/11/2026]. See the Terms and Conditions (https://onlinelibrary.wiley.com/terms-and-conditions) on Wiley Online Library for rules of use; OA articles are governed by the applicable Creative Commons License

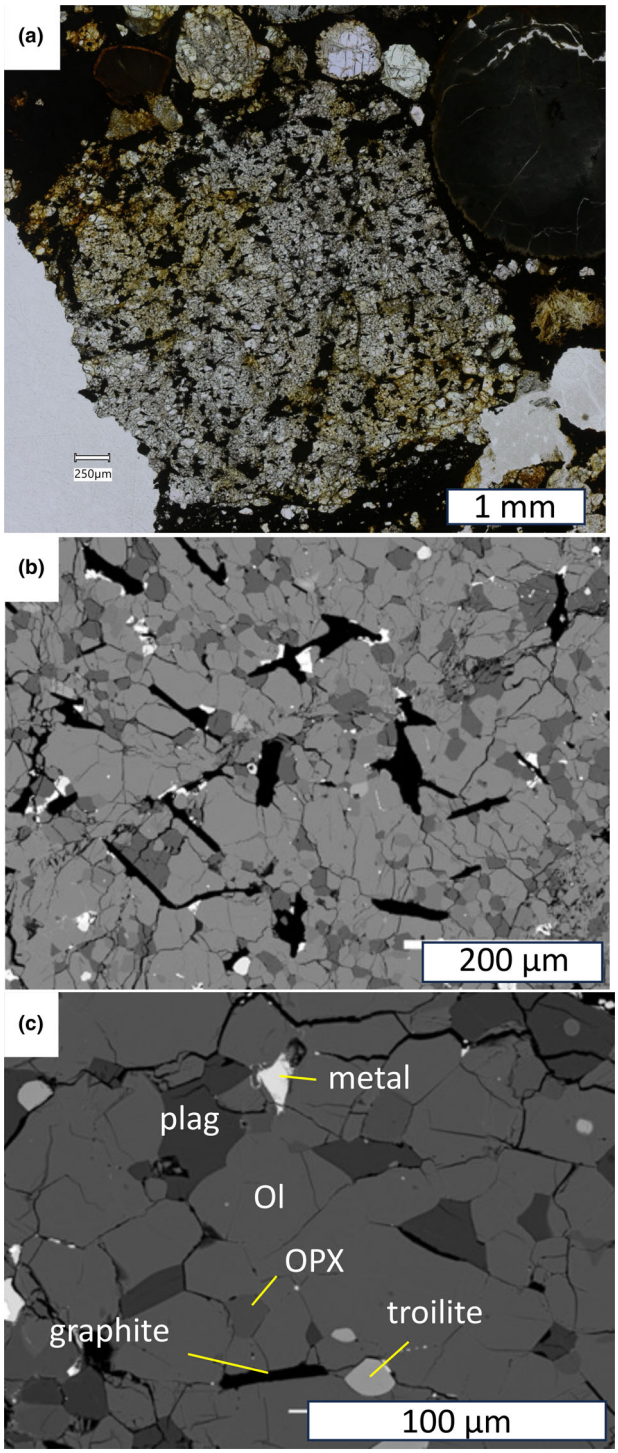


FIGURE 7. Xenolith in GRO 06054. (a) Plane polarized light image, with clast on the left side. (b, c) BSE images of the clast. Mineral abbreviations: plag = plagioclase, Ol = olivine, OPX = orthopyroxene.

chondrites, and plots below the H chondrite trend on a $\Delta^{17}O$ versus $\delta^{18}O$ plot (Table 2, Figure 11). This igneous clast is therefore a true xenolith, although the presence of matrix mantle around the clast suggests that it was incorporated during the initial accretion of the chondrite, suggesting a proximal origin.

Chondritic Clasts in LL3 Chondrites

NWA 16109 contains several similar-looking dark clasts, including a 45 × 45 mm angular one that has a thickness of 59 mm. With a volume of about 100 cm^3, this is by far the largest clast that we studied (Figure 10a). These clasts have a clastic texture, with unequilibrated chondrules with an average apparent diameter of 445 ± 229 µm (n = 40), chondrule fragments, and mineral fragments set in an abundant (55 vol%) fine-grained matrix (Figure 10b). Metal and troilite are abundant (6.8 and 15.1 vol%, respectively), and are often found as complex composite kamacite–taenite–troilite subspherical grains (Figure 10d), sometimes with micrometer-sized Na-Fe phosphate associated with chromite at metal grain sub-boundaries (Figure 10e). This Na-Fe phosphate is also found as grains up to 10 µm within large composite opaque grains. The clast has a bulk susceptibility of logχ = 4.92 (measured on 190 mg of material, with χ in 10^{-9} m^3/kg), in agreement with its elevated metal content.

The silicate composition $Fa_{17.4\pm9.4}$ (n = 28) and $Fs_{13.0\pm10.5}Wo_{1.1\pm1.0}$ (n = 22) is in the range observed in H3 chondrites, but the highly unequilibrated nature does not allow us to exclude that it can be a L3 or LL3. The Cr_2O_3 content of ferroan olivine is 0.119 ± 0.077 wt% (n = 25), indicating a petrographic subtype ≥3.2 (Grossman & Brearley, 2005). The clast has a much higher metal abundance than the host. The metal abundance in the clast (6.8 vol%) is similar to the 7.8 ± 0.62 vol% observed in H chondrites (Eschrig et al., 2022). This is reflected by the elevated magnetic susceptibility of the clast (logχ = 4.92), compared to the host (logχ = 3.45). This elevated value excludes a LL chondrite classification of the clast, and in view of the weathering grade of the meteorite (W2), it is best compatible with a H classification (Rochette et al., 2003). The bulk oxygen isotopic composition, measured by laser fluorination, is $\delta^{18}O$ = 5.232‰, $\delta^{18}O$ = 3.037‰, $\Delta^{17}O$ = 0.290‰, close to the H trend, in particular to the H3 data (Table 2, Figure 11). We conclude that this clast is of H parentage, although it does not have a typical texture of brecciated H3 chondrite.

NWA 13271 contains a 2.7 × 1.6 mm dark angular clast (Figure 10f). It consists almost entirely of recrystallized and equilibrated chondrite matrix-like material that amounts to 91 vol% of the meteorite (Figure 10g). The dominant mineral is olivine with grain size 2–10 µm (Figure 10h), with a small amount of clinopyroxene in the form of ~10 µm crystals, sometimes

19455100, 0, Downloaded from https://onlinelibrary.wiley.com/doi/10.1111/maps.70233 by Portland State University, Wiley Online Library on [06/11/2026]. See the Terms and Conditions (https://onlinelibrary.wiley.com/terms-and-conditions) on Wiley Online Library for rules of use; OA articles are governed by the applicable Creative Commons License

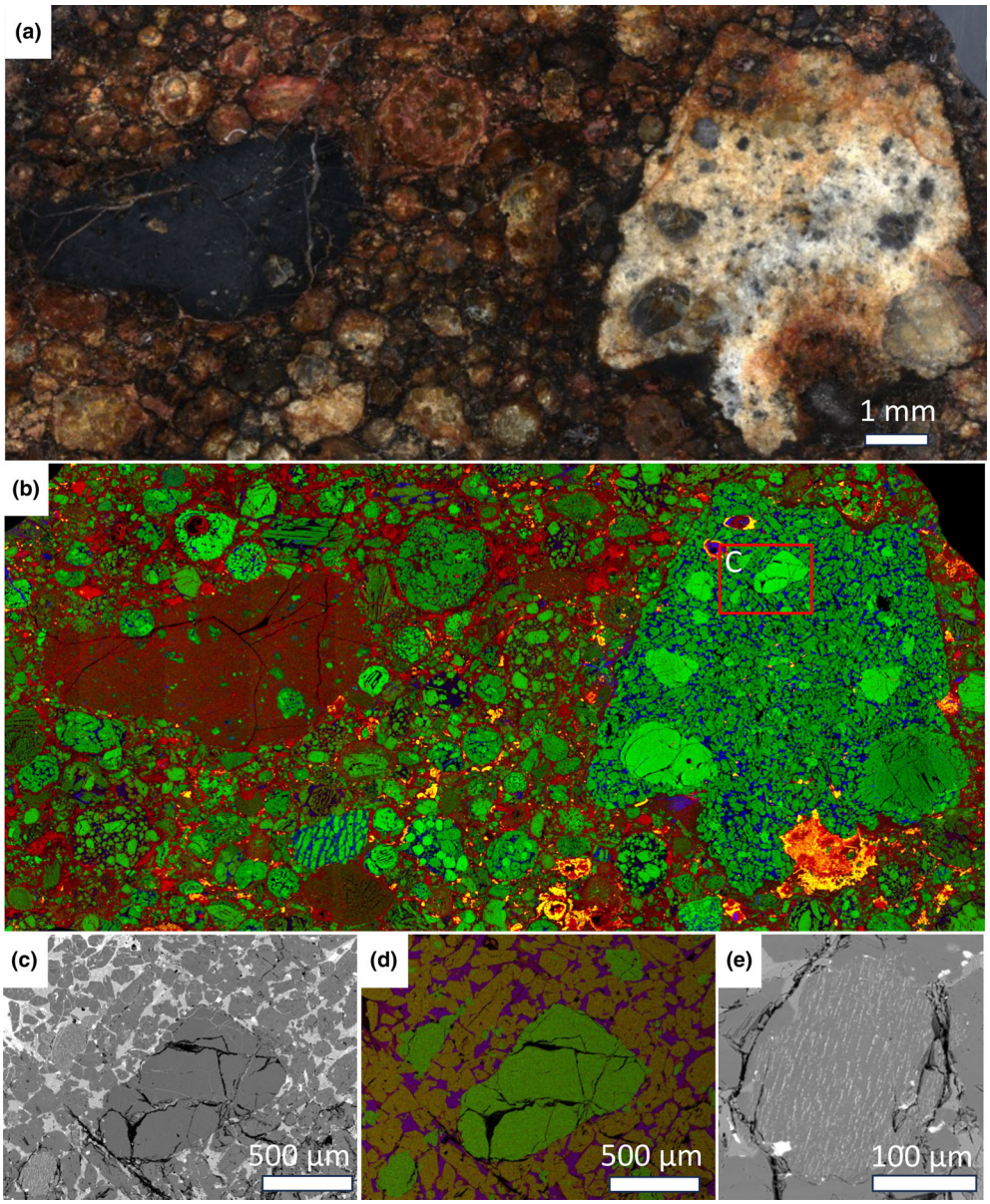


FIGURE 8. Igneous clast in NWA 14826 LL3 chondrite. (a) Optical image of NWA 14826, showing an igneous clast (right), and a dark chondritic inclusion (left). (b) False-color X-ray composite image (red = Fe, green = Mg, blue = Ca, yellow = S) of the same field of view as panel a. (c) BSE image of inset in panel b. (d) RGB composite image (R=Si, G=Mg, B=Al) of the same field of view as panel c, highlighting the silicate mineralogy: olivine is orange, plagioclase is purple, orthopyroxene is green. (e) BSE image of an olivine crystal containing microscopic pure Fe metal.

associated with 50 µm aggregates of K_2O-rich mineral, possibly amphibole or phlogopite (Figure 10i,j). Low-Ca pyroxene is absent. Opaque minerals are rare troilite and rare metal. Metal shows a range of composition, up to 52 at% Ni. Olivine has a composition $Fa_{38.1\pm1.2}$ with 0.17 wt% NiO (n = 9). This is way outside the range for equilibrated LL chondrites that have an upper limit of ~Fa_{33}. The composition of clinopyroxene is $Fs_{9.4\pm1.5}$ $Wo_{26.7\pm0.6}$ (n = 5). The olivine and Ca-pyroxene compositions are in the range of Rumuruti chondrites. The nickel content of olivine (0.17 wt%) is also reminiscent of Rumuruti chondrites. The oxygen isotopic composition, measured in situ on an olivine crystal in the recrystallized matrix, is ^{18}O-rich compared to both LL and R chondrites ($\delta^{18}O$ = 9.3‰, $\delta^{17}O$ = 5.9‰, $\Delta^{17}O$ = 1.06‰). However, it lies along an extension of the LL trend rather than the Rumuruti chondrite trend (Figure 11), and could represent a matrix-rich cognate

19455100, 0, Downloaded from https://onlinelibrary.wiley.com/doi/10.1111/maps.70233 by Portland State University, Wiley Online Library on [06/11/2026]. See the Terms and Conditions (https://onlinelibrary.wiley.com/terms-and-conditions) on Wiley Online Library for rules of use; OA articles are governed by the applicable Creative Commons License

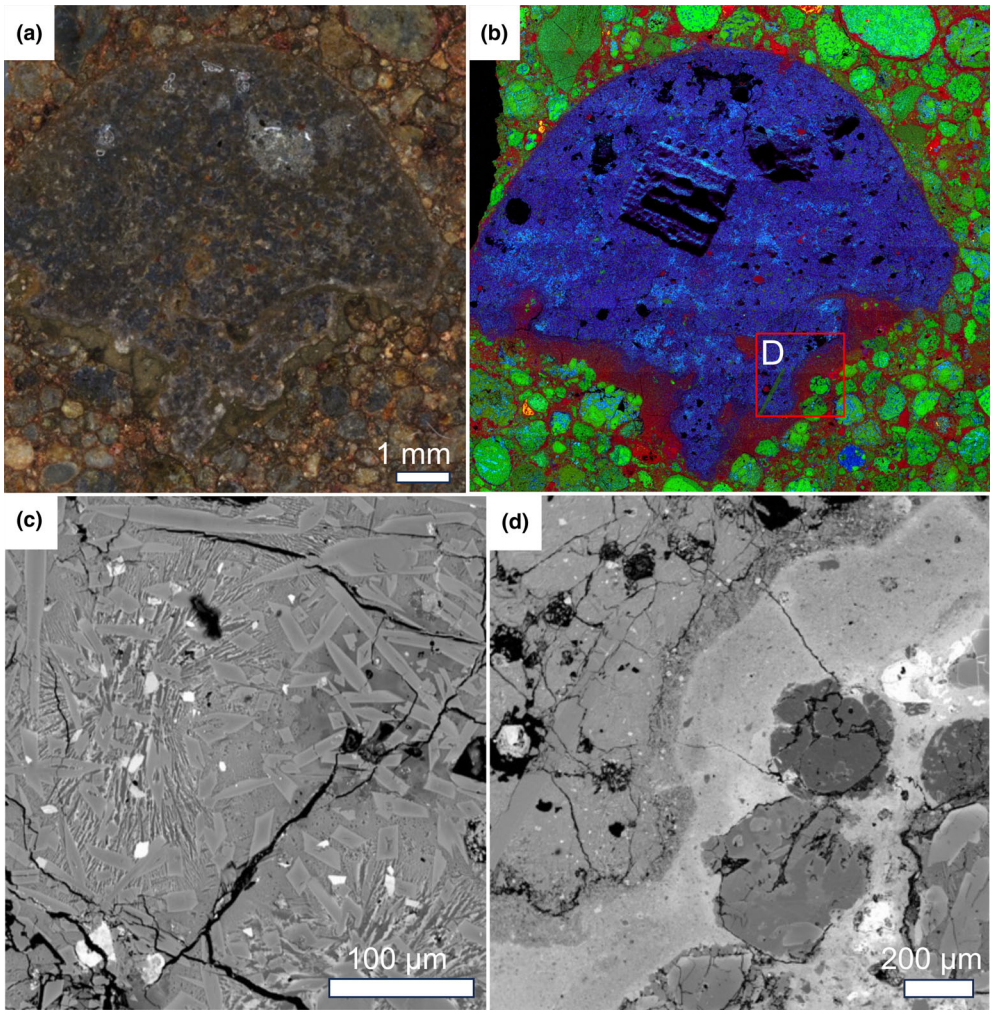


FIGURE 9. Igneous clast in NWA 15116 LL3 chondrite. Optical (a) and compositional composite (b) image (red = Fe, green = Mg, blue = Ca, cyan = Na, yellow = S) of the clast. The square area at the center of the clast in (b) is the area that was microdrilled for oxygen isotopic composition measurement. (c) BSE image. The small bright euhedral crystals are olivine. (d) BSE image of the contact between the clast and the host, evidencing the composite rim mantling the clast with a 10 µm thin inner clastic rim and a 40 m fine-grained dust rim.

inclusion. Although this single SIMS analysis is not decisive to attribute the clast to the LL or R group, or to an ungrouped ordinary chondrite, we did not consider this clast as a xenolith.

Other Remarkable Clasts

The meteorites described in this section do not contain xenoliths, but they contain clasts that are unusual enough to be mentioned briefly.

DaG 417 R3-4 chondrite contains a dark clast (Figure S4a) composed almost exclusively of relatively coarse and porous matrix with olivine equilibrated around Fa_{40}, sulfides, and chromite (Figure S4b). Olivine in the matrix shows complex zoning patterns (Figure S4c). In view of its mineralogy and mineral composition, this clast is interpreted as a cognate equilibrated R chondrite matrix clast.

Sahara 97158 EH3 chondrite contains a centimeter-size clast (Figure S4d) that is relatively similar to the host (chondrule size, enstatite composition, sulfide mineralogy), with the notable exception that it is totally deprived of metal (Figure S4e).

NWA 13385 $CV_{Red}3$ chondrite contains a 7.8 mm^2 clast, dark in optical observations (Figure S4f). The overall mineralogy of the inclusion and the host is similar, with presence of Mg-rich olivine and pyroxene, FeNi metal, absence of carbonates. The clast is matrix-rich (71 vol%), contains chondrules (average apparent diameter 176 ± 50 µm based only on five observed intact chondrules), chondrule fragments and mineral clasts set in a very fine-grained matrix (Figure S4g,h). Olivine is

19455100, 0, Downloaded from https://onlinelibrary.wiley.com/doi/10.1111/maps.70233 by Portland State University, Wiley Online Library on [06/11/2026]. See the Terms and Conditions (https://onlinelibrary.wiley.com/terms-and-conditions) on Wiley Online Library for rules of use; OA articles are governed by the applicable Creative Commons License

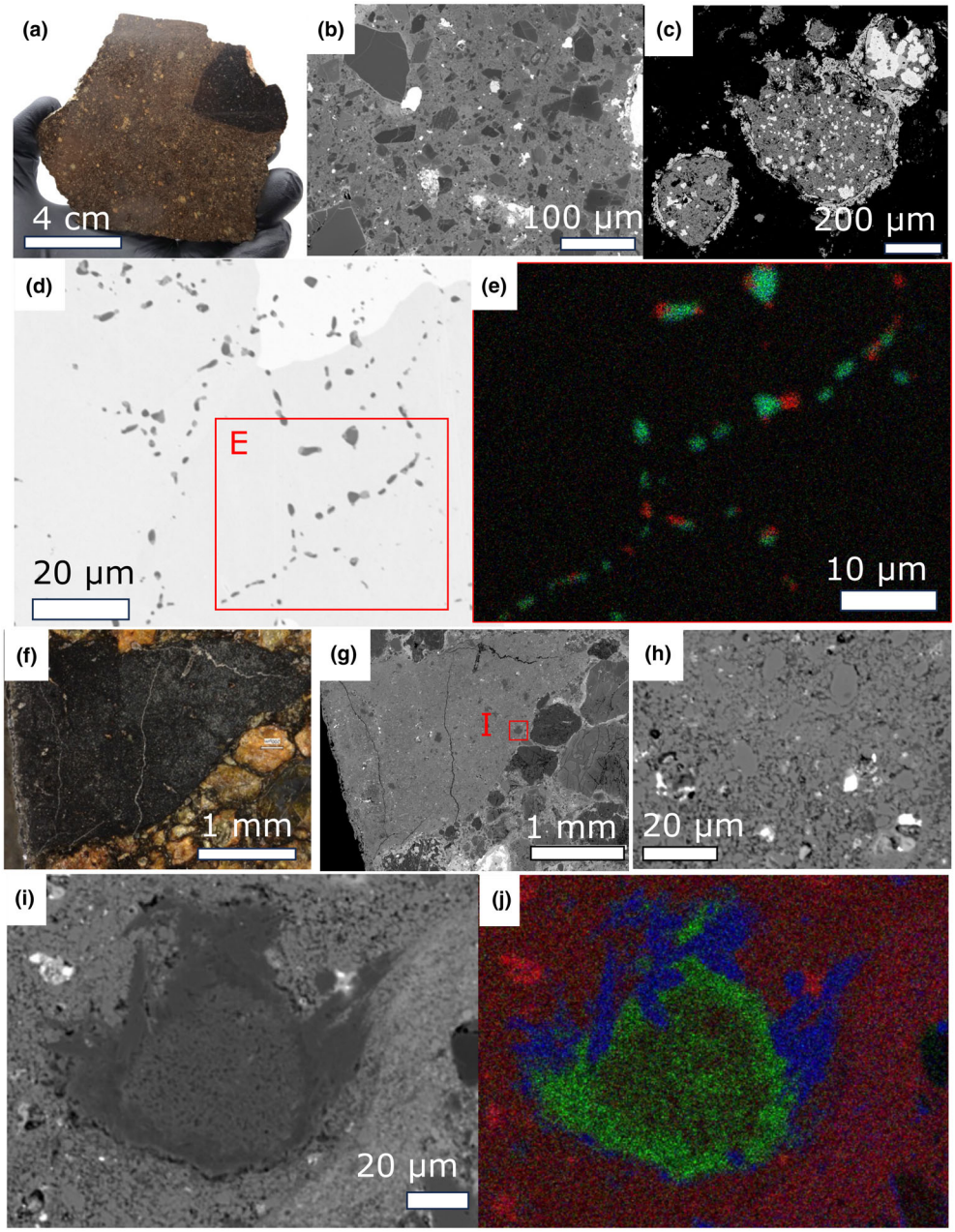
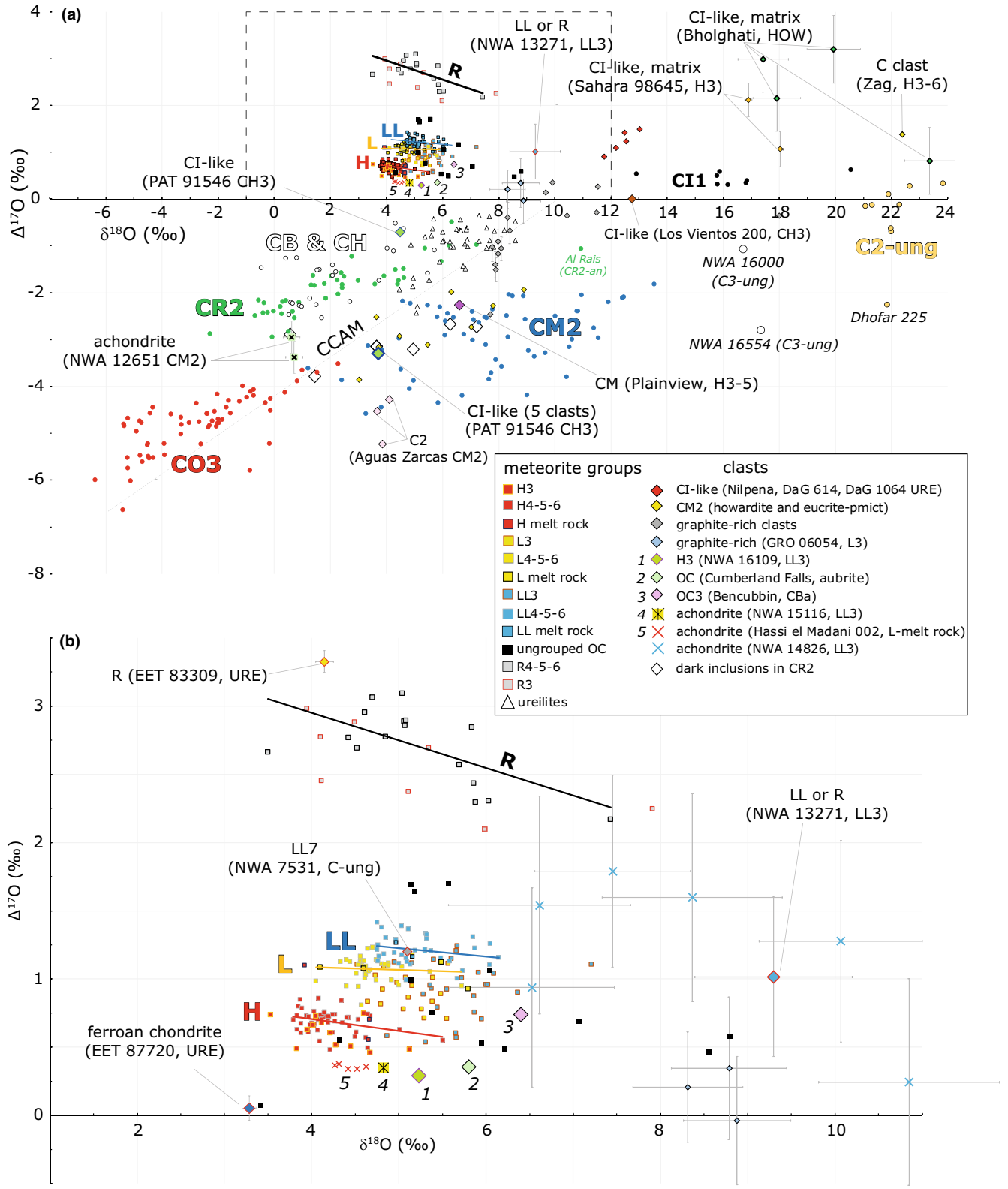


FIGURE 10. Chondritic xenoliths in LL3 chondrites. (a) Optical image of a slice of NWA 16109 showing a large angular chondritic clast on the top right (Credit Preston Allen). (b) BSE image of the chondritic clast in NWA 16109. (c) BSE image of assemblages of troilite, kamacite, and taenite (from darker to brighter) in the chondritic clast in NWA 16109. (d) BSE image of a metal grain in the chondritic clast in NWA 16109. (e) RGB composite image (R = Cr, G = P, B=Na) of the red inset in panel d, highlighting phosphate (green) and chromite (red). (f) Optical image of the angular chondritic clast in NWA 13271. (g) BSE image of the chondritic clast in NWA 13271. The red inset is shown in panel i. (h) BSE image of the matrix of the chondritic clast in NWA 13271. (i) BSE image of a detail of the chondritic clast in NWA 13271. (j) RGB image of the same field of view as in panel i, highlighting olivine in red, clinopyroxene in blue, and a K_2O-rich phase in green.

slightly more magnesian in the clast than in the host with $Fa_{3.2\pm2.1}$ (n = 4) in the clast and $Fa_{5.8\pm7.4}$ (n = 22) in the host. Low-Ca pyroxene has the same composition in the clast and the host, $Fs_{1.6\pm1.1}$ (n = 5) and $Fs_{1.2\pm0.4}$ (n = 12), respectively. The FeO content of the matrix is higher for the host than for the clast (45.4 wt% FeO in the host matrix, 35.1 wt% FeO in the clast matrix). The host matrix is coarser than the clast matrix. Although the inclusion shows significant differences with its host lithology (in terms of matrix abundance and texture,

19455100, 0, Downloaded from https://onlinelibrary.wiley.com/doi/10.1111/maps.70233 by Portland State University, Wiley Online Library on [06/11/2026]. See the Terms and Conditions (https://onlinelibrary.wiley.com/terms-and-conditions) on Wiley Online Library for rules of use; OA articles are governed by the applicable Creative Commons License



19455100, 0, Downloaded from https://onlinelibrary.wiley.com/doi/10.1111/maps.70233 by Portland State University, Wiley Online Library on [06/11/2026]. See the Terms and Conditions (https://onlinelibrary.wiley.com/terms-and-conditions) on Wiley Online Library for rules of use; OA articles are governed by the applicable Creative Commons License

FIGURE 11. Oxygen isotopic composition of xenoliths and individual meteorites from a selection of meteorite groups. (b) It is a zoom of the inset in (a). For readability, not all data given in Table S4 are included in the plot. Circles = carbonaceous chondrites, boxes = ordinary and Rumuruti chondrites, triangles = ureilites, diamonds = chondritic clasts, and crosses = achondritic clasts. A few special meteorites are indicated by their name in italics. For the three ordinary chondrite groups and Rumuruti chondrites, a linear fit is shown for the equilibrated meteorites of the groups (type 4, 5, and 6). The carbonaceous chondrite anhydrous mineral trend (CCAM) is shown by a broken line. In situ SIMS analyses of anhydrous silicate in chondritic clasts, that are less diagnostic for classification than matrix analyses, are shown by small circles. For SIMS analyses, error bars are 1 standard deviation. For analyses from the literature, when the precisions were not available (data from Sokol et al., 2007), we used fixed values of 1 *SD*. = 0.89‰ for $\delta^{18}O$ and 1 *SD*. = 0.63‰ for $\Delta^{17}O$ (average values of the analytical uncertainties for our analyses). Error bars for analyses obtained by fluorination of bulk samples are negligible at the scale of the figure. The cluster formed by the C2-ung meteorites include Dhofar 735, Dhofar 2066, Yamato 86029, Yamato 82162, Yamato 86789, and Belgica 7904. These latter four meteorites, sometimes referred to as "CY" chondrites (Suttle et al., 2023), although this group is not officially defined, are now interpreted as thermally metamorphosed CI-like or CM-like chondrites (Schrader et al., 2025; Tonui et al., 2014).

chondrule size, and matrix Fe content), the similar mineralogy of the inclusion and the host, and the overall unbrecciated nature of NWA 13385, suggest that this clast is better referred to as a matrix-rich cognate inclusion than a xenolith.

We also report mesosiderite clasts in NWA 10472 howardite and NWA 14981 polymict eucrite (Table 1). In NWA 14981, the two mesosiderite clasts represent 4.4% of the surface of the 16.5 cm^2 investigated slice (Figure S5a,b). These clasts consist of pyroxene (including zoned pyroxene and pyroxene with exsolution lamellae), plagioclase, silica, troilite and abundant Fe,Ni metal (Figure S5c–d). The larger clast in NWA 14981 contains olivine surrounded by an orthopyroxene corona (Figure S5e), as described in many mesosiderites (Nehru et al., 1980). The silicate composition in the clast in NWA 14981 (low-Ca pyroxene $Fs_{40.8\pm0.1}Wo_{3.9\pm0.1}$, FeO/MnO 22–36, $n = 10$; Ca-pyroxene exsolutions $Fs_{23.3\pm1.9}Wo_{38.7\pm1.4}$, FeO/MnO 20–23, $n = 10$; zoned pyroxene $Fs_{30.5\pm7.5}Wo_{2.5\pm0.8}$, FeO/MnO 24–33, $n = 12$) and in NWA 10472 (pigeonite $Fs_{55.7\pm1.6}Wo_{11.7\pm1.6}$, Fe/Mn = 34 ± 1 $n = 5$; Ca-pyroxene $Fs_{28.9\pm3.4}Wo_{38.0\pm4.7}$, Fe/Mn = 27 ± 2, $n = 6$), plagioclase $An_{89.6\pm4.6}$ ($n = 2$) is similar to that in mesosiderite silicates. A 10 × 15 mm mesosiderite clast was reported previously in the polymict eucrite DaG 779 (Rosing & Haack, 2004). Although these clasts are unusual in HED meteorites, geochronological data suggest that mesosiderites, like HED achondrites, derive from Vesta (Haba et al., 2019). As such, the mesosiderites clasts in eucrites and howardites cannot be considered as xenoliths.

XENOLITH TYPOLOGY

Xenoliths in HED Achondrites

Chondritic xenoliths in HED meteorites are relatively common and have already been extensively studied (e.g., Patzek et al., 2018; Zolensky et al., 1996). The majority of these clasts are CM2 clasts. They have the petrographic characteristics of CM2 chondrites (e.g., Bunch et al., 1979; Patzek et al., 2018; Zolensky et al., 1996) and the same aqueous alteration ages (Visser et al., 2020). They also have the same sulfur (Visser et al., 2019), hydrogen (Patzek et al., 2020), and oxygen (Patzek et al., 2025; Van Drongelen et al., 2016) isotopic compositions than CM2 chondrites. A lesser proportion of these clasts (~15%, 5 occurrences in Kapoeta, 4 in Jodzie, 2 in Yamato 793497, 1 in Bholghati) were reported as CR2 clasts but without oxygen isotopic evidence (Zolensky et al., 1996). Such clasts were later interpreted as CI-like clasts (Patzek et al., 2018), and their hydrogen isotopic composition has indeed a similar range to that measured in CI1 chondrites (Patzek et al., 2020). However, no bulk oxygen isotopic composition data is available for these CI-like xenoliths. Oxygen isotopic composition of presolar grains and organic matter have been measured in CI-like clasts in Kapoeta (Liu et al., 2020), but they cannot constrain the linkage between the clasts and the meteorite groups that require bulk analyses by fluorination or a least in situ fine-grained matrix analyses by SIMS. Clasts in LEW 85300 polymict eucrites had been attributed to the CV group based on their mineralogy (Zolensky et al., 1992), but this interpretation remains tentative (Zolensky et al., 1996).

Most of the clasts we observed in NWA 10472, NWA 11490, NWA 13143, NWA 14804, NWA 17470, and in Bholghati have petrography (matrix abundance, chondrule size), matrix and mineral composition similar to CM2 chondrites, in agreement with previously described CM2-like clasts in HED meteorites. Our observations fully agree with the conclusion that these clasts are xenoliths of various CM2 lithologies implanted in the Vesta regolith during low-speed collisions (Patzek et al., 2018; Zolensky et al., 1996). We observed a slightly lower proportion of CM2 xenoliths (68%, 17 out of 25 clasts, observed in 6 HED meteorites) compared to Zolensky et al. (1996), but a similar proportion if we

19455100, 0, Downloaded from https://onlinelibrary.wiley.com/doi/10.1111/maps.70233 by Portland State University, Wiley Online Library on [06/11/2026]. See the Terms and Conditions (https://onlinelibrary.wiley.com/terms-and-conditions) on Wiley Online Library for rules of use; OA articles are governed by the applicable Creative Commons License

restrict to carbonaceous chondrite clasts (77%, 17 out of 22 clasts).

We observed four C2-ung clasts in Bholghati (our clasts Bholghati#5-7-10-11). Identical clasts were already described in Bholghati (fig. 9 in Buchanan et al., 1993) and Kapoeta (fig. 10 in Zolensky et al., 1996), and referred to as C1 or CR2 clasts. They have also been reported in NWA 7542 polymict eucrite (fig. 6e,f in Patzek et al., 2018). These latter authors interpreted them as CI-like clasts. But their description, with absence of small-grained magnetite framboid, paucity of sulfides, and dominance of large (>10 μm) magnetite grains is at odd with the usual opaque mineralogy of CI1chondrites. In the four C2-ung clasts in Bholghati, we did not observe magnetite plaquettes and framboids made of small (<μm) individual magnetic crystals that are ubiquitous in CI1 chondrites or, for instance, in the "CR2-like" clast described in in Yamato 793497 by Zolensky et al., 1996 (Figure 12 therein) and in the CI1-like clast described in Bholghati by Reid et al. (1990). The C2-ung clasts in Bholghati also differ from CI1 lithologies by the paucity of sulfides that is a major component in CI1 chondrites with an average 5.8 ± 1.3 vol% in Orgueil, Alais, Ivuna, and Oued Chebeika 002 (Gattacceca et al., 2025; King et al., 2015). The sulfur isotopic composition of CI-like clasts in NWA 7542 was shown to be different from that of CI1 chondrites (Visser et al., 2019). With the SIMS analyses of our clast #5 in Bholghati, we provide the first oxygen isotopic composition data for a "CI-like" clast in HED meteorites other than the NanoSIMS data of Liu et al. (2020). The composition measured for this clast #5 is close to the CI1 meteorite cluster, but significantly different (Figure 11). The closest isotopic match is the matrix of "CI-like" clast analyzed by SIMS in Sahara 98645 H3 chondrite (Bischoff et al., 2018). Matrix FeO contents of 20.6 ± 2.4 wt% (n = 21), 19.2 ± 1.6 wt% (n = 22), and 14.5 ± 1.6 wt% (n = 14) were measured for three "CI-like" clasts in Sahara 98645 (Patzek et al., 2018). These values, like the 20.1 ± 3.0 wt% FeO we measured in the Bholghati C2-ung clasts, are in the CI1 range (e.g., Gattacceca et al., 2025, and references therein). However, The EPMA totals for the same three "CI-like" clasts in Bholghati are 84.0 ± 2.2, 84.8 ± 2.8, and 83.6 ± 1.6 wt% (Patzek et al., 2018) significantly higher than the average 76.4 ± 5.9 wt% for similar analyses in the matrix of CI1 chondrites (average computed using average data from McSween and Richardson (1977), Zolensky et al. (1993) and Gattacceca et al. (2025) for Alais, Ivuna, Orgueil, and Oued Chebeika 002). Moreover, the mineralogy of these CI-like clasts, with large magnetite grains to 20 μm (figs. 8d and 11e in Patzek et al., 2018), rare magnetite plaquettes or small-scale magnetite framboids, and rare sulfides set them apart from CI1 chondrites, although CI1 meteorites show a variety of lithologies (e.g., Alfing et al., 2019; Morlok et al., 2006). The CI1-like clast reported in Bholghati by Reid et al. (1990) also has large magnetite grains (their Figure 5) and matrix EPMA matrix totals of 89.0 wt%, and despite the presence of pyrrhotite we suggest that it is also a C2-ung clast.

Overall, our observations confirm that howardites and polymict eucrites are rich in chondritic xenoliths, with a dominance of CM2 clasts which make up ~70% of the total clast population. We expand significantly the diversity of known xenoliths in HED meteorites with the report of a CO3 clast in NWA 17470 (Figure 1e), a pallasite clast in NWA 10472 (Figure 2k), and ordinary chondrite clasts in NWA 3197, NWA 10674, and NWA 17597 (Figure 2). We also question the nomenclature of "CI-like" (Buchanan et al., 1993; Patzek et al., 2018) or "CR2-like" (Zolensky et al., 1996) for clasts similar to our clasts #5-7-11-12 in Bholghati. We propose that most of them should better be described as ungrouped C2 chondrite material. We note that the clasts described as CI-like clasts in Sahara 98645 H3 chondrite by Patzek et al. (2018) may represent similar material.

Therefore, HED meteorites contain xenoliths from at least five different parent bodies: H, CM2, CO3, pallasite, and an ungrouped C2 body. It is remarkable that different clasts can coexist at sub-centimeter scale: CM2 and C2-ung in Kapoeta, CM2 and CO3 at mm distance in NWA 17470, CM2 and pallasite at mm distance in NWA 10472, CM2 and C2-ung at a distance of 50 μm in Bholghati.

Xenoliths in Ureilites

Polymict ureilites, that make up about 5% of all ureilites, contain xenoliths with abundances up to 10 vol % (Downes et al., 2008; Goodrich et al., 2004, 2021; Ikeda et al., 2000, 2003; Patzek et al., 2018, 2020). These xenoliths include CI-like material, ungrouped carbonaceous chondrites, R chondrites, ordinary chondrites, ungrouped ferroan chondrite (in EET 87720), enstatite chondrites, angrite, ungrouped achondrites, an extreme case being Almahata Sitta anomalous ureilite that contains xenoliths from about all of these groups (e.g., Goodrich et al., 2021; Horstmann & Bischoff, 2014). Polymict ureilites are therefore particularly rich in xenoliths, both in quantity and diversity. Our observations of dozens of xenoliths in the two polymict ureilites selected for this study (NWA 14086, NWA 16454) are in agreement with this. All the clasts we observed were CI-like, which is the most abundant type of clast in brecciated ureilites.

As noted by Patzek et al. (2018), the composition of the phyllosilicates in these CI-like clasts is more similar to that of CM chondrites. The hydrogen isotopic composition of CI-like clasts in ureilites also suggests that

19455100, 0, Downloaded from https://onlinelibrary.wiley.com/doi/10.1111/maps.70233 by Portland State University, Wiley Online Library on [06/11/2026]. See the Terms and Conditions (https://onlinelibrary.wiley.com/terms-and-conditions) on Wiley Online Library for rules of use; OA articles are governed by the applicable Creative Commons License

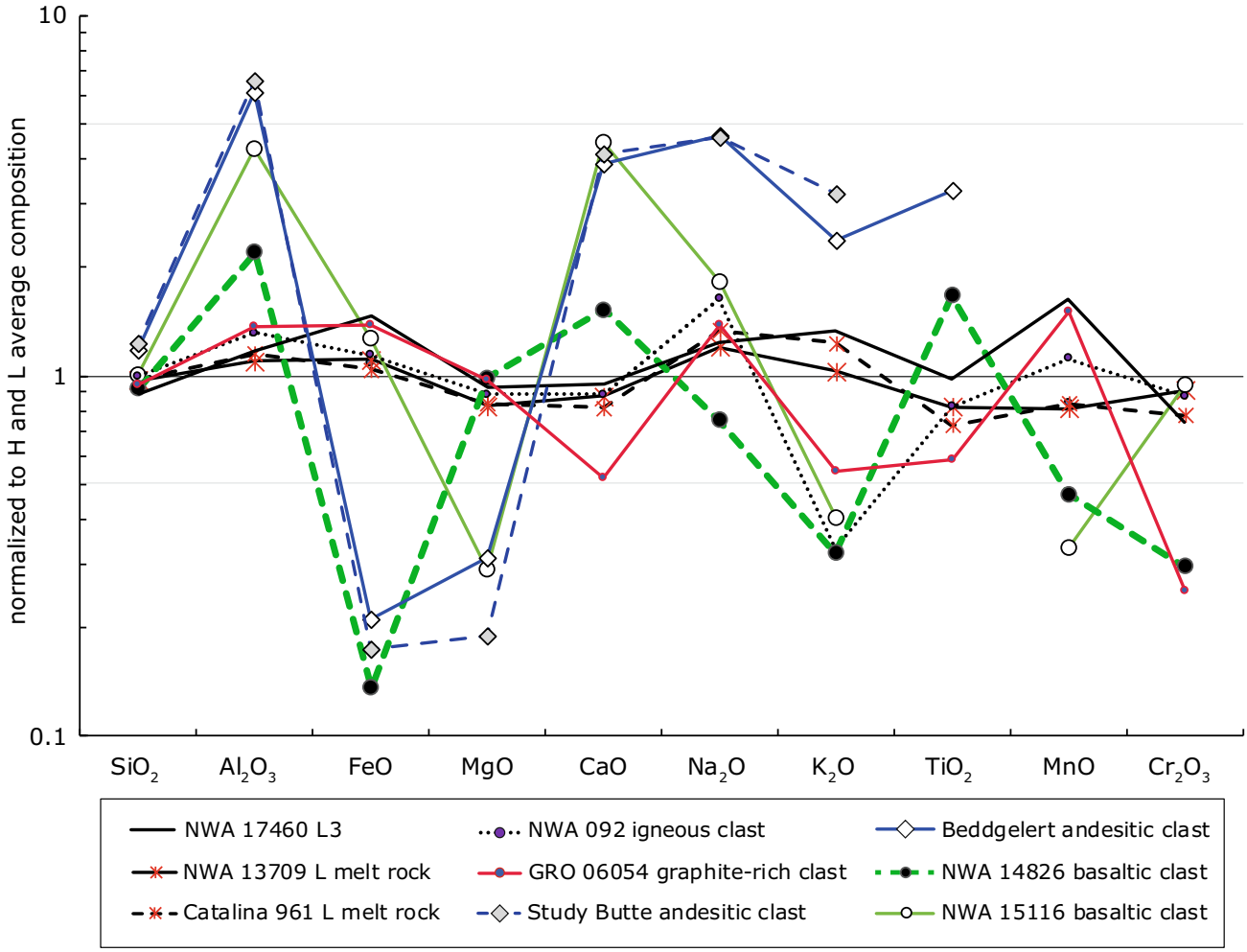


FIGURE 12. Bulk composition of a selection of clasts in chondrites, normalized to the average composition of L and H chondrites (not including metal and troilite) from Jarosewich (1990). We include data acquired with the same methodology for several melt rock clasts (from Catalina 961, NWA 13709, and NWA 16981), as well as data for the host L3 lithology and a chondritic clast in NWA 17460. Data for clasts previously interpreted as achondritic in the following meteorites are given for comparison: Study Butte (Fredriksson et al., 1989), Beddgelert (Fredriksson et al., 1989). Data for a clast previously interpreted as chondritic in NWA 092are also shown for comparison (Goodrich et al., 2021).

these clasts are indeed not CI1 chondrites (Patzek et al., 2020), although CI1 material has been shown to have heterogeneous D/H ratios (Marrocchi et al., 2026). The sulfur isotopic composition of sulfides in CI-like clasts in ureilites is different from that of CI1 chondrites (Visser et al., 2019). The oxygen isotopic composition of CI-like clasts in ureilites is also different from CI1 chondrites (Clayton & Mayeda, 1988; Patzek et al., 2025). This difference in oxygen isotopic composition was interpreted by Brearley and Prinz (1992) as a different water/rock ratio for the clasts in Nilpena ureilite than that for CI1 chondrites, but combined with the observation of different hydrogen and sulfur isotopic compositions, a different parent body seems a more plausible explanation. It is also noteworthy that some "CI-like" clasts previously described in polymict ureilites have petrographic features markedly different from CI1 chondrites: large magnetite grains, low abundance of sulfides, and presence of non-altered chondrules (see fig. 10 of Patzek et al., 2018). Overall, the petrographic and isotopic evidence indicate that the "CI-like" xenoliths described in polymict ureilites are not genetically related to CI1 chondrites, and some of them are not type 1 material since they contain significant amounts of anhydrous silicates and even chondrules.

Xenoliths in CH3 Chondrites

The xenoliths we observed in Los Vientos 200 are very similar to xenoliths observed in other CH3

19455100, 0, Downloaded from https://onlinelibrary.wiley.com/doi/10.1111/maps.70233 by Portland State University, Wiley Online Library on [06/11/2026]. See the Terms and Conditions (https://onlinelibrary.wiley.com/terms-and-conditions) on Wiley Online Library for rules of use; OA articles are governed by the applicable Creative Commons License

chondrites (Bischoff, Palme, et al., 1993; Greshake et al., 2002; Patzek et al., 2018), and in the related CB chondrites (e.g., Greshake et al., 2002). The usual size range of such clasts in CH3 chondrites is well below 1 mm, although exceptions exist like a 1.3 × 0.8 mm clast found in QUE 94411 (Greshake et al., 2002) or a 3.1 × 2.8 mm clast that we observed in Los Vientos 200. These clasts have been described as CI1-like (e.g., Patzek et al., 2018), but the isotopic composition measured for a single large clast in PAT 91546 (Weisberg et al., 1995) is very different from that of CI1 chondrites, and within the CM2 oxygen isotopic composition cluster (Figure 11). The isotopic composition measured in the same meteorite on a combination of five smaller clasts is not far from the CR-CB-CH cluster (Weisberg et al., 1995), but the interpretation is not straightforward due to the aggregation of five different clasts. The bulk oxygen isotopic composition we measured for a "CI-like" clast in Los Vientos 200 is close to, but significantly outside the CI1/Bennu/Ryugu cluster (Figure 11). The sulfur isotopic composition of a CI-like clast in Acfer 182 CH3 is also distinct from that of CI1 chondrites (Visser et al., 2019). Overall, the isotopic data set indicates that these CI-like clasts are not related to CI1 meteorites.

Dark Inclusions in CR2 Chondrites

Dark inclusions reaching several mm in size have been described in almost all CR2 chondrites with modal abundances of ~2–4 vol% (Endress et al., 1994; Weisberg et al., 1991; Zolensky, Abreu, et al., 2018). They are called dark inclusions (DI) rather than clasts since they are found in meteorites that are not obviously brecciated. They share similar mineralogy, with mostly a phyllosilicate-rich fine-grained matrix containing anhydrous silicates (including chondrules with smaller diameter than in the host CR2 chondrites), magnetite framboids and plaquettes, carbonates, and Fe- and Fe,Ni-sulfides. More such inclusions were described and categorized as CI-like clasts in Renazzo and Acfer 087 (Patzek et al., 2018).

We observed such inclusions in four CR2 chondrites: NWA 7502, NWA 13724, NWA 14250, and NWA 15175. The FeO content of the matrix in these inclusions is in the 19–31 wt% range, lower on average than the usual range observed in CR2 matrix. However, the highest FeO contents measured in these inclusions, like in NWA 15175 inclusion, overlap with the CR2 host matrix analyses that yield an average FeO content of 32.5 ± 5.9 wt% FeO, computed from 23 defocused EPMA of CR2 matrix (McSween & Richardson, 1977; Zolensky et al., 1993, and our analyses, Table S2). The variability of matrix composition suggests that the dark inclusions in CR2 have suffered a range of secondary processes (aqueous alteration and heating). The opaque mineralogy, although reminiscent of that of CI1 chondrites, has noticeable textural differences with CI1 with relatively few magnetite framboids and more abundant euhedral magnetite crystals with size ~10 μm. Also, some inclusions, like those in NWA 14250, contain metal-bearing chondrules, a noticeable difference with CI1 chondrites. All these observations are similar to those on dark inclusions previously observed in CR2 chondrites (Endress et al., 1994; Patzek et al., 2018; Weisberg et al., 1991).

The abundance of anhydrous minerals, including chondrules and chondrule fragments, in the dark inclusions of CR2 is higher than that in CI1 chondrites that contain less than a few % of anhydrous silicates (King et al., 2015), and sometimes none, like Oued Chebeika 002 (Gattacceca et al., 2025). The hydrogen isotopic composition of "CI-like clasts" in CR2 chondrites indicates that these clasts are indeed not CI1 chondrites (Patzek et al., 2020). The oxygen isotopic composition of "CI-like clasts" in CR2 chondrites (Endress et al., 1994; Patzek et al., 2025; Weisberg et al., 1995) is also very different from that of CI1 chondrites and closer, yet distinct, to that of CR2 chondrites (Figure 11). Therefore, the majority, if not all, of the "CI-like clasts" described in CR2 chondrites are likely not genetically related to CI1 chondrites. Although some of these inclusions are referred to as C1 clasts (Patzek et al., 2020), the presence of relatively abundant anhydrous silicates rather points to a C2 classification. Finally, the bulk composition of the dark inclusions is identical to that of their host CR2 lithology (Weisberg et al., 1991).

Therefore, the dark inclusions described in CR2 chondrites are likely all related to their CR2 host material, as already proposed by, for example, Patzek et al. (2025). Textural and size consideration suggest that they were incorporated in the meteorite during the initial accretion of the CR2 parent body (Endress et al., 1994; Patzek et al., 2018). Their difference in oxygen isotopic composition with the bulk CR2 chondrites is small and may be compatible with a scenario where they have been formed with material similar to CR2 material, but altered previous to accretion. In that case, these inclusions may not be referred to as xenoliths, and are best qualified as dark inclusions, that is, lithified and variably altered matrix-rich aggregate of CR2 material incorporated in CR2 chondrites during initial accretion.

Recently, it has been proposed that some dark clasts in NWA 14250 CR2 chondrite could originate from the comet-forming region of the outer disk, based on their (i) CI-like chemistry, (ii) isotopic signatures (^{15}N-rich, D/H heterogeneities, ^{16}O-poor values), and (iii) nucleosynthetic anomalies supposedly distinct from CI1 chondrites, together with local similarities to cometary IDPs (van Kooten et al., 2024). While this interpretation is intriguing, we do not favor a cometary origin for several reasons.

19455100, 0, Downloaded from https://onlinelibrary.wiley.com/doi/10.1111/maps.70233 by Portland State University, Wiley Online Library on [06/11/2026]. See the Terms and Conditions (https://onlinelibrary.wiley.com/terms-and-conditions) on Wiley Online Library for rules of use; OA articles are governed by the applicable Creative Commons License

First, the oxygen isotopic compositions of these dark clasts do not reach the extreme ^{16}O-poor values reported in earlier work for microxenoliths in LA 02342 CR2 chondrite (e.g., Nittler et al., 2019), and potential analytical biases (e.g., ^{16}OH interference) are not discussed. In addition, key cometary indicators such as very high carbon contents are not demonstrated, and the clasts contain relatively abundant, sometimes large, type I chondrules, unlike those observed in samples from Stardust. A simpler interpretation is that these clasts represent matrix-rich CR lithologies incorporated into more matrix-poor CR chondrites. Such materials naturally explain the CI-like chemistry, CR-like isotopic signatures, and petrographic features. Overall, the data appear consistent with a CR–in–CR origin rather than requiring a cometary contribution.

Graphite-Rich Clasts in Chondrites

The graphite-rich clast observed in GRO 06054 (LL3.1) is texturally similar to graphite-rich clasts previously described in eight unequilibrated chondrites, mostly in L3 and LL3 chondrites (Bischoff et al., 2018; Semenenko et al., 2004; Storz et al., 2021; Zolensky, Johnson, et al., 2018). The opaque mineralogy is also similar. In GRO 06054, the rare metal is under a Ni-rich form (taenite or tetrataenite), similar to what was observed in the graphite-rich clasts in Krymka (Semenenko et al., 2004). With the clast in GRO 06054, there are now nine known occurrences of such graphite-rich clasts. Their main properties are summarized in Table S7. In most graphite-rich clasts, olivine and pyroxene are equilibrated but their compositions are variable from clast to clast, and even within a single meteorite in the case of Krymka. The silicate compositions do not seem related to the mineral chemistry of equilibrated material from the group of their host meteorite, suggesting that they are xenoliths.

The oxygen isotopic composition was measured for the graphite-rich clasts in NWA 5697, Adrar 003 (Bischoff et al., 2018), NWA 8330 and NWA 6169 (Zolensky, Johnson, et al., 2018), and GRO 06054 (this study). The compositions are close to the ureilite range or along the terrestrial fractionation line. Overall, these graphite-bearing clasts show a variety of oxygen isotopic signatures and cannot easily be ascribed to a single meteoritic source. However, except for one outlier analysis of a clast in NWA 6169 with $\delta^{18}O \sim 18‰$ (Zolensky, Johnson, et al., 2018), the oxygen isotopic compositions of graphite-rich clasts are clustered close to the ureilite trend and the terrestrial fractionation line, suggesting an origin from the NC reservoir. The carbon isotopic composition of the graphite was measured for the graphite-rich clasts in Krymka (Semenenko et al., 2004), NWA 5697, NWA 3358, and Adrar 003 (Storz et al., 2021): the carbon isotopic composition is compatible with that in enstatite chondrites, but the results are not really conclusive in terms of origin of the clast in view of the overlap of carbon isotopic composition of graphite in different meteorite groups.

These graphite-bearing clasts share a similar texture, but show a wide range of silicate composition and oxygen isotopic composition. Therefore, although they may all derive from NC precursors, their similar texture and mineralogy are rather the result of similar high-temperature petrogenetic processes than an indication of a common chondritic precursor.

Achondrite Xenoliths in Ordinary Chondrites

We report an achondritic xenolith in NWA 15116 (LL3). Igneous clasts with non-chondritic bulk compositions are rare in ordinary chondrites, with only a few occurrences previously described in five meteorites: two in Parnallee LL3.6, a microgabbro (Kennedy et al., 1992) and a feldspar-nepheline clast (Bridges & Hutchison, 1997), one in Villalbeto de la Peña L6 (Bischoff et al., 2013), andesitic clasts in Study Butte H3-6 and in Beddgelert H4 (Fredriksson et al., 1989), and a plagioclase-bearing dunite in Hassi el Madani 002 L chondrite (Agee et al., 2024). Based on their fractionated chemical composition, these clasts have been interpreted as igneous differentiates. It is not known if the andesitic clast in Beddgelert is derived from the melting of a H precursor or not and it is therefore not counted as a xenolith. The xenolithic nature of the microgabbro clast in Parnallee has been established based on the bulk and mineral compositions and rare earth element content of the clast (Kennedy et al., 1992). For the other clasts, the xenolithic nature has been confirmed by their oxygen isotopic composition (Figure 11). The oxygen isotopic composition lies in the winonaite and ureilite field for the clast in Villabeto de la Peña (Dyl et al., 2012) and the feldspar-nepheline clast in Parnallee (Bridges et al., 1995). It lies in the LL field for the andesitic clast in Study Butte H3-6 (Sokol et al., 2007). The achondritic clast in NWA 15116 plot below the H chondrite trend on a $\Delta^{17}O$ versus $\delta^{18}O$ plot. It is noteworthy that this composition is similar to that of the achondritic clast reported in Hassi el Madani 002, although the mineralogy and mineral composition of the two clasts is markedly different (Agee et al., 2024).

Eventually, for the few occurrences of achondritic xenoliths in ordinary chondrites for which oxygen isotopic composition is available, the origin of the clast is from another ordinary chondrite parent body, or from an unidentified parent body with oxygen isotopic composition close to the ureilite/winonaite cluster. All these source bodies are non-carbonaceous bodies. The

19455100, 0, Downloaded from https://onlinelibrary.wiley.com/doi/10.1111/maps.70233 by Portland State University, Wiley Online Library on [06/11/2026]. See the Terms and Conditions (https://onlinelibrary.wiley.com/terms-and-conditions) on Wiley Online Library for rules of use; OA articles are governed by the applicable Creative Commons License

only known example of an achondritic xenolith from the CC reservoir is a 70-μm-clast in NWA 12651 CM2 chondrite (Ebert et al., 2019). Other clasts with granoblastic textures have been found in CV chondrites (Jogo et al., 2013) and CM chondrites (e.g., Kerraouch et al., 2019), but they have all been interpreted as cognate clasts.

Chondritic Xenoliths in Ordinary Chondrites

Xenoliths of ordinary chondrites are rare in ordinary chondrites (see review in Goodrich et al., 2021). Despite the tens of thousands of ordinary chondrites available for study, only five such occurrences have been reported in the literature: Dimmitt (LL5 in H), Glanerbrug (L in LL4-6), St-Mesmin (H4 in LL6), NWA 5674 (L4 in LL6), and Krymka (H3 in LL3). Adzhi-Bogdo (LL3-6) may be a sixth occurrence with some clasts containing olivine in the upper range of L composition, but these could also represent uncommon LL lithologies (Bischoff, Geiger, et al., 1993). We report the occurrence of a 100 cm^3 ordinary chondrite clast, tentatively classified as H3, in NWA 16109 LL3 chondrite.

Because of the existing ambiguity in the interpretation of the oxygen isotopic composition data, the equilibrated clast we observed in NWA 13271 (LL3) is not considered a R xenolith despite its unusual olivine composition ($Fa_{38.1\pm1.2}$, NiO 0.17 wt%). This clast is similar in texture and mineralogy to some clasts up to 2.5 mm in size that have been described in Weatherford CBa and interpreted as possible R chondrite material based on the olivine composition Fa_{41} and absence of orthopyroxene (Prinz et al., 1993). However, in the absence of oxygen isotopic composition data, this attribution to the R group remains tentative and this clast is not considered a confirmed xenolith either. It is noteworthy that mineralogy and silicate composition are often not sufficient to attribute a clast to a given chondrite group and confirm its xenolithic nature. For instance, a chondritic recrystallized equilibrated clast in Murchison with olivine composition Fa_{37} was interpreted as a R clast (Isa et al., 2014) before the measurement of the oxygen isotopic composition of the same clast indicated that it had close relationship with CM chondrites (Kerraouch et al., 2019).

A variety of carbonaceous chondrite xenoliths have been described in 11 H chondrites (Table S3). Some of these, like in Abbott and Willard, are several mm in size (Briani et al., 2012). They are mostly CM2 xenoliths, but a well-characterized CI1 xenolith has been reported in Tsukuba (Nakashima et al., 2003). Two carbonaceous chondrite xenoliths in H chondrites have had their oxygen isotopic composition measured: a CI-like clast in Sahara 98645 that plots close to but significantly outside the CI1 cluster (Bischoff et al., 2018), and a C clast in Zag that plots close to the "CY" cluster formed by a number of ungrouped C2 chondrites (Kebukawa et al., 2019). The sulfur isotopic composition of a CI-like clast in Sahara 98645 (H3) is distinct from that of CI1 chondrites (Visser et al., 2019). We propose that the xenolith in Sahara 98645 is better described as C2-ung rather than as CI-like (see discussion in section §5.1).

In the present study, we describe a 1-mm CM2 clast in NWA 13177 (L3-6), the first description of such a xenolith in an L chondrite. Indeed, carbonaceous chondrite clasts had never been convincingly reported in L or LL chondrites. A hypothetical C clast reported in Cynthiana L/LL4 by Van Schmus (1967) was later shown to be a cognate clast (Sears & Wasson, 1981). Hypothetical carbonaceous clasts in Mezö Madaras (Van Schmus, 1967) were also later shown to be cognate clasts (Christophe Michel-Lévy, 1988). Another carbonaceous clast in Tennasilm is mentioned in Van Schmus (1967) but with no details available.

Xenoliths in CO and CM Chondrites

No xenoliths have been convincingly described in CO3 chondrites in the literature, in line with the low proportion of breccias in this group (Bischoff et al., 2006). A basaltic clast has been described in Lancé (Kurat & Kracher, 1980), but its petrogenesis and xenolithic nature are unclear. A ~ 500 μm, possibly hydrated (type 2), matrix-rich clast has been reported in Lancé as well (Kurat, 1975), but its description is compatible with an unusual matrix-rich inclusion of CO-related material. In this work, we report two CO3 chondrites containing CM2 xenoliths, NWA 15819, and NWA 17518. These are the first descriptions of xenoliths in CO3 chondrites.

Only three xenolithic clasts have been convincingly described in CM2 chondrites. This low number may be attributable to the difficulty of distinguishing xenoliths due to the coexistence in most CM chondrites of CM clasts with a variety of aqueous alteration degrees (e.g., Kerraouch et al., 2021; Lentfort et al., 2021; Verdier-Paoletti et al., 2019). A remarkable xenolith is a large clast (at least 2 × 1 cm) metal-rich chondritic lithology was reported in Aguas Zarcas CM2 and interpreted as a unique carbonaceous chondrite with proposed affinities with both CM and CR chondrites (Kerraouch et al., 2021, 2022). The chondrule size and matrix abundance are significantly different from CM and CR chondrites, and are similar to those of CO3 chondrites. The bulk oxygen isotopic composition of this xenolith clast lies in between the CM and the CO clusters (Figure 11), close to compositions reported for Jbilet Winselwan and Dhofar 1619 CM2 chondrites, but its Cr, Ti, and Te isotopic

19455100, 0, Downloaded from https://onlinelibrary.wiley.com/doi/10.1111/maps.70233 by Portland State University, Wiley Online Library on [06/11/2026]. See the Terms and Conditions (https://onlinelibrary.wiley.com/terms-and-conditions) on Wiley Online Library for rules of use; OA articles are governed by the applicable Creative Commons License

compositions are best consistent with CM chondrites. This clast was interpreted as a C2 xenolith with CM affinities (Kerraouch et al., 2022).

DISCUSSION

Xenolith Abundances

The 18 new xenolith-bearing meteorites described in this work increase the number of known xenolith-bearing meteorites by 20%, for a total number of 107 (Table 3). A significant proportion of these meteorites contain xenoliths of various types. For instance, Isheyevo CB/CH contains at least three different types of ungrouped carbonaceous chondrite xenoliths (Bonal et al., 2010; Briani et al., 2009), Bholghati howardite contains CM2 and C2-ung xenoliths (Zolensky et al., 1996; Reid et al., 1990; this work), and DaG 319 ureilite contains xenoliths from at least four different parent bodies (angrite, OC, R, CI-like).

The 107 xenolith-bearing meteorites represent only 0.14% of the total collection of 79,000 meteorites registered in the Meteoritical Bulletin Database (https://www.lpi.usra.edu/meteor/) as of March 2026. It is possible that some meteorite groups contain meteorites originating from different planetesimals whose material share undistinguishable petrographic properties. This has been proposed, for instance, for CM chondrites (Sanderson et al., 2026). In that case, recognizing a CM xenolith in a CM chondrite would be impossible based on petrographic observations. It is also possible that small xenoliths whose petrography is relatively similar to their host (L and H chondrites, CVox and CVred chondrites, CV3 and CK3 chondrites, etc.) can be overlooked. The 0.13% xenolith occurrence must therefore be regarded as a lower limit.

This overall rarity hides a large variability among meteorite groups (Table 3). Xenoliths are exceedingly rare in ordinary chondrites, CO, CM, CV, and CK chondrites where they are present in ~0.1–0.2% of meteorites. In ordinary chondrites, xenolith occurrences are four times more frequent in LL than in H and L chondrites. This scales with the ~4 times higher relative abundance of brecciated meteorites within the LL group compared to the H and L groups (79% vs 23%, Bischoff et al., 2018). It is noteworthy that LL chondrites do not contain xenoliths from the CC reservoir, that only one such xenolith out of 12 known xenoliths has been described in L chondrites (in NWA 13177, this study), whereas carbonaceous chondrite xenoliths make up 79% of the 14 known xenoliths in H chondrites. A single xenolith-bearing meteorite has been identified in the relatively abundant R chondrite group (n = 346). No macroscopic xenolith has been convincingly evidenced in other chondrite groups, including groups containing large numbers of meteorites like EL (n = 240), EH (n = 224), and CR chondrites (n = 216). Many CR chondrites contain abundant dark inclusions, but these are best interpreted as cognate matrix-rich inclusions accreted on the CR parent body at the same time as the other CR chondrite components (e.g., Bischoff et al., 2006, and discussion above). The proportion of xenolith-bearing meteorites is higher in aubrites (2.1%), ureilites (4.4%, but ~100% of polymict ureilites), and HED achondrites (1.6% for the overall population, 4.2% of polymict eucrites and 6.5% of howardites) than in all chondrite groups (0 to 0.15% range, except 18% for CB and CH chondrites).

The vast majority of xenoliths are found in regolith breccia meteorites. These breccias, characterized by their elevated content of solar wind-implanted noble gases (and therefore also called gas-rich meteorites), originate from the surface of the asteroids where meteorites will naturally accumulate. Polymict ureilites, that are regolith breccias (although some of them do not contain solar wind implanted gases, see discussion in Goodrich et al., 2004), all contain xenoliths. All xenolith-bearing ordinary chondrites in which the noble gas content was measured are regolith (gas-rich) breccias (Abbott, Dimmitt, Magombedze, Ipiranga, Tysnes Island, Leighton, Tsukuba, Willard (b), Zag), except NWA 5764 (Gattacceca et al., 2017). The higher proportion of xenolith-bearing H chondrites compared to L and LL chondrites also aligns with the higher proportion of regolith breccias in the H group than in the LL and L groups (e.g., Bischoff et al., 2018; Osawa & Nagao, 2006), with 15.3%, 5.5%, and 3.0% occurrence, respectively (Bischoff et al., 2006). It is noteworthy that more xenoliths may be discovered in brecciated equilibrated ordinary chondrites, a meteorite population that we did not investigate but that contains a relatively high proportion of regolith breccias (Bischoff et al., 2018).

On the other hand, no xenoliths are known in meteorites from meteorite groups that have no regolith breccia members, like angrites or Martian meteorites. However, the proportion of xenolith-bearing meteorites in the regolith breccia members of a group is highly variable. Indeed, some chondrite groups in which most or all meteorites are regolith breccias (CR, R, CM) have no or very few xenolith-bearing members. The Rumuruti chondrite case is noteworthy since more than half of the Rumuruti chondrites are regolith breccias (Bischoff et al., 2011) but to date, a single xenolith, a melt rock of possible L chondrite parentage, has been described in these well-studied meteorites (Lunning et al., 2020). Some carbonaceous chondrite groups contain no xenoliths (CR, CV_{Ox}) or very few xenoliths (CV_{Red}, CK, CO, CM with ~0.1–0.2% occurrences).

19455100, 0, Downloaded from https://onlinelibrary.wiley.com/doi/10.1111/maps.70233 by Portland State University, Wiley Online Library on [06/11/2026]. See the Terms and Conditions (https://onlinelibrary.wiley.com/terms-and-conditions) on Wiley Online Library for rules of use; OA articles are governed by the applicable Creative Commons License

TABLE 3. Statistics of xenolith-bearing meteorites.

			CC xenoliths								NC xenoliths												
		f (‰)	CM2	CI-like[b]	C2-ung	CR2	CV_{Ox}	CO3	C[f]	Ach.	H	L	LL	OC	OC-Ach[h]	R	EH	EL	Ung. ferroan chondrite	Graphite-bearing	Angrite	Pallasite	Ach.
NC host	H	0.47	7	2	1[d]				1				1							1			1
	L	0.47	1												5					5			2
	LL[a]	1.62									3	2		1	3		1			3			2
	R	2.89										1											
	Ureilite-pmict	345		11[c]		1					1	1	1	1		3[e]	1	1	1		3[c]		
	Aubrite	20.8		1										1									
	Howardite	64.8	19		9[e]	1					1			1									
	Eucrite-pmict	41.6	13		4[e]			1			1											1	
	Diogenite	50.2	1																				
CC host	CH3	172		4					1[g]														
	CBa	222							1					2		2							
	CBb	161		2																			
	CV_{Red}	1.3					1																
	CK	1.7					1																
	CO3	2.5	2																				
	CM2	3.9							2	1													
	C-ung												1										

Note: *f*: fraction of xenolith-bearing meteorites within group (in ‰, *f* is the ratio of the number of xenolith-bearing meteorite in a group and the total number of meteorites in that group). Ach. = achondrite. The names of meteorites in each cell of this table are given in Table S11.

[a]The graphite-bearing clast in Adrar 003 L/LL chondrite is counted with LL chondrites.

[b]The "CI-like" clasts in polymict ureilites, HED achondrites, and CH3 are likely unrelated to CI1 meteorites and should be better referred to as C1 (see text).

[c]The ureilites DaG 164, DaG 165, DaG 319, DaG 665, DaG 976, DaG 999, and DaG 1000, all polymict ureilites containing CI-like clasts, were found within 5 km and are very likely paired. They were counted here as a single meteorite.

[d]Xenolith in Sahara 98645 originally described as CI-like (Patzek et al., 2018).

[e]It includes the xenoliths originally described as "CI-like" clasts (Patzek et al., 2018), and "CR2-like" (Zolensky et al., 1996), except for Yamato 793497.

[f]It includes xenoliths reported as C, C1/2, C2, and C3.

[g]Isheyevo (CB/CH) is counted as CH3.

[h]Achondrite derived from an OC protolith. The numbers provided are the numbers of meteorites of a given group containing a xenolith of a given group. Meteorites that contain different types of clasts (like Bholghati, that contains CM2 and C2-ung clasts) are counted several times. Therefore, to derive the number of xenolith-bearing meteorites regardless of the diversity of xenoliths that individual meteorites may contain, the following numbers must be subtracted from the sum of all the table cells: 16 for HED, 3 for CB chondrites, 2 for LL chondrites, and 14 for polymict ureilites.

19455100, 0, Downloaded from https://onlinelibrary.wiley.com/doi/10.1111/maps.70233 by Portland State University, Wiley Online Library on [06/11/2026]. See the Terms and Conditions (https://onlinelibrary.wiley.com/terms-and-conditions) on Wiley Online Library for rules of use; OA articles are governed by the applicable Creative Commons License

If we restrict our reasoning to regolith breccia meteorites, we still see striking differences in xenolith abundance between meteorite groups, from about 100% in polymict ureilites to almost null in Rumuruti chondrites. A key factor controlling the xenolith abundance in an asteroid regolith is likely the age of the regolith. Indeed, assuming a broadly constant influx of meteorites, the xenolith density will increase with the age of the regolith. It is noteworthy that the meteorite groups with the highest proportion of xenolith-bearing members and the highest diversity of xenoliths (with xenoliths from different sources sometimes found at the infra cm-scale) are from supposedly large parent bodies. HED originate from asteroid Vesta that has a diameter of ~530 km. A large size, of at least 1000 km in diameter, has been proposed for the ureilite parent body (e.g., Nabiei et al., 2018), and the aubrite parent body (e.g., Cartier et al., 2024). Gravitational focusing of meteoroids cannot account for this observation since it is negligible even for asteroids the size of Vesta. A possible explanation for this observation is that larger asteroids are expected to retain regolith more efficiently than smaller ones. Old regoliths can incorporate xenoliths over long periods, and impact gardening can mix efficiently xenoliths of different origins. For smaller asteroids, regolith accumulation and maturation is limited by ejection of surface material during impacts (e.g., Hsu et al., 2022).

The CB and CH groups, with ~20% of xenolith-bearing members are a special case where the high abundance of xenoliths can be directly linked to a petrogenesis that is markedly different from other meteorites, with parent body assembly in a vapor-melt plume around 5 Myr after the start of solar system formation (e.g., Bollard et al., 2015; Krot et al., 2005; Wölfer et al., 2023). This process led to a mixture of collisional products and of a minor fraction of nebular products that include the matrix-rich clasts described here, but also a population of porphyritic chondrules (Malhé et al., 2024). Therefore, compared to other xenoliths, the xenoliths in CB and CH chondrites were not transferred between two asteroids under the form of meteoroids, but are the direct results of reaccretion of debris following the collision of two asteroids.

Xenolith Implantation

It is noteworthy that in most xenolith-bearing meteorites characterized in this study, the contact between the xenoliths and the host lithology show no shock features such as deformation or localized melting, and the clasts themselves do not show shock features either. The same applies to many xenoliths described in the literature (see, e.g., Marrocchi et al., 2021). The fine-grained matrix of all the CM2 and C2-ung clasts that we studied in howardites and polymict eucrites yielded EPMA totals in the 77.4–89.5 wt% range, indicating that the clasts are hydrated. Raman spectroscopy of 16 CI-like and 14 CM-like hydrated xenoliths in ureilites, eucrites, and howardites, shows that the xenoliths were not significantly heated during their implantation (Visser et al., 2018). Examples of xenoliths shocked during their implantation have been described previously, based on the observation of shock effects like silicate darkening (e.g., a shocked LL5 clast in Dimmitt H3-5, Rubin et al., 1983), or by the dehydration of the fine-grained chondritic matrix revealed by the absence phyllosilicates (e.g., clast PV3 in Plainview H5, Rubin & Bottke, 2009). But in most cases, xenoliths are unshocked and must have been implanted at relatively low speed. For instance, the preservation of intact organic molecules, the abundance of volatiles and the presence of phyllosilicates in the CM2 clasts in Jodzie howardite preclude heating above about 200°C for these clasts (Bunch et al., 1979). The maximum survivable collision speed for a chondrite is in the 1.5–2 km s^{-1} range (Bland, 2001). Modeling shows low collision speed below 2 km s^{-1}, although relatively rare, do occur for about 5% of collisions between main belt asteroids (e.g., Bottke Jr. et al., 1994). The unshocked xenoliths may originate from this ~5% fraction of impactors that has a low collision velocity. A similar conclusion was reached by Gounelle et al. (2003) about the carbonaceous microxenoliths in howardites, that may represent the 10% fraction of asteroidal dust colliding with Vesta at speeds below 1 km s^{-1} (Gounelle et al., 2003). However, a small fraction of an impactor with high speed may be spalled off the rear side of the impactor and reach the surface with a lower speed (Melosh, 1989), providing an alternative mechanism for the implantation of unshocked xenoliths. Also, the orbit of small meteoroids in the mm-size range can be efficiently circularized by the Poynting–Robertson effect over a Myr time scale, providing another mechanism for low-speed collision with asteroids. Notable exceptions to this low-velocity incorporation of the xenoliths are the H chondrite clasts we observed in NWA 3197 howardite and NWA 10674 polymict eucrite. These clasts show evidence for high shock, like mosaicism in olivine, and are mantled by a 1-mm thick layer of eucrite melt rock, indicating a highly energetic incorporation of the clasts in the host eucrite/howardite lithologies.

It is noteworthy that the largest chondritic xenoliths are chondrites of petrologic type 3 and above: 1 × 1.5 cm in size for a R4 clast in Bencubbin CBa (Isa et al. 2014), >5.4 cm^2 of exposure for a H6 xenolith in St-Mesmin LL6 chondrite (Dood, 1974), >16 cm^3 for a L4 xenolith in NWA 5764 LL6 (Gattacceca et al., 2017), >100 cm^3 for a H3 xenolith in NWA 16109 LL3 (this work), and up to 8 × 8 × 5 cm for a LL7 clast in NWA 7531 C-ung

19455100, 0, Downloaded from https://onlinelibrary.wiley.com/doi/10.1111/maps.70233 by Portland State University, Wiley Online Library on [06/11/2026]. See the Terms and Conditions (https://onlinelibrary.wiley.com/terms-and-conditions) on Wiley Online Library for rules of use; OA articles are governed by the applicable Creative Commons License

(Bunch et al., 2013). Conversely, chondritic xenoliths of petrologictype 1 and 2 are most often inframillimetric. This is in line with the more robust mechanical behaviour of metamorphosed chondrites, ordinary chondrites in particular, compared to the friable aqueously altered chondrites like CM2 and CI1 (Pohl and Britt, 2020). Therefore, there is very likely a strong control of the mechanical properties of the xenolith material on the size of its precursor meteoroid and its ability to survive collision and be implanted as a xenolith.

Xenoliths and the NC/CC Dichotomy

Chondritic xenoliths (including a few ones with igneous texture but chondritic composition) are dominant in the xenolith population. They represent 98% and 74% of the xenoliths in CC and NC host meteorites, respectively. Xenoliths from both the NC and CC reservoirs are found in meteorites from both reservoirs. Xenoliths from the CC and NC reservoirs are found in similar abundances, in 53% and 47% of xenolith-bearing meteorites, respectively. However, CC xenoliths are ultra-dominant in CC meteorites where they represent 88% of xenoliths. There are only very few occurrences of NC xenoliths in CC meteorites: OC3 and R clasts in Weatherford and Bencubbin CBa (Hutchison, 1986; Isa et al., 2014; Prinz et al., 1993; Weisberg et al., 1990) and angular LL7 clasts in NWA 7531 C-ung (Bunch et al., 2013). The attribution of these xenoliths to the NC reservoir is well established by their oxygen isotopic composition (Bunch et al., 2013; Clayton & Mayeda, 1978; Isa et al., 2014; Prinz et al., 1993). The deficit in CC meteorites with NC xenolith may reflect the fact that the outer belt, that hosts the majority of CC-related asteroids (with spectral types Ch, Cgh, B, C, Cb, Cg) is depleted in NC-asteroids (with spectral type S), whereas the middle belt, that hosts the majority of NC-asteroids is still dominated by CC-asteroids (e.g., Anderson et al., 2025).

Age of Xenolith Implantation

In the absence of strong shock effects during implantation, the age the implantation is difficult to estimate precisely using isotopic dating. To our knowledge, implantation ages of xenoliths have never been measured directly. In view of the long collisional history of the asteroid belt, the implantation of xenoliths likely extends for most of the solar system history, and may vary among meteorite groups (e.g., Goodrich et al., 2021).

In a few cases where clasts in chondrites are mantled by fine-grained matrix, such as the achondritic clasts in NWA 12651 (Ebert et al., 2019), or in NWA 15116 (the present study), an implantation during the accretion of the chondritic parent body is likely. In other instances, the preservation of equilibrated chondritic xenoliths of lower petrologic type than their chondritic host (e.g., the L4 clasts in the LL6 NWA 5764 [Gattacceca et al., 2017]) indicate implantation after thermal metamorphism of the host, that is several tens of Myr after solar system formation (e.g., Blackburn et al., 2017).

We note that in CO, CK, and CV_{Red} chondrites, the chondritic xenoliths always belong to the same clan as the host chondrite: CO-CM breccias (NWA 15819 and NWA 17518), CK3-CV_{Ox}3 breccias (Camel Donga 003), CV_{Ox}3-CV_{Red}3 breccias (Vigarano). These xenoliths are also relatively large even for lithologies that are relatively friable like CM chondrites: the two CM2 clasts we described in CO3 chondrites are both several mm in size, the xenolith with CM affinities in Aguas Zarcas is at least 2×1 cm in size, the CV_{Ox}3 clasts in Camel Donga CK3 are cm-sized (Alevy et al., 2025), and the CV_{Ox}3 clast in Vigarano CV_{Red}3 is 2×1 cm in size (Krot et al., 2000). Chondrite clans contain chondrite groups whose parent planetesimals were formed over a narrow range of heliocentric distance, as suggested by mineralogical, chemical, and isotopic similarities (e.g., Weisberg et al., 2006). The observation that implantation of xenoliths within a clan was more frequent and led to the implantation of large xenoliths suggests that this implantation occurred while the parent bodies of this clan were still orbiting in a relatively narrow range of heliocentric distance. Indeed, orbital proximity would increase the likelihood of exchange of material at low collisional speed between these parent bodies. This has the important implication that the implantation of these large xenoliths within a clan likely occurred before the major orbital disturbance of asteroids triggered by the formation of Jupiter a few Myr after the formation of the solar system.

However, the majority of xenoliths were not implanted in an asteroid belonging to the same clan. For these xenoliths, the broad match, described in the previous section, between the overall xenolith population and the present-day architecture of the asteroid belt suggests an implantation occurring mostly after the major redistribution of asteroids triggered by the giant planet formation. The unshocked nature of CC xenoliths in NC meteorites (and vice-versa) also favors an implantation after the two asteroid reservoirs were mixed. Indeed, a direct exchange between the two still separated reservoirs would imply very high collision velocities and the non-preservation of pristine exchanged material, unless gas-drag was still efficient enough to circularize the meteoroid orbits.

The transit durations of xenoliths between their original parent body to their host parent body have been estimated for a CM2 clast in Jodzie howardite (Bunch

19455100, 0, Downloaded from https://onlinelibrary.wiley.com/doi/10.1111/maps.70233 by Portland State University, Wiley Online Library on [06/11/2026]. See the Terms and Conditions (https://onlinelibrary.wiley.com/terms-and-conditions) on Wiley Online Library for rules of use; OA articles are governed by the applicable Creative Commons License

et al., 1979), for the CM2 clast in Plainview H3-5 (Wilkening & Clayton, 1974), and for the L4 clast in NWA 5764 LL6 (Gattacceca et al., 2017) by looking for a possible excess of cosmogenic ^{21}Ne in the xenolith compared to the host lithology that would reflect a pre-irradiation of the xenolith during its transit. In all these meteorites, no significant ^{21}Ne excess was measured in the xenoliths. For Plainview and NWA 5764, the CRE durations in the xenolith and the host were identical within uncertainty and imply short xenolith transit times of 0.1 ± 0.6 Myr for Plainview and 0.1 ± 8.1 Myr for NWA 5764 (although the uncertainty is relatively high for NWA 5764). For the CM2 clast in Plainview, the short transfer age further suggests that the clast was incorporated after the implantation of the CC asteroids in the main asteroid belt.

Xenolith and Meteorite Groups

The relative abundances of meteorite groups in the xenolith population and in the meteorite collection are markedly different. A few chondrite groups are absent from the xenolith population: K, CB, CH, CL chondrites. This material is also very rare in the meteorite collection, with only 4, 28, 29, and 7 meteorites, respectively. Brachinites, martian and lunar meteorites, as well as iron meteorites, are also absent from the xenolith population. On the other hand, CM material represents less than 1% of meteorites (an upper limit in view of the strong under-declaration of ordinary chondrites) but 40% of xenoliths, and CI chondrite material represents less than 0.01% of meteorites but 25% of xenoliths. The situation is opposite for ordinary chondrites that are more abundant in the meteorite collection (a lower limit of 85%) than in the xenolith population (25%). However, fragmentation and ablation in the terrestrial atmosphere makes meteorite statistics a poor reflect of the asteroid population, with underrepresentation of friable material like CM and CI (e.g., Brož et al., 2024b), and overrepresentation of hard material like iron meteorites. Therefore, the xenolith statistics should rather be compared to the asteroid statistics, but this discussion is limited by the absence of precise matches between asteroid spectral types and meteorite groups.

A significant proportion of xenoliths does not seem to be represented in the existing meteorite groups and can be qualified as ungrouped. This includes in particular the relatively abundant "CI-like" clasts reported in polymict ureilites, HED achondrites, and CH3 chondrites. These clasts are not type 1 material and their oxygen isotopic composition, when it has been measured, is different from CI1 chondrites. Therefore, as previously observed (Patzek et al., 2018; Visser et al., 2019), these clasts cannot be linked to CI1 chondrites and should be better referred to as ungrouped C2 clasts. Ungrouped xenoliths also include, for example, some achondritic clasts in ordinary chondrites, the reduced ordinary chondrite material found in Cumberland Falls aubrite, or the type 3 ordinary chondrite clasts in CBa chondrites. Overall, the proportion of ungrouped xenoliths amounts to at least 40% of the total xenolith population. The meteorite collection represents material that fell on Earth over relatively short periods: the last 200 years for falls, the last ~200 kyr for Antarctica meteorites (e.g., Welten et al., 2006), and a maximum of ~2 Myr for meteorites from Atacama (e.g., Drouard et al., 2019; Sadaka et al., 2026). This material is provided to the Earth mostly by young asteroid families formed in the last ~50 Myr (Brož et al., 2024a). Therefore, it is not surprising that many xenoliths are not represented in the groups defined based on the meteorite collection, if they were implanted more than ~50 Myr ago, which seems likely in view of the protracted collisional history of the asteroid belt.

CONCLUSIONS

We provide a review of the occurrence of macroscopic xenoliths in meteorites, based on a critical review of the literature and a search for new xenolith-bearing meteorites. An exhaustive survey of large meteorite slices in the MNHN collection revealed no new xenolith-bearing meteorites. An exhaustive survey of the CEREGE meteorite collection (except for equilibrated ordinary chondrites), and the study of recently classified meteorites selected from other collections, allowed identifying 18 new meteorites containing xenoliths. This confirms that macroscopic xenoliths are exceedingly rare, and better looked for in new samples from collections with an ongoing classification activity, rather than in large collections of historical, already well-studied meteorites. This study brings the total of confirmed xenolith-bearing meteorites to 107, which represents 0.14% of the total number of meteorites.

Most of the new xenoliths described in the present work are xenolith lithologies that had already been described previously, such as CM2 xenoliths in HED achondrites and CI-like xenoliths in polymict ureilites and CH3 chondrites. However, we also report less usual occurrences such as a graphite-rich granoblastic xenolith in GRO 06054 (LL3) or a 100 cm^3 H3-related chondritic clast in NWA 16109 (LL3). A few exceptional xenolith/host meteorite pairs are reported. NWA 13177 (L3-6) contains a CM2 clast. This is the first description of a carbonaceous chondrite xenolith in an L chondrite. We also report the first description of CO3 chondrites containing CM2 xenoliths (NWA 15819 and NWA 17518). CM2 clasts were known only in H chondrites and HED achondrites so far. We expand the diversity of

19455100, 0, Downloaded from https://onlinelibrary.wiley.com/doi/10.1111/maps.70233 by Portland State University, Wiley Online Library on [06/11/2026]. See the Terms and Conditions (https://onlinelibrary.wiley.com/terms-and-conditions) on Wiley Online Library for rules of use; OA articles are governed by the applicable Creative Commons License

known xenoliths in HED achondrites where only "CI-like" and CM2 clasts had been described so far: NWA 17470 polymict eucrite contains a CO3 clast (together with CM2 clasts), NWA 10472 contains a pallasite clast, and NWA 3197 and NWA 10674 contain H chondrite clasts. We also identified a centimeter-sized achondritic xenolith formed by crystallization of a differentiated melt in NWA 15116 LL3 chondrite.

Based on mineralogy, texture, oxygen isotopic composition, we interpret the population of clasts previously described in HED meteorites as "CR2-like" (Zolensky et al., 1996) or "CI-like" (Patzek et al., 2018) as type 2 ungrouped carbonaceous chondrite material. The same may be applicable to most "CI-like" clasts in polymict ureilites and CH3 chondrites. At least 40% of xenoliths cannot be readily assigned to a known meteorite group and must be classified as ungrouped. This suggests that they sampled a flux of meteoroids different from the present-day one. This is in agreement with the fact that meteorites are provided by asteroid families formed by recent (~<50 Ma) collisions in a favorable location close to a dynamical resonance (Brož et al., 2024), and as such, do not capture the full variety of asteroidal material. Xenoliths are therefore a valuable source of material not represented in the meteorite collection.

Xenoliths are found mostly in regolith breccia meteorites. They seem to be more frequent in meteorites from supposedly large parent bodies (ureilites, aubrites, HED achondrites) than in meteorites from smaller parent bodies (chondrites), in agreement with the possibility for large bodies to maintain an older and more mature regolith than smaller ones.

Although the relatively low total number of xenolith-bearing meteorites (n = 107) precludes a robust statistical interpretation in terms of clasts delivery dynamics within the asteroid belt, a few general observations can be made. Chondritic xenoliths represent 95% of occurrences, in line with a higher number of chondritic asteroids with respect to achondritic ones. Xenoliths from the CC and NC reservoirs are found in host meteorites from both reservoirs, and a majority was implanted at low collisional speed (<~2 km s^{-1}). The low proportion of CC-meteorites with NC-xenoliths can be related to the fact that the present day outer asteroid belt hosts the majority of CC asteroids but is depleted in NC asteroids. This observation and the low collisional speed between CC and NC materials suggest that most xenoliths were implanted after the main asteroid scattering event triggered by the formation of Jupiter a few Myr after the formation of the solar system. Conversely, chondritic xenoliths in CV, CK, and CO chondrites are all from a member of the same clan (CV_{Ox} in CV_{Red}, CV_{Ox} in CK, CM in CO) and relatively large suggesting that they were implanted while their parent bodies were still orbiting in a narrow range of heliocentric distance, that is, before the main asteroid scattering event triggered by the formation of Jupiter. Eventually, a few xenoliths were incorporated on their host parent body during its initial accretion phase. Xenolith implantation seems to have been a universal and protracted phenomenon, active for most of solar system history.

Acknowledgments—We thank Markus Patzek and an anonymous reviewer for their relevant and constructive comments. This work was supported by the CLASTS project (grant ANR-22-CE49-0013) of the French Agence Nationale de la Recherche, and the French Programme National de Planétologie (INSU/CNES). R.T. acknowledges funding from the University of Manchester and the UK Science and Technology Facilities Council (STFC) (grant #ST/S002170/1) for funding the LA-ICP-MS facility in Manchester, and the Royal Society for funding the benchtop SEM in Manchester. We thank Fabien Kutz for providing material for this study. We acknowledge sample loans from CEREGE, MNHN Paris, Appalachian State University, University of Washington, the Cascadia Meteorite laboratory of Portland State University, and ANSMET. The US Antarctic meteorite samples are recovered by the ANSMET program, which has been funded by NSF and NASA, and characterized and curated by the Department of Mineral Sciences of the Smithsonian Institution and Astromaterials Acquisition and Curation Office at NASA Johnson Space Center. We thank Jolantha Eschrig for detecting the graphite-rich xenolith in GRO 06054. Open access publication funding provided by COUPERIN CY26.

Data Availability Statement—The data that supports the findings of this study are available in the Supporting Information of this article.

Editorial Handling—Dr. Christopher Herd

REFERENCES

Agee, C. B., Ross, A. J., Spilde, M. N., and Ziegler, K. 2024. Hassi el Madani 002: Ungrouped Polymict Achondrite With Two Distinct Oxygen Isotope Lithologies. *55th Lunar and Planetary Science Conference*, abstract #2074.

Alevy, E. G., Dunn, T. L., Krot, A. N., Cardon-Pilotaz, P., and Gross, J. 2025. Multiple CV Chondrite Lithologies in Camel Donga 003 (CK3): Implications for the CV and CK Parent Bodies. *Meteoritics & Planetary Science* 60: 1336–64.

Alfing, J., Patzek, M., and Bischoff, A. 2019. Modal Abundances of Coarse-Grained (>5 μm) Components within CI-Chondrites and their Individual Clasts – Mixing of Various Lithologies on the CI Parent Body(ies). *Geochemistry* 79: 125532.

Anderson, S. E., Vernazza, P., and Brož, M. 2025. Different Arrival Times of CM- and CI-Like Bodies from the Outer

19455100, 0, Downloaded from https://onlinelibrary.wiley.com/doi/10.1111/maps.70233 by Portland State University, Wiley Online Library on [06/11/2026]. See the Terms and Conditions (https://onlinelibrary.wiley.com/terms-and-conditions) on Wiley Online Library for rules of use; OA articles are governed by the applicable Creative Commons License

Solar System in the Asteroid Belt. *Nature Astronomy* 9: 1464–75. https://doi.org/10.1038/s41550-025-02635-2.
Bischoff, A., Dyl, K. A., Horstmann, M., Ziegler, K., Wimmer, K., and Young, E. D. 2013. Reclassification of Villalbeto de la Peña—Occurrence of a Winonaite-Related Fragment in a Hydrothermally Metamorphosed Polymict L Chondritic Breccia. *Meteoritics & Planetary Science* 48: 628–640.
Bischoff, A., Geiger, T., Palme, H., Spettel, B., Schultz, L., Scherer, P., Schluter, J., and Lkhamsuren, J. 1993. Mineralogy, Chemistry, and Noble Gas Contents of Adzhi-Bogdo- an LL3-6 Chondritic Breccia with L-Chondritic and Granitoidal Clasts. *Meteoritics* 28: 570–78.
Bischoff, A., Palme, H., Schultz, L., Weber, D., Weber, H. W., and Spettel, B. 1993. Acfer 182 and Paired Samples, an Iron-Rich Carbonaceous Chondrite: Similarities with ALH 85085 and Relationship to CR Chondrites. *Geochimica et Cosmochimica Acta* 57: 2631–48.
Bischoff, A., Schleiting, M., Wieler, R., and Patzek, M. 2018. Brecciation Among 2280 Ordinary Chondrites – Constraints on the Evolution of Their Parent Bodies. *Geochimica et Cosmochimica Acta* 238: 516–541. https://doi.org/10.1016/j.gca.2018.07.020.
Bischoff, A., Scott, E. R. D., Metzler, K., and Goodrich, C. A. 2006. Nature and Origins of Meteoritic Breccias. In *Meteorites and the Early Solar System II*, edited by D. S. Lauretta, and H. Y. McSween, Jr., 679–712. Tucson: University of Arizona Press.
Bischoff, A., Vogel, N., and Roszjar, J. 2011. The Rumuruti Chondrite Group. *Chemie der Erde* 71: 101–133.
Blackburn, T., Alexander, C. M. O'D., Carlson, R., and Elkins-Tanton, L. T. 2017. The Accretion and Impact History of the Ordinary Chondrite Parent Bodies. *Geochimica et Cosmochimica Acta* 200: 201–217.
Bland, P. A. 2001. Quantification of Meteorite Infall Rates from Accumulations in Deserts, and Meteorite Accumulations on Mars. In *Accretion of Extraterrestrial Matter throughout Earth's History*, edited by B. Peucker-Ehrenbrink, and B. Schmitz, 267–303. New York: Kluwer Academic/Plenum Publishers.
Bollard, J., Connelly, J. N., and Bizzarro, M. 2015. Pb-Pb Dating of Individual Chondrules from the CBa Chondrite Gujba: Assessment of the Impact Plume Formation Model. *Meteoritics & Planetary Science* 50: 1197–1216.
Bonal, L., Huss, G. R., Krot, A. N., and Nagashima, K. 2010. Chondritic Lithic Clasts in the CB/CH-Like Meteorite Isheyevo: Fragments of Previously Unsampled Parent Bodies. *Geochimica et Cosmochimica Acta* 74: 2500–2522.
Bonal, L., Quirico, E., Flandinet, L., and Montagnac, G. 2016. Thermal History of Type 3 Chondrites from the Antarctic Meteorite Collection Determined by Raman Spectroscopy of their Polyaromatic Carbonaceous Matter. *Geochimica et Cosmochimica Acta* 189: 312–337.
Bottke, W. F., Jr., Nolan, M., Greenberg, R., and Kolvoord, R. A. 1994. Velocity Distribution among Colliding Asteroids. *Icarus* 107: 255–268.
Bottke, W. F., Brož, M., O'Brien, D. P., Campo Bagatin, A., Morbidelli, A., and Marchi, S. 2015. The Collisional Evolution of the Main Asteroid Belt. In *Asteroids IV*, edited by P. Michel, F. E. DeMeo, and W. F. Bottke, 701–724. Tucson: Univ. of Arizona. https://doi.org/10.2458/azu_uapress_9780816532131-ch036.
Bouden, N., Villeneuve, J., Marrocchi, Y., Deloule, E., Füri, E., Gurenko, A., Piani, L., Thomassot, E., Peres, P., and Fernandes, F. 2021. Triple Oxygen Isotope Measurements by Multi-Collector Secondary Ion Mass Spectrometry. *Frontiers in Earth Science* 8: 9.
Brearley, A. J., and Prinz, M. 1992. CI Chondrite-like Clasts in the Nilpena Polymict Ureilite: Implications for Aqueous Alteration Processes in CI Chondrites. *Geochimica et Cosmochimica Acta* 56: 1373–86.
Briani, G., Gounelle, M., Bourot-Denise, M., and Zolensky, M. 2012. Xenoliths and Microxenoliths in H Chondrites: Sampling the Zodiacal Cloud in the Asteroid Main Belt. *Meteoritics & Planetary Science* 47: 880–902.
Briani, G., Gounelle, M., Marrocchi, Y., Mostefaoui, S., Leroux, H., Quirico, E., and Meibom, A. 2009. Pristine Extraterrestrial Material with Unprecedented Nitrogen Isotopic Variation. *Proceedings of the National Academy of Science* 106: 10522–27.
Bridges, J. C., and Hutchison, R. 1997. A Survey of Clasts and Large Chondrules in Ordinary Chondrites. *Meteoritics & Planetary Science* 32: 389–394.
Bridges, J. C., Hutchison, R., Franchi, I. A., Alexander, C. M. O'D., and Pillinger, C. T. 1995. A Feldspar-Nepheline Achondrite Clast in Parnallee. *Proceedings, National Institute of Polar Research Symposium on Antarctic Meteorites* 8: 195–203.
Brož, M., Vernazza, P., Marsset, M., Binzel, R. P., DeMeo, F., Birlan, M., Colas, F., et al. 2024b. Source Regions of Carbonaceous Meteorites and Near-Earth Objects. *Astronomy and Astrophysics* 689: A183.
Brož, M., Vernazza, P., Marsset, M., DeMeo, F. E., Binzel, R. P., Vokrouhlicky, D., and Nesvorny, D. 2024a. Young Asteroid Families as the Primary Source of Meteorites. *Nature* 634: 566–571.
Buchanan, P. C., Zolensky, M. E., and Reid, A. M. 1993. Carbonaceous Chondrite Clasts in the Howardites Bholghati and EET87513. *Meteoritics* 28: 659–682.
Buchanan, P. C., Zolensky, M. E., and Reid, A. M. 1997. Petrology of Allende Dark Inclusions. *Geochimica et Cosmochimica Acta* 61: 1733–43.
Bunch, T. E., Chang, S., Frick, U., Neil, J., and Moreland, G. 1979. Carbonaceous Chondrites - I. Characterization and Significance of Carbonaceous Chondrite (CM) Xenoliths in the Jodzie Howardite. *Geochimica et Cosmochimica Acta* 43: 1727–42.
Bunch, T. E., Rumble, I. I. I. D., Wittke, J. H., Irving, A. J., and Pitt, D. 2010. Multilithologic, ExtraOrdinary Chondrite Northwest Africa 5717: Further Evidence for Unrecognized Metal-Poor, Non-Carbonaceous Chondritic Parent Bodies. *41st Lunar and Planetary Science Conference*, abstract #1280.
Bunch, T., Wittke, J. H., Irving, A. J., and Rumble, D., III. 2013. Unique Polymict Breccia Northwest Africa 7531 Composed of Recrystallized LL Clasts Associated with CR Metachondrite Material: Evidence for Highly Equilibrated Ordinary Chondritic Impactors onto the CR Chondrite Parent Body. *44th Lunar and Planetary Science Conference*, abstract #2214.
Burbine, T. H., McCoy, T. J., Gladman, B., and Keil, K. 2002. Meteoritic Parent Bodies: Their Number and Identification. In *Asteroids III*, edited by J. R. W. Bottke, A. Cellino, P. M. Paolicchi, and R. P. Binzel, 653–667. Tucson: University of Arizona Press.
Cartier, C., Llado, L., Pirotte, H., Tissandier, L., Namur, O., Collinet, M., Wang, s.-J., and Charlier, B. 2024. Partitioning of Nickel and Cobalt between Metal and

19455100, 0, Downloaded from https://onlinelibrary.wiley.com/doi/10.1111/maps.70233 by Portland State University, Wiley Online Library on [06/11/2026]. See the Terms and Conditions (https://onlinelibrary.wiley.com/terms-and-conditions) on Wiley Online Library for rules of use; OA articles are governed by the applicable Creative Commons License

Silicate Melts: Expanding the Oxy-Barometer to Reducing Conditions. *Geochimica et Cosmochimica Acta* 367: 142–164.
Chaumard, N., Devouard, B., Bouvier, A., and Wadhwa, M. 2014. Metamorphosed Calcium-Aluminum-Rich Inclusions in CK Carbonaceous Chondrites. *Meteoritics & Planetary Science* 49: 419–452.
Christophe Michel-Lévy, M. 1988. A New Component of the Mezö-Madaras Breccia: A Microchondrule- and Carbon-Bearing L-Related Chondrite. *Meteoritics* 23: 45–48.
Clayton, R. N., and Mayeda, T. K. 1978. Multiple Parent Bodies of Polymict Brecciated Meteorites. *Geochimica et Cosmochimica Acta* 42: 325–27.
Clayton, R. N., and Mayeda, T. K. 1988. Formation of Ureilites by Nebular Processes. *Geochimica et Cosmochimica Acta* 52: 1313–18.
Corrigan, C. M., and Lunning, N. G. 2016. A Variety of Melt Clasts in Ordinary Chondrite Breccia Meteorite Hills (MET) 01004. *47th Lunar and Planetary Science Conference*, abstract #2729.
Corrigan, C. M., Lunning, N. G., Friedrich, J. M., and McCoy, T. J. 2015. An H Chondrite Clast in an LL Chondrite: Impact Melt or Incipient Partial Melt? *78th Annual Meeting of the Meteoritical Society*, abstract #6005.
Dauphas, N., Hopp, T., and Nesvorny, D. 2024. Bayesian Inference on the Isotopic Building Blocks of Mars and Earth. *Icarus* 408: 115805.
Deienno, R., Izidoro, A., Morbidelli, A., Gomes, R. S., Nesvorný, D., and Raymond, S. 2018. Excitation of a Primordial Cold Asteroid Belt as an Outcome of Planetary Instability. *The Astrophysical Journal* 864: 50.
Delbo, M., Walsh, K., Bolin, B., Avdellidou, C., and Morbidelli, A. 2017. Identification of a Primordial Asteroid Family Constrains the Original Planetesimal Population. *Science* 357: 1026–29.
Dodd, R. T., Jr., Van Schmus, W. R., and Koffman, D. M. 1967. A Survey of Unequilibrated Ordinary Chondrites. *Geochimica et Cosmochimica Acta* 31: 921–951.
Dodd, R. T. 1974. Petrology of the St. Mesmin Chondrite. *Contributions to Mineralogy and Petrology* 46: 129–145.
Downes, H., Mittlefehhldt, D. W., Kita, N. T., and Valley, J. W. 2008. Evidence from Polymict Ureilite Meteorites for a Disrupted and re-Accreted Single Ureilite Parent Asteroid Gardened by Several Distinct Impactors. *Geochimica et Cosmochimica Acta* 72: 4825–44.
Drouard, A., Gattacceca, J., Hutzler, A., Rochette, P., Braucher, R., Bourlès, D., ASTER Team, et al. 2019. The Meteorite Flux of the Past 2 m.y. Recorded in the Atacama Desert. *Geology* 47: 673–76.
Dyl, K. A., Bischoff, A., Ziegler, K., Young, E. D., Wimmer, K., and Bland, P. A. 2012. Early Solar System Hydrothermal Activity in Chondritic Asteroids on 1-10-Year Timescales. *Proceedings on the National Academy of Sciences* 6: 18306–11.
Ebert, S., Patzek, M., Lentfort, S., and Bischoff, A. 2019. Accretion of Differentiated Achondritic and Aqueously Altered Chondritic Materials in the Early Solar System—Significance of an Igneous Fragment in the CM Chondrite NWA 12651. *Meteoritics & Planetary Science* 54: 2985–95.
Ebert, S., Bischoff, A., Harries, D., Lentfort, S., Barrat, J.-A., Pack, A., Gattacceca, J., Visser, R., Schmid-Beurmann, P., and Kimpel, S. 2018. Northwest Africa 11024—A Heated and Dehydrated Unique Carbonaceous (CM) Chondrite. *Meteoritics & Planetary Science* 54: 328–356. https://doi.org/10.1111/maps.13212.
Endress, M., Keil, K., Bischoff, A., Spettel, B., Clayton, R. N., and Mayeda, T. K. 1994. Origin of Dark Clasts in the Acfer 059/EI Djouf 001 CR2 Chondrite. *Meteoritics* 29: 26–40.
Eschrig, J., Bonal, L., Mahlke, M., Carry, B., Beck, P., and Gattacceca, J. 2022. Investigating S-Type Asteroid Surfaces through Reflectance Spectra of Ordinary Chondrites. *Icarus* 381: 115012. https://doi.org/10.1016/j.icarus.2022.115012.
Floyd, C. J., Benito, S., Martin, P.-E., Jenkins, L. E., Dunham, E., Daly, L., and Lee, M. R. 2024. Chondrule Sizes within the CM Carbonaceous Chondrites and Measurement Methodologies. *Meteoritics & Planetary Science* 59: 2769–88.
Fredriksson, K., Jarosewich, E., and Wlotzka, F. 1989. Study Butte: A Chaotic Chondrite Breccia with Normal H-Group Chemistry. *Zeitschrift für Naturforschung A* 44a: 945–962.
Funk, C., Bischoff, A., and Schlüter, J. 2011. Xenoliths in Carbonaceous and Ordinary Chondrites. *74th Annual Meteoritical Society Meeting*, abstract #5318.
Gattacceca, J., Bonal, L., Sonzogni, C., and Longerey, J. 2020. CV Chondrites: More than One Parent Body. *Earth and Planetary Science Letters* 147: 116467. https://doi.org/10.1016/j.epsl.2020.116467.
Gattacceca, J., Gounelle, M., Devouard, B., Barrat, J.-A., Bonal, L., King, A. J., Maurel, C., Beck, P., Roskosz, M., et al. 2025. Oued Chebeika 002: A New CI1 Meteorite Linked to Outer Solar System Bodies. *Meteoritics & Planetary Science* 60: 1684–1947. https://doi.org/10.1111/maps.14359.
Gattacceca, J., Krzesinska, A. M., Marrocchi, Y., Meier, M. M., Bourot-Denise, M., and Lenssen, R. 2017. Young Asteroid Mixing Revealed in Ordinary Chondrites: The Case of NWA 5764, a Polymict LL Breccia with L Clasts. *Meteoritics & Planetary Science* 52: 2289–2304.
Goodrich, C. A., Kring, D. A., and Greenwood, R. C. 2021. Xenoliths in Ordinary Chondrites and Ureilites: Implications for Early Solar System Dynamics. *Meteoritics & Planetary Science* 56: 1949–87.
Goodrich, C. A., Scott, E. R. D., and Fioretti, A. M. 2004. Ureilitic Breccias: Clues to the Petrologic Structure and Impact Disruption of the Ureilite Parent Asteroid. *Geochemistry* 64: 283–327.
Gounelle, M., Zolensky, M., Liou, J.-C., Bland, P. A., and Alard, O. 2003. Mineralogy of Carbonaceous Chondritic Microclasts in Howardites: Identification of C2 Fossil Micrometeorites. *Geochimica et Cosmochimica Acta* 67: 507–527.
Grant, H., Tartèse, R., Jones, R., Piani, L., and Marrocchi, Y. 2024. Identification of a Primordial High D/H Component in the Matrix of Unequilibrated Ordinary Chondrites. *Geochimica et Cosmochimica Acta* 378: 58–70.
Greenwood, R. C., Burbine, T. H., and Franchi, I. A. 2020. Linking Asteroids and Meteorites to the Primordial Planetesimal Population. *Geochimica et Cosmochimica Acta* 277: 377–406.
Greshake, A. 2014. A Strongly Hydrated Microclast in the Rumuruti Chondrite NWA 6828: Implications for the Distribution of Hydrous Material in the Solar System. *Meteoritics & Planetary Science* 49: 824–841.
Greshake, A., Krot, A. N., Meibom, A., Weisberg, M. K., Zolensky, M. E., and Keil, K. 2002. Heavily-Hydrated Lithic

19455100, 0, Downloaded from https://onlinelibrary.wiley.com/doi/10.1111/maps.70233 by Portland State University, Wiley Online Library on [06/11/2026]. See the Terms and Conditions (https://onlinelibrary.wiley.com/terms-and-conditions) on Wiley Online Library for rules of use; OA articles are governed by the applicable Creative Commons License

Clasts in CH Chondrites and the Related, Metal-Rich Chondrites Queen Alexandra Range 94411 and Hammadah al Hamra 237. *Meteoritics & Planetary Science* 37: 281–293.
Grossman, L., Allen, J. M., and MacPherson, G. J. 1980. Electron Microprobe Study of a "Mysterite"-Bearing Inclusion from the Krymka LL-Chondrite. *Geochimica et Cosmochimica Acta* 44: 211–16.
Grossman, J. N., and Brearley, A. J. 2005. The Onset of Metamorphism in Ordinary and Carbonaceous Chondrites. *Meteoritics & Planetary Science* 40(1): 87–122.
Haba, M. K., Wotzlaw, J.-F., Lai, Y.-J., Yamaguchi, A., and Schönbächler, M. 2019. Mesosiderite Formation on Asteroid 4 Vesta by a Hit-and-Run Collision. *Nature Geoscience* 12: 510–15. https://doi.org/10.1038/s41561-019-0377-8.
Hopp, T., Dauphas, N., Abe, Y., Aléon, J. O'D., Alexander, C. M., Amari, S., et al. 2022. Ryugu's Nucleosynthetic Heritage from the Outskirts of the Solar System. *Science Advances* 8: eadd8141.
Horstmann, M., and Bischoff, A. 2014. The Almahata Sitta Polymict Breccia and the Late Accretion of Asteroid 2008 TC3. *Chemie der Erde* 74: 149–184.
Hsu, H.-W., Wang, X., Carroll, A., Hood, N., and Horányi, M. 2022. Fine-Grained Regolith Loss on Sub-Km Asteroids. *Nature Astronomy* 6: 1043–50.
Hutchison, R. 1986. New Data on the Bencubbin Polymict Stony Iron Breccia. *Lunar and Planetary Science* 17: 374–75.
Ikeda, Y., Kimura, M., Mori, H., and Takeda, H. 1981. Chemical Compositions of Matrices of Unequilibrated Ordinary Chondrites. *Memoirs of National Institute of Polar Research. Special issue* 20: 124–144.
Ikeda, Y., Kita, N. T., Morishita, Y., and Weisberg, M. K. 2003. Primitive Clasts in the Dar al Gani 319 Polymict Ureilite: Precursors of the Ureilites. *Antarctic Meteorite Research* 16: 105–127.
Ikeda, Y., Prinz, M., and Nehru, C. E. 2000. Lithic and Mineral Clasts in the Dar al Gani., DAG. 319 Polymict Ureilites. *Antarctic Meteorite Research* 13: 177–221.
Isa, J., Rubin, A. E., and Wasson, J. T. 2014. R-Chondrite Bulk-Chemical Compositions and Diverse Oxides: Implications for Parent-Body Processes. *Geochimica et Cosmochimica Acta* 124: 131–151.
Itoh, D., and Tomeoka, K. 2003. Dark Inclusions in CO_3 Chondrites: New Indicators of Parent-Body Processes. *Geochimica et Cosmochimica Acta* 67: 153–169.
Jarosewich, E. 1990. Chemical Analyses of Meteorites: A Compilation of Stony and Iron Meteorite Analyses. *Meteoritics* 25: 323–337.
Jogo, K., Nagashima, K., Hutcheon, I. D., Krot, A. N., and Nakamura, T. 2013. Heavily Metamorphosed Clasts from the CV Chondrite Breccias Mokoia and Yamato-86009. *Meteoritics & Planetary Science* 47: 2251–68.
Johnson, C. A., Prinz, M., Weisberg, M., Clayton, R. N., and Mayeda, T. 1990. Dark Inclusions in Allende, Leoville, and Vigarano: Evidence for Nebular Oxidation of CV3 Constituents. *Geochimica et Cosmochimica Acta* 54: 819–830.
Kebukawa, Y., Ito, M., Zolensky, M. E., Grenwood, R. C., Rahman, Z., Suga, H., Nakato, A., et al. 2019. A Novel Organic-Rich Meteoritic Clast from the Outer Solar System. *Scientific Reports* 9: 3169. https://doi.org/10.1038/s41598-019-39357-1.
Keil, K. 1982. Composition and Origin of Chondritic Breccias. In *Workshop on Lunar Breccias and Soils and Their Meteoritic Analogs*, edited by G. J. Taylor, and L. L. Wilkening, 65–83. Houston, Texas: Lunar and Planetary Institute.
Keil, K., and Fodor, R. V. 1980. Origin and History of the Polymict Brecciated Tysnes Island Chondrite and its Carbonaceous and Non-Carbonaceous Lithic Fragments. *Chemie der Erde* 39: 1–26.
Kennedy, A. K., Hutchison, R., Hutcheon, I. D., and Agrell, S. O. 1992. A Unique High Mn/Fe Microgabbro in the Parnallee (LL3) Ordinary Chondrite: Nebular Mixture or Planetary Differentiate from a Previously Unrecognized Planetary Body? *Earth and Planetary Science Letters* 113: 191–205.
Kerraouch, I., Bischoff, A., Zolensky, M. E., Pack, A., Patzek, M., Hanna, R. D., Fries, M. D., et al. 2021. The Polymict Carbonaceous Breccia Aguas Zarcas: A Potential Analog to Samples Being Returned by the OSIRIS-REx and Hayabusa2 Mission. *Meteoritics & Planetary Science* 56: 277–310.
Kerraouch, I., Ebert, S., Patzek, M., Bischoff, A., Zolensky, M. E., Pack, A., Schmitt-Kopplin, P., Bekhai, D., Bendaoud, A., and Le, L. 2019. A Light, Chondritic Xenolith in the Murchison (CM) Chondrite – Formation by Fluid-Assisted Percolation during Metasomatism? *Geochemistry* 79: 125518.
Kerraouch, I., Kebukawa, Y., Bischoff, A., Zolensky, M. E., Wölfer, E., Hellmann, J. L., Ito, M., et al. 2022. Heterogeneous Nature of the Carbonaceous Chondrite Breccia Aguas Zarcas – Cosmochemical Characterization and Origin of New Carbonaceous Chondrite Lithologies. *Geochimica et Cosmochimica Acta* 334: 155–186.
Kimura, M., and El Goresy, A. 1989. Discovery of E-Chondrite Assemblages, SiC, and Silica-Bearing Objects in ALH85085: Link between E- and C- Chondrite. *Meteoritics* 24: 286.
King, A. J., Schofield, P. F., Howard, K. T., and Russell, S. S. 2015. Modal Mineralogy of CI and CI-Like Chondrites by X-Ray Diffraction. *Geochimica et Cosmochimica Acta* 165: 148–160.
Kita, N. T., Ikeda, Y., Togashi, S., Liu, Y., Morishita, Y., and Weisberg, M. K. 2003. Origin of Ureilites Inferred from a SIMS Oxygen Isotopic and Trace Element Study of Clasts in the Dar al Gani 319 Polymict Ureilite. *Geochimica et Cosmochimica Acta* 68: 4213–35.
Krämer Ruggiu, L., Devouard, B., Gattacceca, J., Bonal, L., Leroux, H., Eschrig, J., Borschneck, D., et al. 2022. Detection of Incipient Aqueous Alteration in Carbonaceous Chondrites. *Geochimica et Cosmochimica Acta* 336: 308–331.
Krot, A., Meibom, A., and Keil, K. 2000. A Clast of Bali-Like Oxidized CV Material in the Reduced CV Chondrite Breccia Vigarano. *Meteoritics & Planetary Science* 35: 817–825.
Krot, A. N., Amelin, Y., Cassen, P., and Meibom, A. 2005. Young Chondrules in CB Chondrites from a Giant Impact in the Early Solar System. *Nature* 436: 989–992.
Krot, A. N., Brearley, A. J., Ulyanov, A. A., Biryukov, V. V., Swindle, T. D., Keil, K., Mittlefehldt, D. W., Scott, E. R. D., Clayton, R. N., and Mayeda, T. K. 1999. Mineralogy, Petrography, Bulk Chemical, Iodine-Xenon, and Oxygen-Isotopic Compositions of Dark Inclusions in the Reduced CV3 Chondrite Efremovka. *Meteoritics & Planetary Science* 34: 67–89.
Kruijer, T. S., Borg, L. E., Render, J., Brennecka, G. A., Wimpenny, J., Shearer, C. K., and Agee, C. B. 2025.

19455100, 0, Downloaded from https://onlinelibrary.wiley.com/doi/10.1111/maps.70233 by Portland State University, Wiley Online Library on [06/11/2026]. See the Terms and Conditions (https://onlinelibrary.wiley.com/terms-and-conditions) on Wiley Online Library for rules of use; OA articles are governed by the applicable Creative Commons License

Isotopic Constraints on the Origin of a Differentiated Achondrite From Hassi el Madani 002. *56th Lunar and Planetary Science Conference*, abstract #1130.
Kruijer, T. S., Burkhardt, C., Budde, G., and Kleine, T. 2017. Age of Jupiter Inferred from the Distinct Genetics and Formation Times of Meteorites. *Proceedings of the National Academy of Science* 114: 6712–16.
Kurat, G. 1975. Der Kohlige Chondrit Lancé: Eine Petrologische Analyse der Komplexen Genese Eines Chondriten. *Tschermaks Mineralogische Und Petrographische Mitteilungen* 22: 38–78.
Kurat, G., and Kracher, A. 1980. Basalts in the Lancé Carbonaceous Chondrite. *Zeitschrift für Naturforschung A* 35: 180–190.
Lee, M. R., Alexander, C. M. O., Bischoff, A., et al. 2025. Low-Temperature Aqueous Alteration of Chondrites. *Space Science Reviews* 221: 11. https://doi.org/10.1007/s11214-024-01132-8.
Leitch, C. A., and Grossman, L. 1977. Lithic Clasts in the Supuhee Chondrite. *Meteoritics* 12: 125–139.
Lentfort, S., Bischoff, A., Ebert, S., and Patzek, M. 2021. Classification of CM Chondrite Breccias—Implications for the Evaluation of Samples from the OSIRIS-REx and Hayabusa 2 Missions. *Meteoritics and Planetary Science Letters* 56: 127–147.
Liu, N., Ogliore, R. C., and Vacher, L. G. 2020. NanoSIMS Isotopic Investigation of Xenolithic Carbonaceous Clasts from the Kapoeta Howardite. *Geochimica et Cosmochimica Acta* 283: 243–264.
Lovering, J. F. 1962. The Evolution of the Meteorites--Evidence for the co-Existence of Chondritic, Achondritic and Iron Meteorites in a Typical Parent Meteorite Body. In *Researches on Meteorites*, edited by C. B. Moore, 179–197. New York: Wiley.
Lunning, N. G., Bischoff, A., Gross, J., Patzek, M., Corrigan, C. M., and McCoy, T. J. 2020. Insights into the Formation of Silica-Rich Achondrites from Impact Melts in Rumuruti-Type Chondrites. *Meteoritics & Planetary Science* 55: 130–148.
Malhé, T., Marrocchi, Y., Neukampf, J., Villeneuve, J., and Jacquet, E. 2024. The Last Generation of Nebular Chondrules Possibly Sampled in the Ch/CBb Chondrite Isheyevo. *Geochimica et Cosmochimica Acta* 385: 74–86.
Marrocchi, Y., Delbo, M., Gounelle, M., and Timothy Jull, A. J. 2021. The Astrophysical Context of Collision Processes in Meteorites. *Meteoritics & Planetary Science* 56: 1406–21.
Marrocchi, Y., Füri, E., Zimmermann, L., and Piani, L. 2026. H-N Budgets and Isotopic Signatures of Oued Chebeika 002 and CI Reservoir Heterogeneity. *Geochemical Perspectives Letters* 39: 7–11. https://doi.org/10.7185/geochemlet.2605.
Marrocchi, Y., Jones, R. H., Russell, S. S., Hezel, D. C., Barosch, J., and Kuznetsova, A. 2024. Chondrule Properties and Formation Conditions. *Space Science Reviews* 220: 69.
Marrocchi, Y., Piralla, M., and Tissot, F. L. H. 2023. Iron Isotope Constraints on the Structure of the Early Solar System. *The Astrophysical Journal Letters* 954: L27.
McCall, G. J. H. 1968. The Bencubbin Meteorite: Further Details, Including Microscopic Character of the Host Material and Two Chondrite Enclaves. *Mineralogical Magazine* 36: 726–739.
McSween, H. Y., and Richardson, S. 1977. The Composition of Carbonaceous Chondrite Matrix. *Geochimica et Cosmochimica Acta* 41: 1145–61.
Melosh, H. J. 1989. *Impact Cratering: A Geologic Process*. New York: Oxford University Press. 245.
Morbidelli, A., Walsh, K. J., O'Brien, D. P., Minton, D. A., and Bottke, W. F. 2015. The Dynamical Evolution of the Asteroid Belt. In *Asteroids IV*, edited by P. Michel, F. E. DeMeo, and W. F. Bottke, 493–507. Tucson: Univ. of Arizona. https://doi.org/10.2458/azu_uapress_9780816532131-ch026.
Morin, G. L. F., Marrocchi, Y., Villeneuve, J., and Jacquet, E. 2022. ^{16}O-Rich Anhydrous Silicates in CI Chondrites: Implications for the Nature and Dynamics of Dust in the Solar Accretion Disk. *Geochimica et Cosmochimica Acta* 332: 203–219.
Morlok, A., Bischoff, A., Stephan, T., Floss, C., Zinner, E., and Jessberger, E. K. 2006. Brecciation and Chemical Heterogeneities of CI Chondrites. *Geochimica et Cosmochimica Acta* 70: 5371–94.
Musolino, A., Suttle, M. D., Folco, L., King, A. J., Poggiali, G., Bates, H. C., Brucato, J. R., and Brearley, A. 2024. Early Fluid Migration and Alteration Fronts in the CM Chondrite Reckling Peak 17085. *Meteoritics & Planetary Science* 59: 3021–43.
Nabiei, F., Badro, J., Dennenwaldt, T., Oveisi, E., Cantoni, M., Hébert, C., El Goresy, A., Barrat, J.-A., and Gillet, P. 2018. A Large Planetary Body Inferred from Diamond Inclusions in a Ureilite Meteorite. *Nature Communications* 9: 1327. https://doi.org/10.1038/s41467-018-03808-6.
Nakashima, D., Nakamura, T., and Noguchi, T. 2003. Formation History of CI-Like Phyllosilicate-Rich Clasts in the Tsukuba Meteorite Inferred from Mineralogy and Noble Gas Signatures. *Earth and Planetary Science Letters* 212: 321–336.
Nehru, C. E., Zucker, S. M., Harlow, G. E., and Prinz, M. 1980. Olivines and Olivine Coronas in Mesosiderites. *Geochimica et Cosmochimica Acta* 44: 1103–18.
Nittler, L. R., Stroud, R. M., Trigo-Rodriguez, J. M., De Gregorio, B. T., Alexander, C. M. O'D., Davidson, J., Moyano-Cambero, C. E., and Tanbakouei, S. 2019. A Cometary Building Block in a Primitive Asteroidal Meteorite. *Nature Astronomy* 3: 659–666.
Osawa, T., and Nagao, K. 2006. Noble Gases in Solar-Gas-Rich and Solar-Gas-Free Polymict Breccias. *Antarctic Meteorite Research* 19: 58–78.
Outrequin, C., Alexandre, A., Vallet-Coulomb, C., Piel, C., Devidal, S., Landais, A., Couapel, M., et al. 2021. The Triple Oxygen Isotope Composition of Phytoliths, a New Proxy of Atmospheric Relative Humidity: Controls of Soil Water Isotope Composition, Temperature, CO_2 Concentration and Relative Humidity. *Climate of the Past* 17: 881–1902.
Papike, J. J., Karner, J. M., and Shearer, C. K. 2003. Determination of Planetary Basalt Parentage: A Simple Technique Using the Electron Microprobe. *American Mineralogist* 88: 469–472.
Patzek, M., Bischoff, A., Visser, R., and John, T. 2018. Mineralogy of Volatile-Rich Clasts in Brecciated Meteorites. *Meteoritics & Planetary Science* 53: 2519–40.
Patzek, M., Hoppe, P., Bischoff, A., Visser, R., and John, T. 2020. Hydrogen Isotopic Composition of CI- and CM-Like Clasts from Meteorite Breccias – Sampling Unknown

19455100, 0, Downloaded from https://onlinelibrary.wiley.com/doi/10.1111/maps.70233 by Portland State University, Wiley Online Library on [06/11/2026]. See the Terms and Conditions (https://onlinelibrary.wiley.com/terms-and-conditions) on Wiley Online Library for rules of use; OA articles are governed by the applicable Creative Commons License

Sources of Carbonaceous Chondrite Materials. *Geochimica et Cosmochimica Acta* 272: 177–197.

Patzek, M., Kadlag, Y., Rüfenacht, M., Füri, E., Pack, A., Bischoff, A., Becker, H., Visser, R., John, T., and Schönbächler, M. 2025. Multi-Isotope (N, O, Ti, and Cr) Study of C1 and CM-Like Clasts—Probing Unsampled C1 Material. *Meteoritics & Planetary Science* 60: 1073–94.

Pohl, L., and Britt, D. T. 2020. Strengths of Meteorites—An Overview and Analysis of Available Data. *Meteoritics & Planetary Science* 55: 962–987.

Prêt, D., Sammartino, S., Beaufort, D., Fialin, M., Sardini, P., Cosenza, P., and Meunier, A. 2010. A New Method for Quantitative Petrography Based on Image Processing of Chemical Element Maps: Part II. Semi-Quantitative Porosity Maps Superimposed on Mineral Maps. *American Mineralogist* 95: 1389–98.

Prinz, M., Weisberg, M. K., Clayton, R. N., and Mayeda, T. K. 1993. Ordinary and Carlisle Lakes-Like Chondrite Clasts in the Weatherford Chondrite Breccia. *Meteoritics* 28: 419–420.

Prinz, M., Weisberg, M. K., Nehru, C. E., and Delaney, J. S. 1986. North Haig and Nilpena: Paired Polymict Ureilites with Angra dos Reis-Related and Other Clasts. *Lunar and Planetary Science* 17: 681–82.

Raymond, S. N., and Izidoro, A. 2017. The Empty Primordial Asteroid Belt. *Science Advances* 3: e1701138.

Reid, A. M., Buchanan, P., Zolensky, M. E., and Barrett, R. A. 1990. The Bholghati Howardite: Petrography and Mineral Chemistry. *Geochimica et Cosmochimica Acta* 54: 2161–66.

Rochette, P., Gattacceca, J., Bonal, L., Bourot-Denise, M., Chevrier, V., Clerc, J.-P., Consolmagno, G., et al. 2008. Magnetic Classification of Stony Meteorites: 2. Non-Ordinary Chondrites. *Meteoritics & Planetary Science* 43: 959–980.

Rochette, P., Sagnotti, L., Bourot-Denise, M., Consolmagno, G., Folco, L., Gattacceca, J., Osete, M. L., and Pesonen, L. 2003. Magnetic Classification of Stony Meteorites: 1. Ordinary Chondrites. *Meteoritics & Planetary Science* 38: 251–58.

Rosing, M. T., and Haack, H. 2004. The First Mesosiderite-Like Clast in a Howardite. *35th Lunar and Planetary Conference*, abstract #1487.

Rubin, A. E., and Bottke, W. F. 2009. On the Origin of Shocked and Unshocked CM Clasts in H-Chondrite Regolith Breccias. *Meteoritics & Planetary Science* 44: 701–724.

Rubin, A. E., and Grosmann, J. N. 2010. Meteorite and Meteoroid: New Comprehensive Definitions. *Meteoritics & Planetary Science* 45: 114–122.

Rubin, A. E., Keil, K., Taylor, G. J., Ma, M. S., Schmitt, R. A., and Bogard, D. D. 1981. Derivation of a Heterogeneous Lithic Fragment in the Bovedy L-Group Chondrite from Impact-Melted Porphyritic Chondrules. *Geochimica et Cosmochimica Acta* 45: 2213–28.

Rubin, A. E., Scott, E. R. D., Taylor, G. J., Mayeda, T. K., Clayton, R. N., and Bogard, D. D. 1983. Nature of the H Chondrite Parent Body: Evidence from the Dimmitt Breccia. Proc. 13th Lunar and Planetary Conference. *Journal of Geophysical Research* 88: A741–A754.

Ruzicka, A., Snyder, G. A., and Taylor, L. A. 1998. Megachondrules and Large, Igneous-Textured Clasts in Julesberg (L3) and Other Ordinary Chondrites: Vapor-Fractionation, Shock-Melting, and Chondrule Formation. *Geochimica et Cosmochimica Acta* 62: 1419–42.

Ruzicka, A. M., Greenwood, R. C., Armstrong, K., Schepker, K. L., and Franchi, I. A. 2019. Petrology and Oxygen Isotopic Composition of Large Igneous Inclusions in Ordinary Chondrites: Early Solar System Igneous Processes and Oxygen Reservoirs. *Geochimica et Cosmochimica Acta* 266: 497–528.

Sadaka, C., Gattacceca, J., Dumas, F., Braucher, R., ASTER Team, Leya, I., Tauseef, M., et al. 2026. Terrestrial Ages of Meteorites from the Atacama Desert (Chile) and Insights in the Past Meteorite Flux to the Earth. *Meteoritics & Planetary Science*. 61: 644–663. https://doi.org/10.1111/maps.70125.

Sanderson, H. R., Courville, S. W., Harrison, C. S., Rider-Stokes, B. G., Davies, F. A., Suttle, M. D., and Davison, T. M. 2026. Insights into the Size and Number of CM Chondrite Parent Bodies from Thermal Modelling and Links to Asteroids. *Journal of the Geological Society* 183. https://doi.org/10.1144/jgs2026-033.

Schrader, D. L., Torrano, Z. A., Foustoukos, D. I., Alexander, C. M. O'D., Render, J., and Brennecka, G. A. 2025. Reassessing the Proposed "CY Chondrites": Evidence for Multiple Meteorite Types and Parent Bodies from Cr-Ti-H-C-N Isotopes and Bulk Elemental Compositions. *Geochimica et Cosmochimica Acta* 390: 24–37.

Scicchitano, M. R., Rubatto, D., Hermann, J., Shen, T., Padrón-Navarta, J. A., Williams, I. S., and Zheng, Y. 2018. In Situ Oxygen Isotope Determination in Serpentine Minerals by Ion Microprobe: Reference Materials and Applications to Ultrahigh-Pressure Serpentinites. *Geostandards and Geoanalytical Research* 42: 459–479.

Sears, D. W., and Wasson, J. T. 1981. Dark Inclusions in the Abbott, Cynthiana and Abee Chondrites. *22nd Lunar and Planetary Science Conference*, pp. 958–960.

Semenenko, V. P., Bischoff, A., Weber, I., Perron, C., and Girich, A. L. 2001. Mineralogy of Fine-Grained Material in the Krymka (LL3.1) Chondrite. *Meteoritics & Planetary Science* 36: 1067–85.

Semenenko, V. P., Girich, A. L., and Nittler, L. R. 2004. An Exotic Kind of Cosmic Material: Graphite-Containing Xenoliths from the Krymka (LL3.1) Chondrite. *Geochimica et Cosmochimica Acta* 68: 455–475.

Sokol, A. K., Mezger, K., Chaussidon, M., and Bischoff, A. 2007. Achondritic Fragments in Ordinary Chondrite Breccias. *70th Annual Meteoritical Society Meeting*, abstract #5153.

Storz, J., Ludwig, T., Bischoff, A., Schwartz, W. H., and Trieloff, M. 2021. Graphite in Ureilites, Enstatite Chondrites, and Unique Clasts in Ordinary Chondrites – Insights from the Carbon-Isotope Composition. *Geochimica et Cosmochimica Acta* 307: 86–104.

Suttle, M. D., King, A. J., Harrison, C. S., Chan, Q. H. S., Greshake, A., Bartoschewitz, R., Tomkins, A. G., Salge, T., Schofield, P. F., and Russell, S. S. 2023. The Mineralogy and Alteration History of the Yamato-Type (CY) Carbonaceous Chondrites. *Geochimica et Cosmochimica Acta* 361: 245–264.

Tonui, E., Zolensky, M., Hiroi, T., Nakamura, T., Lipschutz, M. E., Wang, M.-S., and Okudaira, K. 2014. Petrographic, Chemical and Spectroscopic Evidence for Thermal Metamorphism in Carbonaceous Chondrites I: CI and CM Chondrites. *Geochimica et Cosmochimica Acta* 126: 284–306.

19455100, 0, Downloaded from https://onlinelibrary.wiley.com/doi/10.1111/maps.70233 by Portland State University, Wiley Online Library on [06/11/2026]. See the Terms and Conditions (https://onlinelibrary.wiley.com/terms-and-conditions) on Wiley Online Library for rules of use; OA articles are governed by the applicable Creative Commons License

Van Drongelen, K. D., Rumble, D., III, and Tait, K. T. 2016. Petrology and Oxygen Isotopic Compositions of Clasts in HED Polymict Breccia NWA 5232. *Meteoritics & Planetary Science* 51: 1184–1200.

van Kooten, E., Zhao, X., Franchi, I., Tung, P.-Y., Fairclough, S., Walmsley, J., Onyett, I., Schiller, M., and Bizzarro, M. 2024. The Nucleosynthetic Fingerprint of the Outermost Protoplanetary Disk and Early Solar System Dynamics. *Science Advances* 10(24). https://doi.org/10.1126/sciadv.adp1613.

Van Schmus, W. R. 1967. Polymict Structure of the Mezö-Madaras Chondrite. *Geochimica et Cosmochimica Acta* 31: 2027–42.

Verdier-Paoletti, M., Marrocchi, Y., Vacher, L. G., Gattacceca, J., Gurenko, A., Sonzogni, C., and Gounelle, M. 2019. Testing the Genetic Relationship between Fluid Alteration and Brecciation in CM Chondrites. *Meteoritics & Planetary Science* 54: 1692–1709.

Visser, R., John, T., Menneken, M., Patzek, M., and Bischoff, A. 2018. Temperature Constraints by Raman Spectroscopy of Organic Matter in Volatile-Rich Clasts and Carbonaceous Chondrites. *Geochimica et Cosmochimica Acta* 241: 38–55.

Visser, R., John, T., Patzek, M., Bischoff, A., and Whitehouse, M. J. 2019. Sulfur Isotope Study of Sulfides in CI, CM, C2ung Chondrites and Volatile-Rich Clasts – Evidence for Different Generations and Reservoirs of Sulfide Formation. *Geochimica et Cosmochimica Acta* 261: 210–223.

Visser, R., John, T., Whitehouse, L. J., Patzek, M., and Bischoff, A. 2020. A Short-Lived ^{26}Al Induced Hydrothermal Alteration Event in the Outer Solar System: Constraints from Mn/Cr Ages of Carbonates. *Earth and Planetary Science Letters* 547: 116440.

Warren, P. H. 2011. Stable-Isotopic Anomalies and the Accretionary Assemblage of the Earth and Mars: A Subordinate Role for Carbonaceous Chondrites. *Earth and Planetary Science Letters* 311: 93–100.

Weidenschilling, S. J. 1988. Formation Processes and Time Scales for Meteorite Parent Bodies. In *Meteorites and the Early Solar System*, 348–371. Tucson, AZ: University of Arizona Press.

Weisberg, M. K., McCoy, T. J., and Krot, A. N. 2006. Systematics and Evaluation of Meteorite Classification. In *Meteorites and the Early Solar System II*, edited by D. S. Lauretta, and H. Y. McSween, Jr., 19–52. Tucson: University of Arizona Press.

Weisberg, M. K., Prinz, M., Chatterjee, N., and Clayton, R. N. 1991. Dark Inclusions in CR2 Chondrites. *Meteoritics* 26: 407.

Weisberg, M. K., Prinz, M., and Cherukupalli, E. N. 1990. The Bencubbin Chondrite Breccia and its Relationship to CR Chondrites and the ALH85085 Chondrite. *Meteoritics* 25: 269–279.

Weisberg, M. K., Prinz, M., Clayton, R. N., Mayeda, T. K., Grady, M. M., and Pillinger, C. 1995. The CR Chondrite Clan. *Proceedings of the NIPR Symposium on Antarctic Meteorites* 8: 11–32.

Welten, K. C., Nishiizumi, K., Caffee, M. W., Hillegonds, D. J., Johnson, J. A., Jull, A. J. T., Wieler, R., and Folco, L. 2006. Terrestrial Ages, Pairing, and Concentration Mechanism of Antarctic Chondrites from Frontier Mountain, Northern Victoria Land. *Meteoritics & Planetary Science* 41: 1081–94.

Wilkening, L. L. 1977. Meteorites in Meteorites: Evidence for Mixing among the Asteroids. In *Comets, Asteroids and Meteorites*, edited by A. H. Delsemme, 389–396. Ohio: Univ. of Toledo.

Wilkening, L. L., and Clayton, R. N. 1974. Foreign Inclusions in Stony Meteorites-II. Rare Gases and Oxygen Isotopes in a Carbonaceous Xenolith in the Plainview Gas-Rich Chondrite. *Geochimica et Cosmochimica Acta* 38: 937–945.

Wölfer, E., Budde, G., and Kleine, T. 2023. Age and Genetic Relationships among CB, CH and CR Chondrites. *Geochimica et Cosmochimica Acta* 361: 288–301.

Yap, T. E., and Tissot, F. L. H. 2023. The NC-CC Dichotomy Explained by Significant Addition of CAI-Like Dust to the Bulk Molecular Cloud (BMC) Composition. *Icarus* 405: 115680.

Zolensky, M., Barrett, R., and Browning, L. 1993. Mineralogy and Composition of Matrix and Chondrule Rims in Carbonaceous Chondrites. *Geochimica et Cosmochimica Acta* 57: 3123–48.

Zolensky, M., and Ivanov, A. 2003. The Kaidun Microbreccia Meteorite: A Harvest from the Inner and Outer Asteroid Belt. *Chemie der Erde* 63: 185–246.

Zolensky, M., Johnson, J., Ziegler, K., Chan, Q., Kebukawa, Y., Bottke, W., Fries, M., Martinez, J., and Le, L. 2018. Meteoritic Evidence for Injection of Trans-Neptunian Objects into the Inner Solar System. *49th Lunar and Planetary Science Conference*, abstract #1789.

Zolensky, M. E., Abreu, N. M., Velbel, M. A., Rubin, A., Chaumard, N., Noguchi, T., and Michikami, T. 2018. Physical, Chemical, and Petrological Characteristics of Chondritic Materials and Their Relationships to Small Solar System Bodies. In *Primitive Meteorites and Asteroids*, 59–204. Amsterdam: Elsevier. https://doi.org/10.1016/B978-0-12-813325-5.00002-1.

Zolensky, M. E., Hewins, R. H., Mittlefehldt, D. W., Lindstrom, M. M., Xiao, X., and Lipschutz, M. E. 1992. Mineralogy, Petrology and Geochemistry of Carbonaceous Chondritic Clasts in the LEW 85300 Polymict Eucrite. *Meteoritics* 27: 596–604.

Zolensky, M. E., Weisberg, M. K., Buchanan, P. C., and Mittlefehldt, D. W. 1996. Mineralogy of Carbonaceous Chondrite Clasts in HED Achondrites and the Moon. *Meteoritics & Planetary Science* 31: 518–537.

SUPPORTING INFORMATION

Additional supporting information may be found in the online version of this article.

Figure S1. (a) CM2 xenolith in NWA 14840 (reflected light image). (b) CM2 xenolith in NWA 17470 (reflected light image).

Figure S2. BSE images of type 1 xenoliths in polymict ureilites NWA 14806 (a), and NWA 16454 (b).

Figure S3. BSE images of xenoliths in Los Vientos 200 CH3 chondrite. (a) Rounded xenolith. (b) Sulfide laths and magnetite spheroids. (c) Sulfide laths and magnetite platelets. (d) Xenolith indented by enstatite crystal from the host.

19455100, 0, Downloaded from https://onlinelibrary.wiley.com/doi/10.1111/maps.70233 by Portland State University, Wiley Online Library on [06/11/2026]. See the Terms and Conditions (https://onlinelibrary.wiley.com/terms-and-conditions) on Wiley Online Library for rules of use; OA articles are governed by the applicable Creative Commons License

Figure S4. Unusual clasts. (a) Plane polarized image of DaG 417 R3-4 showing the brecciated texture, and an unusual dark clast at the center. (b, c) BSE images of the unusual clast in DaG 417. (d) It reflected light image of Sahara 97158 EH3 showing a metal-deprived clast at the center. (e) Reflected light images of Sahara 97158 showing the host lithology (left) and the metal-deprived clast (right). (f) Optical image of NWA 13385 $CV_{Red}3$ showing a matrix-rich inclusion at the center. (g, h) BSE images of the matrix-rich inclusion in NWA 13385.

Figure S5. Mesosiderite clasts in HED meteorites. (a) Optical image of a slice of NWA 14981. (b) Compositional composite image (red = Ni, blue = Mg, yellow = S, cyan = Ca) of the same slice, highlighting the CM2 and mesosiderite clasts. (d) BSE image of an orthopyroxene corona around an olivine crystal in the mesosiderite clast in NWAA 14981. (e) BSE image of the mesosiderite clast in NWA 10472.

Figure S6. CI chondrite-normalized trace element abundances for olivine (a) and low-Ca pyroxene (b) in achondritic clasts in NWA 14826 and NWA 15116. These are compared to literature data for other achondrites, including NWA 7325 (Yang et al., 2020), GRA 06128 (Day et al., 2012), Néma 001 (Tartèse et al., 2025), Martian meteorites Tissint and NWA 1068 (Peel et al., 2025), and the angrite NWA 4590 (Rider-Stokes et al., 2023). CI chondrite element abundances are from Barrat et al. (2012).

Table S1. List of meteorite slices investigated at MNHN.

Table S2: EPMA data for defocused matrix analyses of clasts.

Table S3. Xenoliths described in the literature.

Table S4. Literature data of oxygen isotopic composition of xenoliths.

Table S5. LA-ICP-MS protocol for trace element analysis of achondritic clasts in NWA 14826 and NWA 15116.

Table S6. LA-ICP-MS results on reference materials and achondritic clasts in NWA 14826 and NWA 15116.

Table S7. Review of graphite-rich xenolith properties.

Table S8. EPMA data for achondritic clasts in NWA 14826 and NWA 15116.

Table S9. Bulk composition of clasts and selected meteorites.

Table S10. EPMA data for C2-ung clasts in Bholghati (our clasts #5-7). For comparison, two calcite analyses are provided from a CM2 clast in Bholghati (clast 8).

Table S11. Names of xenolith-bearing meteorites as a function of their host and xenolith classification.

Data S1. References for Figure S6.

19455100, 0, Downloaded from https://onlinelibrary.wiley.com/doi/10.1111/maps.70233 by Portland State University, Wiley Online Library on [06/11/2026]. See the Terms and Conditions (https://onlinelibrary.wiley.com/terms-and-conditions) on Wiley Online Library for rules of use; OA articles are governed by the applicable Creative Commons License